



# Formation of a regular domain structure and wavelength conversion in lithium niobate modified by the proton exchange

Evgenii Savelev

## ► To cite this version:

Evgenii Savelev. Formation of a regular domain structure and wavelength conversion in lithium niobate modified by the proton exchange. Physics [physics]. Université Côte d'Azur; Université d'Oural, 2023. English. NNT : 2023COAZ4141 . tel-04533784

HAL Id: tel-04533784

<https://theses.hal.science/tel-04533784>

Submitted on 5 Apr 2024

**HAL** is a multi-disciplinary open access archive for the deposit and dissemination of scientific research documents, whether they are published or not. The documents may come from teaching and research institutions in France or abroad, or from public or private research centers.

L'archive ouverte pluridisciplinaire **HAL**, est destinée au dépôt et à la diffusion de documents scientifiques de niveau recherche, publiés ou non, émanant des établissements d'enseignement et de recherche français ou étrangers, des laboratoires publics ou privés.



# THÈSE DE DOCTORAT

**FORMATION DE STRUCTURES DE DOMAINES REGULIERES ET CONVERSION DE LONGUEUR  
D'ONDE DANS LE NIOBATE DE LITHIUM MODIFIÉ PAR ÉCHANGE PROTONIQUE**

**Evgenii SAVELEV**

Institut de Physique de Nice (France) et Université fédérale de l'Oural (Russie)

**Présentée en vue de l'obtention  
du grade de docteur en Physique  
d'Université Côte d'Azur  
et d'Ural Federal University**  
**Dirigée par :** Pascal BALDI / Vladimir  
SHUR  
**Soutenue le :** 19.12.2023

**Devant le jury, composé de :**  
Président du jury :  
Fabrice RAINERI, Prof, Institut de Physique de  
Nice, Université Côte d'Azur  
Rapporteurs :  
Ausrine BARTASYTE, Prof, Institut FEMTO-ST,  
Université de Bourgogne Franche-Comté  
Alexander N. VTYURIN, Prof, Institut Kirensky  
de physique SB RAS  
Examinateurs :  
Mikhail P. KASHCHENKO, Prof, Département  
de physique, Université d'ingénierie forestière  
d'État de l'Oural

# **FORMATION DE STRUCTURES DE DOMAINES REGULIERES ET CONVERSION DE LONGUEUR D'ONDE DANS LE NIOBATE DE LITHIUM MODIFIE PAR ECHANGE PROTONIQUE**

Jury:

Président du jury :

Fabrice RAINERI, HDR, Professor, Université Côte d'Azur (France) Teaching in Department of Physics Research at Institut de Physique de Nice (CNRS)

Rapporteurs:

Alexander N. VTYURIN, DSc, Professeur, Responsable de la photonique et des technologies laser, Institut d'ingénierie physique et radioélectronique, Université fédérale de Sibérie, Institut Kirensky de physique SB RAS

Ausrine BARTASYTE, HDR, Professeur des Universités, Institut FEMTO-ST, Université de Bourgogne Franche-Comté

Examinateurs:

Mikhail P. KASHCHENKO, DSc, Professeur, Chef du Département de Physique, Université d'ingénierie forestière d'État de l'Oural Invités

# FORMATION DE STRUCTURES DE DOMAINES REGULIERES ET CONVERSION DE LONGUEUR D'ONDE DANS LE NIOBATE DE LITHIUM MODIFIE PAR ECHANGE PROTONIQUE

## Résumé

Buts de la recherche: (1) étude de l'évolution de la structure de domaine dans les monocristaux CLN modifiés par la méthode d'échange protonique doux lors de la commutation de la polarisation dans le champ électrique homogène et dans le champ créé par un microscope sonde à balayage, (2) analyse de la génération de seconde harmonique dans les monocristaux CLN dopés au magnésium avec une structure de domaine régulière créée au moyen d'un balayage par faisceau d'électrons. Pour atteindre ces buts, les principaux objectifs suivants ont été formulés:

1. Étudier les particularités de la croissance anormale des domaines lamellaires sur la surface polaire pendant la commutation de polarisation dans les monocristaux de niobate de lithium modifiés par échange protonique doux.
  2. Étudier l'influence des paramètres d'échange protonique sur la distribution spatiale de la composition, la cinétique de la structure de domaine et les champs de seuil dans les monocristaux de niobate de lithium modifiés.
  3. Élaborer des méthodes de structures de domaine quasi-périodiques et régulières dans les monocristaux de niobate de lithium modifiés.
  4. Étudier les particularités de la génération de seconde harmonique dans les monocristaux de niobate de lithium dopés au magnésium avec une structure de domaine régulière créée au moyen d'un balayage par faisceau d'électrons focalisés.
- Méthodologie et méthodes de recherche. Des études expérimentales systématiques de la structure de domaine ont été réalisées à l'aide d'équipements analytiques modernes de haute précision. La visualisation *in situ* de l'évolution de DS a été réalisée à l'aide de la microscopie optique avec une caméra à grande vitesse. La distribution spatiale des ions H<sup>+</sup> dans les plaques étudiées a été mesurée à l'aide de la microscopie confocale Raman (CRM). La visualisation non destructive de DS sur la surface a été réalisée par microscopie à force piézoélectrique à balayage (PFM). La visualisation des domaines en volume a été réalisée à l'aide de CRM et de la microscopie à génération de seconde harmonique (SHG). La commutation de polarisation locale à l'aide d'un microscope sonde à balayage a été utilisée pour créer des domaines isolés et des structures de domaine.

## PRINCIPAUX RÉSULTATS ET CONCLUSIONS DE L'ÉTUDE

1. Il a été étudié pour la première fois la croissance anormale de domaines lamellaires sur la surface polaire Z pendant la commutation de polarisation dans des monocristaux de niobate de lithium modifiés par un échange protonique doux.
2. Il a été trouvé que les champs de seuil de formation de domaines anormalement bas sur la surface polaire Z dépendaient de la durée du processus d'échange protonique.
3. Il a été détecté l'effet de la formation de structures de domaine quasi-périodiques pendant la croissance de domaines lamellaires à partir d'une paroi de domaine planaire.

4. La diminution anormale observée des champs de seuil de la croissance des domaines lamellaires à la suite d'un échange protonique doux est attribuée à la formation d'un champ interne de cohérence causé par la présence d'un gradient de composition dans la couche superficielle.
5. Il est démontré que la valeur du gradient de composition dans la couche superficielle croît avec l'augmentation de la durée de l'échange protonique, ce qui conduit à une diminution du champ de seuil.
6. Il est démontré qu'il est possible de créer une structure de domaine régulière et stable avec une période de 500 nm en commutant localement la polarisation à l'aide d'un microscope sonde à balayage.
7. Il a été obtenu pour la première fois une émission de 374 nm de longueur d'onde par génération de seconde harmonique dans un cristal de niobate de lithium dopé au magnésium avec une structure de domaine régulière d'une période de 2  $\mu\text{m}$  créée par balayage à l'aide d'un faisceau d'électrons focalisé.

**Mots clés:** Ferroélectrique, Guides d'ondes, Ingénierie de domaine, Gradient de composition, Nanotechnologie, Conversion de longueur d'onde lumineuse

## FORMATION OF A REGULAR DOMAIN STRUCTURE AND WAVELENGTH CONVERSION IN LITHIUM NIOBATE MODIFIED BY THE PROTON EXCHANGE

### Abstract

1. The abnormal growth of stripe domains on the Z-polar surface during polarization switching in lithium niobate single crystals modified by soft proton exchange was studied for the first time.
2. The dependences of abnormally low values of threshold fields of domain formation on the Z-polar surface on the duration of the proton exchange process are revealed.
3. The effect of the formation of quasi-periodic domain structures with the growth of stripe domains from a planar domain wall was found.
4. The observed anomalous decrease in the threshold field of stripe domain growth as a result of soft proton exchange is attributed to the formation of bound internal field caused by the presence of a composition gradient in the near-surface layer.
5. It is shown that the composition gradient in the near-surface layer increases with an increase in the duration of the proton exchange process, which leads to a decrease in the threshold field.
6. The possibility of creating a stable periodic domain structure with a period of 500 nm by local switching using the probe of a scanning probe microscope is demonstrated.
7. For the first time, radiation with a wavelength of 374 nm was obtained by the method of the second-harmonic generation in a crystal of magnesium doped lithium niobate with a 2- $\mu\text{m}$ -period domain structure created by scanning with a focused electron beam.

**Keywords:** Ferroelectrics, Waveguides, Domain engineering, Composition gradient, Nanotechnology, Light wavelength conversion

## Table of contents

CARACTÉRISTIQUES GÉNÉRALES DE LA THÈSE .....	8
La pertinence du sujet de recherche et la mesure de l'élaboration du sujet.....	8
Importance théorique de la recherche effectuée.....	11
Eléments pour la défense: .....	12
Valorisation des résultats.....	13
Publications et apports personnels de l'auteur.....	13
Structure et portée de la thèse. ....	14
Introduction .....	37
Literature review .....	43
1.1 Domain structure of uniaxial ferroelectrics .....	43
1.1.1 Ferroelectrics. Basic concepts.....	43
1.1.2 Evolution of the domain structure during polarization reversal .....	44
1.1.3 Screening of depolarizing fields .....	45
1.1.4 Kinetic approach to describe the evolution of the domain structure. ....	48
1.1.5 Kinetics of the domain structure under highly nonequilibrium switching conditions .....	50
1.2 Domain imaging methods .....	55
1.2.1 Selective chemical etching .....	56
1.2.2 Optical imaging .....	56
1.2.3 Scanning electron microscopy .....	57
1.2.4 Scanning probe microscopy .....	58
1.2.5 Confocal Raman microscopy .....	60
1.2.6 Second harmonic generation microscopy .....	61

1.3 Lithium niobate .....	62
1.3.1 Basic physical properties.....	62
1.3.2 Domain structure of lithium niobate .....	63
1.3.3 Evolution of the domain structure under pulsed IR laser irradiation....	66
1.3.4 Shape stability effect .....	69
1.4 Regular domain structures.....	70
1.4.1 Quasi phase matching .....	70
1.4.2 Methods for creating regular domain structures. ....	73
1.4.3 Electron beam lithography .....	74
1.5 Optical waveguides .....	76
1.5.1 Basic concepts .....	76
1.5.2 Types of waveguides .....	79
1.5.3 Method for creating waveguides by proton exchange. ....	80
1.6 Brief conclusions.....	83
2 Studied samples, experimental setups, and methods. ....	84
2.1 Studied samples.....	84
2.2 Experimental methods.....	85
2.2.1 Study of the evolution of the domain structure during polarization reversal in a uniform electric field.....	85
2.2.2 Local switching .....	86
2.2 Measuring the dependence of H <sup>+</sup> concentration on depth. ....	86
2.3 Visualization of the domain structure .....	87
2.4 Brief conclusions.....	88
3 Evolution of the domain structure in SPE CLN when switching in a uniform field.	
.....	89

3.1 Anomalous kinetics of stripe domains .....	89
3.2 Quasi-periodic domain structures .....	96
3.3 Change in the evolution of the domain structure because of the long holding of the SPE CLN.....	97
3.4 Dependence of the threshold fields for the growth of stripe domains and the spatial distribution of the composition on the duration of the proton exchange	99
3.5 Computer simulation of proton exchange in lithium niobate .....	101
3.5 Brief conclusions.....	103
<b>4 Local switching and creation of regular structures in SPE CLN .....</b>	<b>105</b>
4.1 Local point switching.....	105
4.2 Line scan switching .....	107
4.3 Creation of regular domain structures.....	109
4.5 Brief conclusions.....	110
<b>5 Second harmonic generation in MgOCLN with PDS created by scanning with a focused electron beam.....</b>	<b>112</b>
5.2 Measurement of second harmonic generation .....	113
5.2 Features of second harmonic generation.....	113
5.3 Brief conclusions.....	115
<b>Conclusion.....</b>	<b>117</b>
<b>List of author's publications on the theme of the thesis .....</b>	<b>119</b>
<b>CITED LITERATURE .....</b>	<b>123</b>

# CARACTÉRISTIQUES GÉNÉRALES DE LA THÈSE

## **La pertinence du sujet de recherche et la mesure de l'élaboration du sujet**

Les cristaux ferroélectriques sont largement utilisés en acoustique [1], en microélectronique [2] et en optique [3]. Ces dernières années, on constate un développement rapide de l'ingénierie des domaines [4], une discipline qui étudie les méthodes permettant de créer une structure de domaines (domain structure, DS) d'une géométrie donnée dans les cristaux ferroélectriques pour des applications pratiques.

Le niobate de lithium ( $\text{LiNbO}_3$ ) est l'un des cristaux ferroélectriques les plus utilisés. Une technologie de croissance du cristal bien développée utilisant la méthode Czochralski produit des cristaux de composition congruente (CLN) de niobate de lithium de haute qualité et de grande taille. Le CLN possède des coefficients piézoélectriques et optiques non linéaires élevés [5] et une haute température de transition de phase, ce qui permet de l'utiliser pour la fabrication de divers dispositifs acousto-optiques, d'optique non linéaire et d'optique intégrée [6].

Dans le cadre des applications de télécommunication et d'optique intégrée, des guides d'ondes optiques sont créés dans les CLN. L'une des méthodes les plus répandues pour créer des guides d'ondes optiques dans les CLN est l'échange protonique (proton exchange, PE) [7]. Dans ce cas, la modification de l'indice de réfraction dans la couche superficielle de la plaque de CLN est due au remplacement partiel des ions lithium par des protons. La source de protons utilisée est généralement l'acide benzoïque. Pour réaliser l'échange protonique doux (soft proton exchange, SPE) du benzoate de lithium est ajouté à l'acide benzoïque, ce qui ralentit le processus d'échange et conduit à la création d'un guide d'ondes avec un gradient de composition [8].

La création de structures de domaine régulières (Regular Domain Structures - RDS) dans les monocristaux CLN permet par l'effet de quasi-accord de phase [9] de réaliser la génération de seconde harmonique (SHG) et la génération de lumière paramétrique avec une efficacité record. La méthode la plus courante pour créer des

RDS est d'appliquer un champ électrique externe à l'aide d'un système **d'**electrodes lamellaires créées par photolithographie. De nouvelles méthodes de création de RDS sont développées récemment en utilisant la commutation de polarisation locale par balayage avec un faisceau focalisé d'électrons ou d'ions, ainsi qu'en appliquant le champ avec une sonde conductrice d'un microscope de sonde à balayage. Il est à noter l'importance pratique de la création de guides d'ondes optiques avec une structure de domaine régulière pour la conversion de la longueur d'onde du rayonnement, ce qui nécessite l'étude de la cinétique de la structure de domaines dans les cristaux de PE CLN. Il faut noter que la faible conductivité de la couche superficielle de PE CLN modifiée [10] rend difficile l'écrantage du champ dépolarisant pendant la commutation de la polarisation. L'évolution de la structure de domaines est dans ce cas un processus fortement déséquilibré, qui est considéré comme un analogue de la transition de phase du premier type. La réalisation de guides d'ondes optiques par la méthode de PE entraîne l'apparition d'un gradient de composition dans la couche superficielle, ce qui crée un champ électrique "incorporé" ayant une influence significative sur la cinétique de la structure de domaine. En outre, la couche superficielle est un vide diélectrique artificiel, ce qui réduit l'efficacité de l'écrantage externe et entraîne un retard dans l'écrantage du champ dépolarisant. Une tâche fondamentale de la physique des ferroélectriques consiste à étudier l'évolution de la structure de domaine au cours de la commutation de polarisation dans des conditions d'écrantage incomplet du champ dépolarisant et en présence d'un gradient de composition.

**Buts de la recherche:** (1) étude de l'évolution de la structure de domaine dans les monocristaux CLN modifiés par la méthode d'échange protonique doux lors de la commutation de la polarisation dans le champ électrique homogène et dans le champ créé par un microscope sonde à balayage, (2) analyse de la génération de seconde harmonique dans les monocristaux CLN dopés au magnésium avec une structure de domaine régulière créée au moyen d'un balayage par faisceau d'électrons.

Pour atteindre ces buts, les **principaux objectifs** suivants ont été formulés:

1. Étudier les particularités de la croissance anormale des domaines lamellaires sur la surface polaire pendant la commutation de polarisation dans les monocristaux de niobate de lithium modifiés par échange protonique doux.
2. Étudier l'influence des paramètres d'échange protonique sur la distribution spatiale de la composition, la cinétique de la structure de domaine et les champs de seuil dans les monocristaux de niobate de lithium modifiés.
3. Élaborer des méthodes de structures de domaine quasi-périodiques et régulières dans les monocristaux de niobate de lithium modifiés.
4. Étudier les particularités de la génération de seconde harmonique dans les monocristaux de niobate de lithium dopés au magnésium avec une structure de domaine régulière créée au moyen d'un balayage par faisceau d'électrons focalisés.

### **Les objets de l'étude.**

Plaques de CLN de 0,5 mm d'épaisseur, coupées perpendiculairement à l'axe polaire et polies jusqu'à une qualité optique. Les plaques ont été soumises à un échange protonique doux de 12 à 72 heures à 300°C dans l'acide benzoïque avec l'ajout de 3,0% de benzoate de lithium.

Plaques de CLN dopé au Mg congruent avec une structure de domaine régulière créée par irradiation par faisceau d'électrons focalisés d'une surface polaire Z- recouverte d'une couche de photorésist.

### **Nouveautés scientifiques de la thèse :**

1. Il a été étudié pour la première fois l'effet de la formation et de la croissance anisotrope des domaines lamellaires sur la surface polaire d'un ferroélectrique uniaxial avec une couche superficielle modifiée dans un champ électrique homogène.
2. Il a été étudié pour la première fois l'effet de la diminution anormale des champs de seuil de formation et de croissance des domaines lamellaires sur la surface polaire d'un ferroélectrique uniaxial avec une couche superficielle modifiée causée par la présence d'un gradient de composition.

3. Il a été démontré pour la première fois que des structures de domaine lamellaire quasi-périodiques se développent à partir d'une paroi de domaine planaire dans des monocristaux modifiés d'un ferroélectrique uniaxial.

### **Importance théorique de la recherche effectuée.**

1. Il est démontré qu'il est nécessaire de considérer l'effet du gradient de composition sur les champs de seuil de formation et de croissance des domaines dans les cristaux dont la composition est spatialement hétérogène.
2. Il est montré que la formation de la structure des domaines lamellaires dans les ferroélectriques uniaxiaux lors de la commutation dans un champ croissant peut être décrite dans le cadre d'un modèle de Kolmogorov-Avrami modifié.

### **Importance pratique de la recherche effectuée.**

1. La croissance anisotrope des domaines lamellaires étudiée offre des possibilités de fabrication de structures de domaine régulières dans des guides d'ondes produits dans des monocristaux de niobate de lithium par échange protonique doux.
2. Les réductions significatives contrôlées des champs de seuil avec l'augmentation de la durée de l'échange protonique sont d'un intérêt considérable pour le développement de techniques d'ingénierie des domaines dans l'optique intégrée.
3. Un intérêt considérable pour la production de rayonnements UV est la génération de rayonnements d'une longueur d'onde de 374 nm par la génération de second harmonique dans des monocristaux de niobate de lithium avec une structure de domaine régulière d'une période de 2 microns, créée par balayage d'un faisceau d'électrons focalisé.

### **Méthodologie et méthodes de recherche.**

Des études expérimentales systématiques de la structure de domaine ont été réalisées à l'aide d'équipements analytiques modernes de haute précision. La visualisation *in situ* de l'évolution de DS a été réalisée à l'aide de la microscopie optique avec une caméra à grande vitesse. La distribution spatiale des ions H<sup>+</sup> dans

les plaques étudiées a été mesurée à l'aide de la microscopie confocale Raman (CRM). La visualisation non destructive de DS sur la surface a été réalisée par microscopie à force piézoélectrique à balayage (PFM). La visualisation des domaines en volume a été réalisée à l'aide de CRM et de la microscopie à génération de seconde harmonique (SHG). La commutation de polarisation locale à l'aide d'un microscope sonde à balayage a été utilisée pour créer des domaines isolés et des structures de domaine.

**La fiabilité des résultats obtenus** est assurée par l'utilisation d'instruments de mesure vérifiés et étalonnés, de procédures de mesure certifiées, de statistiques d'expériences fiables, de l'application de méthodes modernes et indépendantes de traitement des données expérimentales, de l'accord avec les résultats d'autres auteurs et de la cohérence avec les modèles physiques connus. La crédibilité des calculs est confirmée par la validité des hypothèses, ainsi que par la cohérence avec les résultats expérimentaux.

#### **Eléments pour la défense:**

1. La croissance anormale de domaines lamellaires sur la surface polaire pendant la commutation de polarisation dans les monocristaux de niobate de lithium modifiés par échange protonique doux est due à un écrantage inefficace du champ dépolarisant causé par la présence d'une lacune diélectrique.
2. La diminution anormale du champ de seuil de nucléation et de croissance des domaines lamellaires à la suite d'un échange protonique doux est due à la formation d'un champ interne de cohérence proportionnel au gradient de composition dans la couche superficielle.
3. La formation de structures de domaine quasi-périodiques dans la croissance de domaines lamellaires à partir d'une paroi de domaine planaire est due à l'interaction électrostatique des domaines lamellaires avec des parois de domaine chargées.
4. La création d'une structure de domaine régulière stable avec une période de 500 nm lors d'une commutation de polarisation locale par microscope sonde

à balayage à température élevée est due à une augmentation de l'efficacité de l'écrantage et à une réduction des champs de seuil.

5. La génération d'un rayonnement de second harmonique à 374 nm dans un niobate de lithium dopé au magnésium avec une structure de domaine régulière par un faisceau d'électrons focalisé et avec une efficacité normalisée de 0,4%/(W·cm) est due à la bonne reproductibilité de la période de la structure.

### **Valorisation des résultats.**

Les principaux résultats de la recherche ont été présentés lors de 5 conférences et symposiums russes et internationaux: 1) Conférence internationale *Research of ferroelectric materials by Russian scientists. Centenary of the discovery of ferroelectricity (SE-100)* (Ekaterinbourg, 2020), 2) XXIIe conférence russe sur la physique féroélectrique (*All-Russian Conference on Ferroelectric Physics – XXII*) (Ekaterinbourg, 2021), 3) Conférence internationale *Modern Nanotechnologies (IWMN-2022)* (Ekaterinbourg, 2022), 4) Conférence scientifique russe avec participation internationale *YENISEI PHOTONICS 2022* (Krasnoyarsk, 2022), 5) Conférence internationale *International Symposium on Applications of Ferroelectrics (ISAF-PFM-ECAPD-2022)* (Tours, France, 2022) 6 Conférence internationale *Materials Science and Nanotechnology (MNC-2023)* (Ekaterinbourg, 2023)

### **Publications et apports personnels de l'auteur.**

Les principaux résultats ont été publiés dans 9 articles, dont 3 articles dans des revues scientifiques validées par des pairs incluses dans les bases de données internationales de citations Scopus et WoS, dans 6 résumés de conférences internationales et russes et dans un programme informatique. La thèse a été réalisée à l'aide de l'équipement de UCSU (Ural Center for Shared Use) Modern Nanotechnologies de l'Institut des sciences naturelles et des mathématiques de l'UrFU dans le cadre d'une recherche soutenue par la RFBR (Russian Foundation for Basic Research) (subvention 20-32-90192 doctorants).

Les principaux résultats ont été obtenus personnellement par l'auteur ou avec sa participation active. Le choix de l'orientation de la recherche, la discussion des résultats et la formulation des tâches ont été effectués conjointement avec le directeur de recherche, le docteur ès sciences physico-mathématiques, le professeur V.Y. Shur, le directeur de recherche Ph.D., le professeur P. Baldi et le candidat ès sciences physico-mathématiques, le CR (chargé de recherche) A.R. Akhmatkhanov. La fabrication des échantillons, la commutation de la polarisation dans un champ homogène, la visualisation des DS par microscopie optique et méthodes CRM, l'étude des paramètres des DS, l'analyse et le traitement des résultats ont été réalisés par l'auteur lui-même. La commutation locale de la polarisation et la visualisation des DS par la méthode PFM ont été réalisées conjointement avec le candidat ès sciences physico-mathématiques, l'AR (attaché de recherche) B.N. Slautine, l'AR L.V. Guimadeeva et l'AR A.S. Abramov. La visualisation des DS par la méthode SHG a été réalisée conjointement avec le chercheur M.S. Nebogatikov et la candidate ès sciences physico-mathématiques, l'AR A.S. Slautina.

### **Structure et portée de la thèse.**

Le travail de thèse se compose d'une introduction, de cinq chapitres, d'une conclusion, d'une liste d'abréviations et de conventions et d'une liste de littérature. Le volume total de travail est de 138 pages, dont 65 dessins, 1 tableau et une liste de références.

### **Contenu principal du travail**

**L'introduction** justifie la pertinence du sujet du travail scientifique et de qualification et la mesure de son élaboration, formule le but et les objectifs principaux du travail, énonce les éléments à défendre, identifie les objets de la recherche, montre la nouveauté scientifique des résultats, l'importance théorique et pratique de la recherche, décrit la méthodologie et les méthodes de recherche. Les informations sur la fiabilité et la valorisation des résultats, des publications et de la contribution personnelle de l'auteur sont présentées.

**Le premier chapitre** présente un aperçu général. Il présente un examen des concepts actuels de formation et d'évolution de DS dans un champ électrique externe, en tenant compte des processus d'écrantage. Les principales propriétés physiques et caractéristiques de DS du ferroélectrique uniaxial CLN étudié sont décrites. Les principales méthodes de création de guides d'ondes planaires et de canaux dans les monocristaux de CLN sont présentées. Les caractéristiques des différentes méthodes d'échange protonique sont discutées. Les méthodes modernes de visualisation de DS à la surface et en volume des ferroélectriques sont examinées. Les résultats de la création de DS régulières et de la génération de seconde harmonique dans les structures de guides d'ondes sont présentés.

**Le deuxième chapitre** est méthodologique et contient les paramètres des échantillons, une description du dispositif expérimental et les méthodes utilisées.

L'échange protonique a été réalisé à 300°C dans l'acide benzoïque avec l'ajout de benzoate de lithium. Pour l'échange, l'échantillon a été fixé dans la partie supérieure du récipient en zirconium (Figure 1a). Pour réduire les effets de l'eau adsorbée, le récipient d'échantillons a été recuit sous vide à 110°C. Les manipulations ultérieures du récipient ont été effectuées dans une atmosphère sèche. Une source de protons a été placée au fond du récipient (Figure 1a) qui est ensuite fermé et mis sous vide à  $10^{-3}$  mbar.

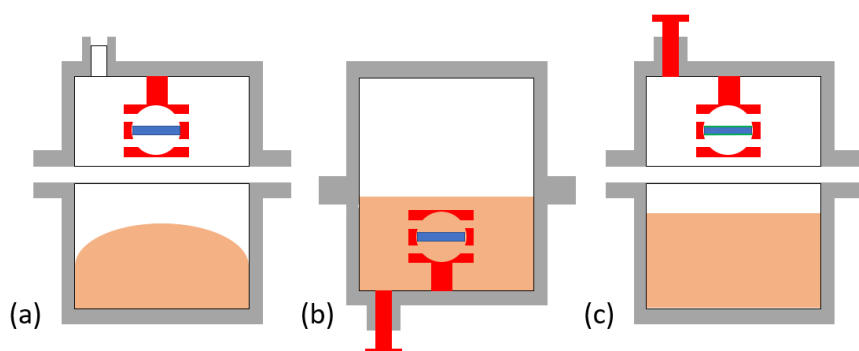


Figure 1. Étapes de l'échange protonique. (a) – assemblage de la cellule, (b) – échange protonique, (c) – achèvement de l'échange protonique.

Le récipient chauffé à 300°C a alors été retourné (Figure 1b) et l'échantillon a ainsi été immergé dans la source de protons. Une fois l'échange terminé, le récipient

a été de nouveau retourné et refroidi à la température ambiante (Figure 1c). Les taux de changement de température n'ont pas dépassé 5°C/min.

Le PE a entraîné la formation de  $H_xLi_{1-x}NbO_3$  dans la couche superficielle, répartie de manière inhomogène en profondeur. Le profil de distribution de la concentration de  $H^+$  ( $C(z)$ ) dans l'échantillon a été mesuré par la méthode CRM avec une résolution submicronique à l'aide d'un microscope confocal Raman Alpha 300 AR, WiTec (Allemagne). Il a été démontré précédemment [11] que l'intensité intégrale de la raie Raman près de  $3492\text{ cm}^{-1}$  causée par les vibrations du groupe OH- est proportionnelle à la concentration de  $H^+$ .

Les paramètres de la raie spectrale Raman  $3492\text{ cm}^{-1}$  ont été mesurés [11] (Figure 2a). L'intensité maximale de la raie a été déterminée par approximation des mesures avec une fonction de Lorenz (Figure 4b).

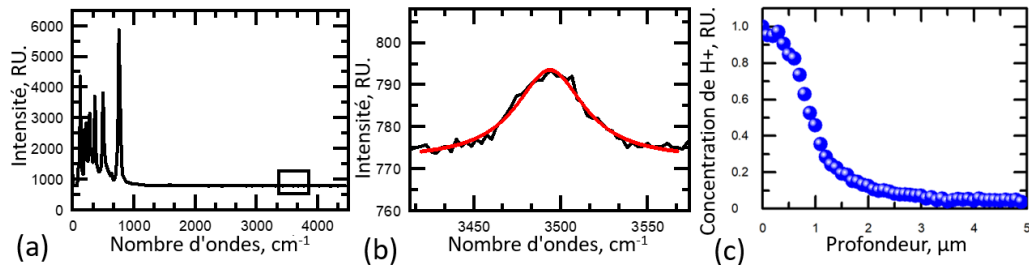


Figure 2. (a) - Spectre de diffusion Raman de SPE CLN. (b) - Raie spectrale  $3492\text{ cm}^{-1}$  approximée par la fonction de Lorenz. (c) - Dépendance envers la profondeur de la concentration relative d'ions  $H^+$ .

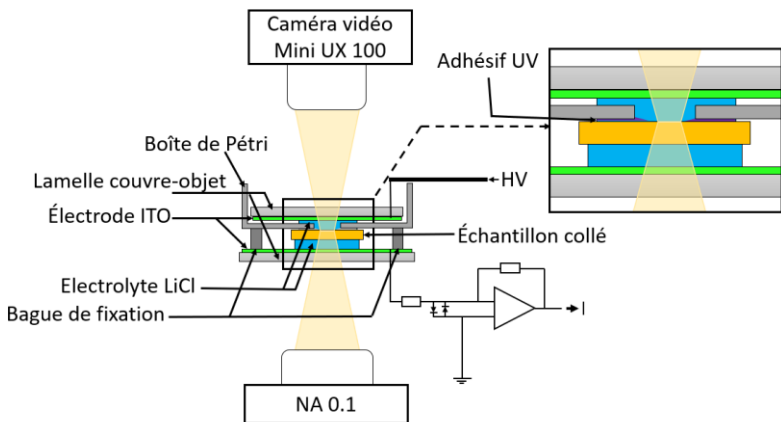


Figure 3. Schéma d'installation de commutation de polarisation de champ homogène avec visualisation in situ de la cinétique de la structure de domaines.

Pour obtenir une commutation de polarisation dans un champ homogène, les échantillons ont été placés dans une cellule avec une électrode ITO transparente et une électrode liquide basée sur une solution saturée de LiCl (Figure 3). La commutation a été réalisée (Figure 4a) par des impulsions rectangulaires (en champ constant) d'une durée allant jusqu'à 300 s et d'une amplitude de 0,1 à 25 kV/mm, et par des impulsions triangulaires (en champ croissant) (Figure 4b) avec une vitesse de croissance du champ de 200 V/(mm·s). Les impulsions ont été générées par une carte ADC/DAC PCI-6251 (National Instruments, USA) ou un générateur de signaux AFG1022 (Tektronix, USA) et amplifiées avec un amplificateur haute tension Trek 20/20C (Trek inc., USA). La commutation du champ croissant a été utilisée pour déterminer les champs de seuil de la croissance des domaines lamellaires et de la formation des domaines hexagonaux.

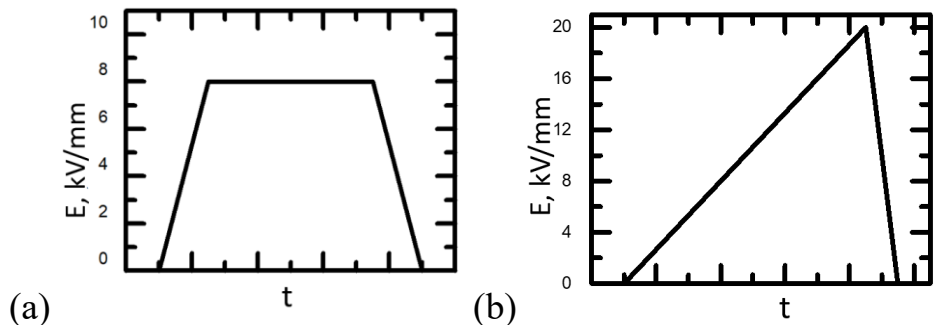


Figure 4. Forme de l'impulsion: (a) – champ constant, (b) – champ croissant.

La visualisation *in situ* de la structure de domaines a été réalisée à l'aide d'un microscope optique LMA10 (Carl Zeiss, Allemagne) équipé d'une caméra vidéo à grande vitesse Fastcam Mini UX100 (Photron, Japon), synchronisée avec les impulsions du champ.

La structure de domaines statiques a été visualisée sur la surface et en volume. Sur la surface - à l'aide de PFM Ntegra Aura (NT-MDT, Russie) et du microscope optique BX-61 (Olympus, Japon). En volume - à l'aide de la méthode CRM avec une résolution allant jusqu'à 300 nm. La distribution spatiale des décalages des raies  $581 \text{ cm}^{-1}$  E(TO8) et  $872 \text{ cm}^{-1}$  A1(LO4) dans les spectres Raman a été mesurée. La

microscopie à SHG a été réalisé à l'aide d'une installation basée sur le Ntegra Spectra (NT-MDT, Russie) avec une résolution d'environ 1  $\mu\text{m}$ .

La création de domaines isolés et de structures de domaines par la méthode de commutation locale, ainsi que leur visualisation sur la surface par la méthode PFM ont été réalisées à l'aide de microscopes sonde à balayage (SPM) MFP-3D (Oxford Instruments, USA) et Ntegra Aura (NT-MDT, Russie). Des sondes en silicium avec des revêtements conducteurs NSC 01 (Mikromash, Estonie) et HA\_NC/W2C (ScanSens, Allemagne) ont été utilisées.

La RDS a été créée en irradiant une surface polaire Z avec un faisceau d'électrons focalisés. La surface irradiée a été recouverte d'une couche photorésist AZ nLOF 2020 (MicroCHemicals, Allemagne) de 2  $\mu\text{m}$  d'épaisseur par la méthode de centrifugation. Sur la surface polaire opposée (Z+), une électrode de cuivre de 100 nm d'épaisseur a été appliquée par pulvérisation magnétron. La période de RDS créée était de 2  $\mu\text{m}$  avec une surface de  $1,5 \times 0,5 \text{ mm}^2$ . Un microscope électronique à balayage Auriga Crossbeam Workstation (Carl Zeiss, Allemagne) avec un système de lithographie par faisceau d'électrons Elphy Multibeam (Raith GmbH, Allemagne) a été utilisé. La tension d'accélération était de 8 kV, le courant de faisceau de 1,29 nA, la vitesse de balayage de 0,52 mm/s et la dose de 2,5  $\mu\text{L}/\text{cm}^2$ .

La SHG a été étudiée à l'aide d'un laser Ti:Sapphire MBR-110 (Coherent, USA) générant une émission de pompage de 100 mW à polarisation linéaire et focalisé par une lentille d'une longueur focale de 30 mm. Le diamètre de l'étranglement de faisceau était de 30  $\mu\text{m}$ .

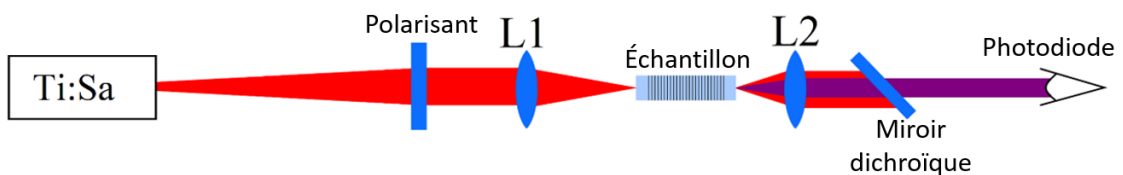


Figure 5. Schéma du dispositif expérimental pour l'étude de la génération de seconde harmonique dans les cristaux avec RDS.

La puissance du signal de SHG extrait avec un filtre à bande unique BrightLine 375/110 nm (Semrock, USA) a été mesurée avec une photodiode S130VC (Thorlabs, USA).

**Le troisième chapitre** est consacré à l'étude des particularités de la formation et de la croissance des domaines lamellaires en SPE CLN pendant la commutation dans un champ électrique homogène.

### ***SPE CLN évolution de la structure de domaine***

On a étudié la cinétique de la structure de domaine pendant la commutation de polarisation dans un champ uniforme dans des plaques dans lesquelles un échange protonique doux de 12 à 48 heures à 300°C et une concentration de benzoate de lithium de 3,0 % a été effectué. Les études ont été réalisées avec une commutation dans un champ croissant et constant deux mois après la fin du processus d'échange.

Dans tous les échantillons de SPE CLN étudiés, la cinétique de la structure des domaines a commencé dans des champs nettement plus petits que dans les CLN lors de la commutation dans le champ croissant. Une évolution anormale de la structure de domaine a été observée, représentant la formation de domaines lamellaires et leur croissance dans les trois directions (Figure 6). La croissance du domaine lamellaire s'est arrêtée à l'approche d'un domaine lamellaire croissant dans l'autre direction. La commutation longue a entraîné la formation d'une structure maillée de domaines lamellaires avec une période effective d'environ 10  $\mu\text{m}$ . Il convient de noter que la formation et la croissance anisotrope de domaines lamellaires d'une largeur submicronique ont été observées précédemment pour une structure de domaines formée au moyen du chauffage du CLN par un rayonnement laser IR impulsif [12].

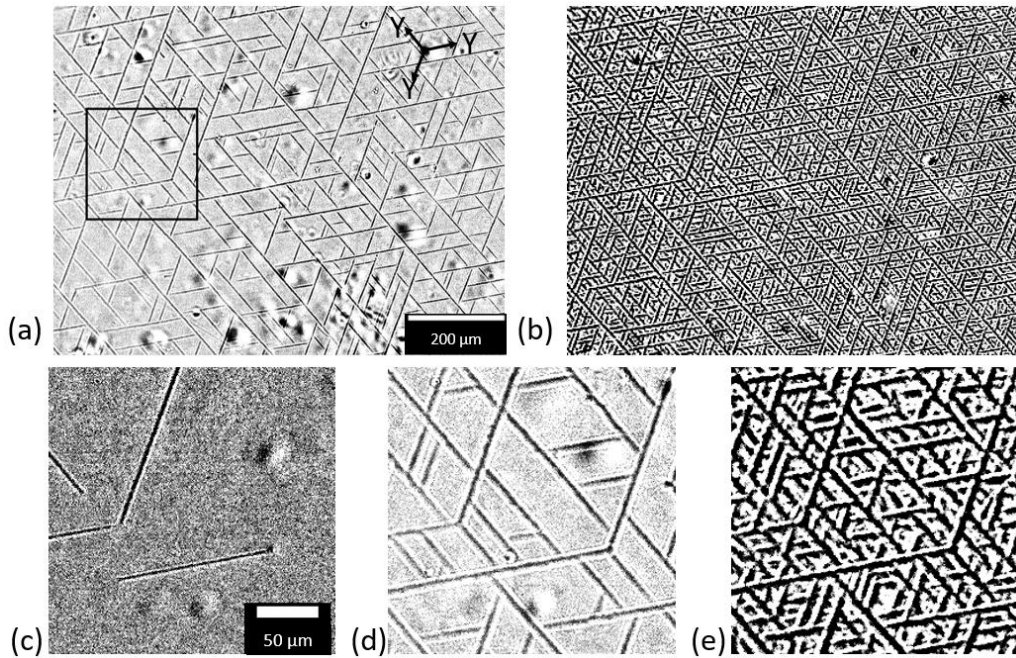


Figure 6. Images optiques instantanées de la structure de domaine pendant la commutation de polarisation dans le champ croissant à des moments du début de la commutation: (a) - 37 s ( $E = 8 \text{ kV/mm}$ ), (b) - 95 s ( $E = 19 \text{ kV/mm}$ ). Le fragment d'image agrandi mis en évidence en (a), à des moments: (c) - 22 s ( $E = 4,5 \text{ kV/mm}$ ), (d) - 37 s ( $E = 8 \text{ kV/mm}$ ), (e) - 95 s ( $E = 19 \text{ kV/mm}$ ). Vitesse de montée du champ est de  $0,2 \text{ kV}/(\text{mm-s})$ . Durée de l'échange protonique de 48 heures, à  $300^\circ\text{C}$ , fraction de benzoate de lithium de 3,0 %.

La visualisation de la structure de domaine statique par CRM a révélé une largeur moyenne des domaines lamellaires d'environ  $4 \mu\text{m}$  et une profondeur allant jusqu'à  $30 \mu\text{m}$  (Figure 7).

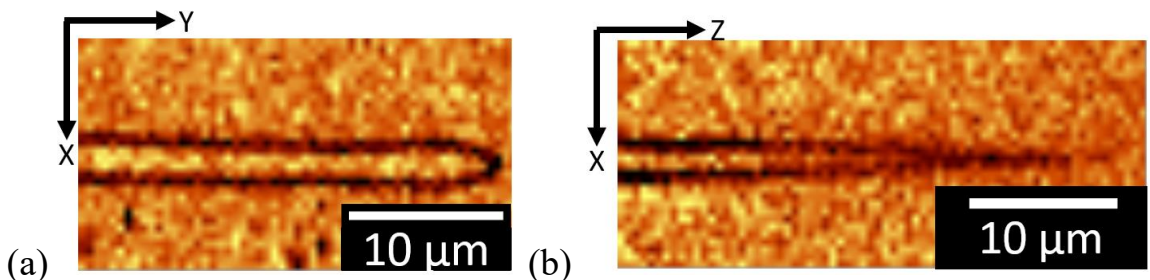


Figure 7. Images CRM du domaine lamellaire obtenu par commutation de polarisation dans un champ constant de  $5 \text{ kV/mm}$ : (a) – à la surface polaire, (b) – dans la section YZ. Durée de l'échange protonique de 48 h, à  $300^\circ\text{C}$  et avec une fraction de benzoate de lithium de 3,0%.

La visualisation des domaines lamellaires en volume par la microscopie à SHG a montré qu'ils sont en forme de peigne (Figure 8) [13]. En surface, les domaines

apparaissent comme une bande continue, mais à une profondeur de plus de 30  $\mu\text{m}$ , ils se séparent en chaînes de domaines d'environ un micron de diamètre.

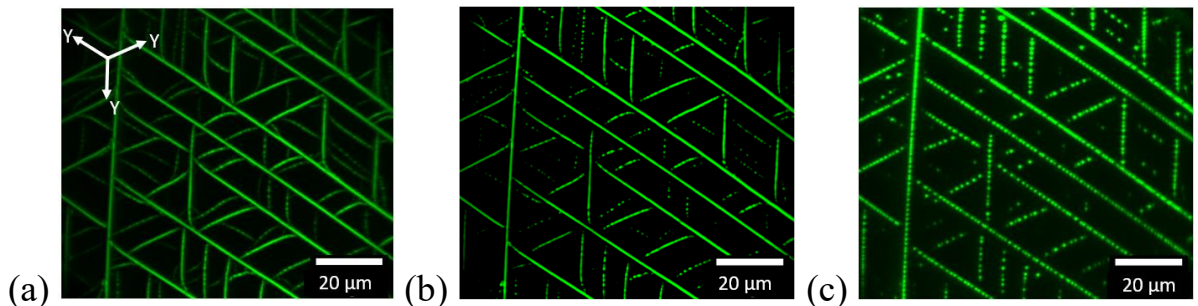


Figure 8. Images CRM de la structure de domaine après commutation partielle dans le champ croissant à différentes profondeurs de la surface du pôle Z,  $\mu\text{m}$ : (a) - 0, (b) - 8, (c) - 32. Amplitude du champ de 20 kV/mm, durée de l'impulsion de 100 s. Durée de l'échange protonique de 12 heures, à 300°C, fraction de benzoate de lithium de 3,0 %.

L'analyse statistique des orientations des domaines lamellaires a été réalisée à partir de la visualisation *in situ* de la cinétique de la structure de domaine à l'aide de l'algorithme suivant (Figure 9):

- 1) L'arrière-plan (première image de l'enregistrement vidéo) a été soustrait de toutes les images instantanées (Figure 9b).
- 2) Les images obtenues ont été binarisées à l'aide de la méthode de Lee[14].
- 3) La transformée de Fourier de l'image binarisée a été calculée (Figure 9c).
- 4) La convolution angulaire de la transformée de Fourier par rapport au centre a été effectuée (Figure 9d).

L'algorithme de traitement de l'enregistrement vidéo et de présentation des résultats a été mis en œuvre à l'aide des bibliothèques OpenCV, scipy, skimage et matplotlib.

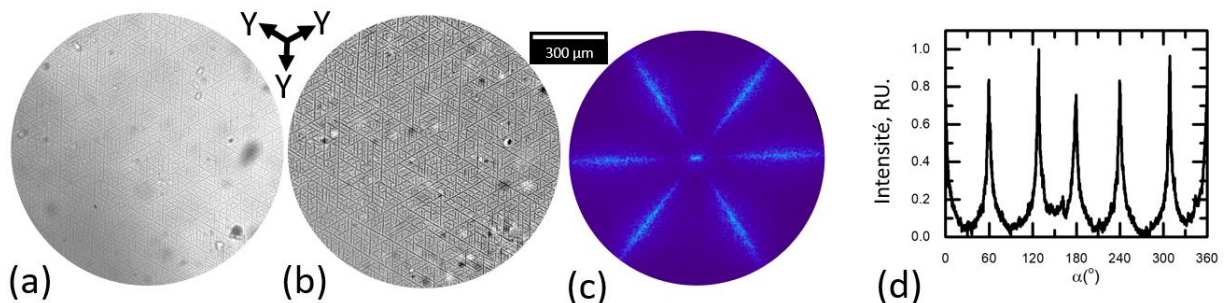


Figure 9. (a) - Image optique instantanée de la structure de domaine, (b) - Image après soustraction de l'arrière-plan, (c) - Transformée de Fourier. (d) - Convolution angulaire de la transformée de Fourier. Commutation dans un champ constant de 8 kV/mm. Durée de l'échange protonique de 48 heures, benzoate de lithium de 3,0% et à 300 °C.

L'analyse a révélé que les domaines lamellaires sont principalement orientés le long des trois directions cristallographiques Y équivalentes en termes de symétrie CLN ( $C_{3v}$ ).

La cinétique de la structure de domaines pendant la commutation dans un champ croissant est décrite quantitativement par l'analyse de la dépendance temporelle de la longueur totale des domaines lamellaires  $L$  (Figure 6a) et de la période effective moyenne de la structure de domaine  $T = A/L$ , où  $A$  est la surface analysée. Une approche de Kolmogorov-Avrami modifiée a été utilisée [15-17], qui a été appliquée pour analyser la dépendance temporelle de la surface totale des domaines [18]. Il a été tenu compte du fait qu'au stade initial, l'augmentation de  $L$  est due à la croissance des domaines lamellaires apparaissant sur les défauts de surface, ce qui correspond au modèle  $\beta$  de Kolmogorov-Avrami. Lors d'une commutation ultérieure au temps  $t_{cat}$ , l'évolution de la structure de domaine change qualitativement et la formation et la croissance de domaines lamellaires résultant du branchement est observée, ce qui correspond au modèle  $\alpha$  de Kolmogorov-Avrami (Figure 6d). Dans le cadre de l'approche modifiée de Kolmogorov-Avrami,  $t_{cat}$  est le moment de la «catastrophe géométrique» où la dimension du processus passe de la 3D à la 2D ou du modèle  $\beta$  au modèle  $\alpha$ .

La dépendance temporelle mesurée expérimentalement de la longueur totale des domaines lamellaires  $L(t)$  a été approximée par la formule (Figure 10a):

$$L(t) = \begin{cases} L_\beta(t), & t \leq t_{cat} \\ L_\alpha(t - \Delta t), & t \geq t_{cat} \end{cases} \quad (1)$$

Lors de la première étape

$$L_\beta(t) = L_{max} \left( 1 - \exp \left( - \left( \frac{t-t_{st}}{t_\beta} \right)^2 \right) \right) \quad (2)$$

où  $t_\beta = (\mu\beta R/2)^{-1/2}$ ,  $\beta$  – concentration des centres de formation des domaines lamellaires,  $\mu$  – mobilité de la paroi,  $t_{st} = E_{th}/R$  – temps de démarrage du processus de commutation,  $E_{th}$  – champ de seuil,  $R = dE/dt$  – taux de croissance du champ,  $L_{max}$  – longueur totale limite des domaines..

Lors de la deuxième étape:

$$L_\alpha(t) = L_{max} \left[ 1 - \exp \left( -a \left[ \frac{-1}{6} R(t^3 - t_{st}^3) + \frac{1}{2} E_{th}(t^2 - t_{st}^2) + \left( \frac{1}{2} R t^2 - E_{th} t \right) (t - t_{st}) \right] \right) \right] \quad (3)$$

où  $a = \alpha\mu$ ,  $\alpha$  – probabilité de branchement par unité de longueur des domaines lamellaires.

La dépendance temporelle de la période effective moyenne de la structure de domaine a été approximée par la formule (Figure 10b):

$$T(t) = \frac{A}{L(t)} \quad (4)$$

L'approximation de  $L(t)$  pour SPE CLN avec un échange protonique de 48 h aux paramètres fixes  $L_{max} = 96$  mm,  $R = 0,2$  kV/(mm·s) и  $E_{th} =$  kV/mm a donné les valeurs de paramètres suivantes:  $a = (7,1 \pm 0,5) \cdot 10^{-5}$  kV/(mm·s<sup>2</sup>),  $\Delta t = -(30 \pm 1)$  s,  $t_\beta = (25 \pm 1)$  s.

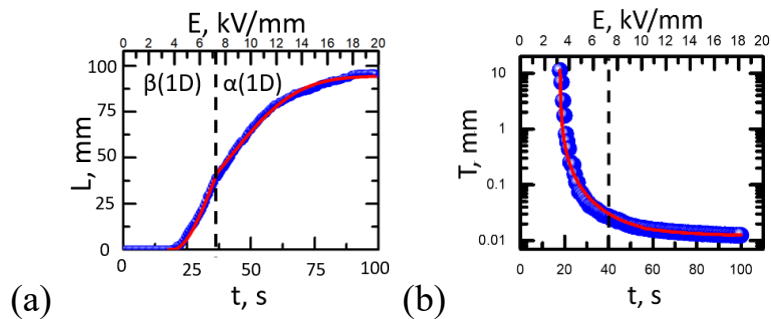


Figure 10. Dépendances temporelles: (a) - de la longueur totale des domaines lamellaires et (b) - de la période effective, approximées par les équations (1) et (4), respectivement. Durée de l'échange protonique de 48 heures, fraction de benzoate de lithium de 3,0 %, température de 300 °C.

La croissance traditionnelle de domaines hexagonaux avec des parois parallèles aux directions cristallographiques Y a été observée dans les champs supérieurs à 21,5 kV/mm, ce qui correspond au champ de seuil pour la commutation de polarisation dans CLN dans tous les échantillons examinés. La forme hexagonale a été rapidement restaurée après la fusion des domaines en raison de la croissance de parois de courte durée ultrarapides, c'est-à-dire qu'un effet de stabilité de la forme caractéristique de CLN a été observé (Figure 11) [19].

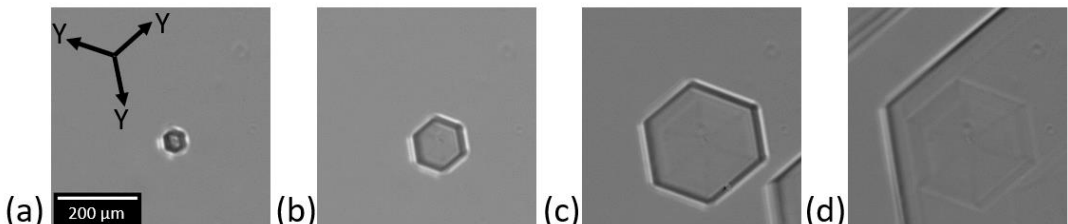


Figure 11. Croissance de domaines hexagonaux pendant la commutation de polarisation dans un champ constant de 22 kV/mm. Images optiques instantanées de la structure de domaine. Intervalles de temps à partir du début de la commutation, ms: (a) - 220, (b) - 228, (c) - 236, (d) - 244. Microscopie optique, lumière transmise. Durée de l'échange protonique de 48 heures, à une fraction de benzoate de lithium de 3,0 % et à une température de 300 °C.

### ***Structures de domaine quasi-périodiques.***

Le processus de formation d'une structure quasi-périodique des domaines lamellaires a été étudié lors du changement du mode de commutation. Dans ce cas,

le processus de commutation s'est déroulé en deux étapes. Lors de la première étape, une paroi de domaine étendue a été créée près du bord de l'électrode en commutant dans le champ de 22 kV/mm. Lors de la deuxième étape, l'échantillon a été recouvert d'une électrode solide et la commutation par une série d'impulsions rectangulaires d'une amplitude de 10 kV/mm et d'une durée de 100 ms avec un intervalle inter-impulsions de 10 s a conduit à la formation d'une structure quasi-périodique de domaines lamellaires se développant à partir de la paroi de domaine créée le long de la direction cristallographique Y (Figure 12 a,b).

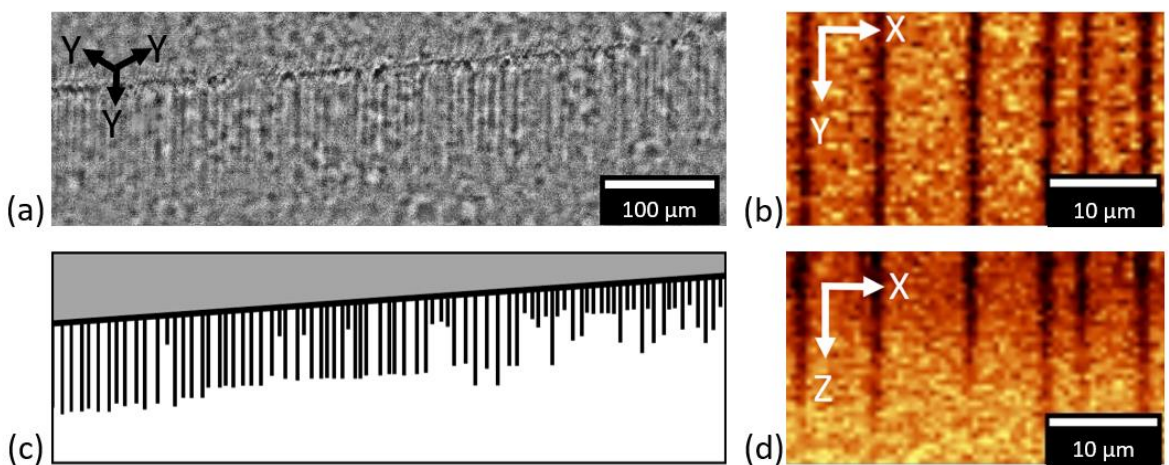


Figure 12. Structure quasi-périodique de domaines lamellaires se développant à partir d'une paroi de domaine planaire lorsque la polarisation est commutée par une série d'impulsions rectangulaires. (a) - Image optique. Images CRM: (b) - Plan XY, (d) - Plan XZ. (c) - Schéma de la structure de domaine.

Les domaines lamellaires présentaient une largeur d'environ 2  $\mu\text{m}$ , une longueur allant jusqu'à 100  $\mu\text{m}$ , une période moyenne d'environ 5  $\mu\text{m}$  (Figure 12c) et une profondeur allant jusqu'à 20  $\mu\text{m}$  (Figure 12d).

La formation d'une structure quasi-périodique constituée de domaines lamellaires parallèles dans un champ homogène est due à l'interaction électrostatique de domaines lamellaires non réticulés avec des parois de domaines chargées. L'effet résultant ouvre la possibilité de générer des RDS dans les guides d'ondes optiques SPE.

**Dépendance des champs de seuil de la croissance des domaines lamellaires et de la distribution spatiale de la composition par rapport à la durée de l'échange protonique.**

Une étude comparative de la distribution spatiale de la composition et des champs de seuil a été réalisée pour les échantillons de SPE CLN avec différentes durées d'échange protonique de 12, 24, 36 et 48 heures à la même température de 300 °C et à une concentration de benzoate de lithium de 3,0 %. Les résultats des mesures du changement de composition en fonction de la profondeur sont présentés dans la Figure 13. Les dépendances de C(z) près de la surface polaire ont été approximées par une dépendance linéaire pour déterminer la valeur du gradient de composition  $dC/dz$  près de la surface (Figure 14b). La dépendance par rapport à la durée de l'échange protonique des champs de seuil mesurés pendant la commutation dans le champ croissant est illustrée dans la Figure 15a. Il ressort que la diminution des champs de seuil par rapport au CLN non modifié augmente avec la durée de l'échange protonique. Il est connu que le gradient de composition dans le cristal peut être considéré comme une source de champ interne [20]. Il est démontré qu'avec l'augmentation de la durée de l'échange protonique, l'épaisseur de la couche de gradient diminue et le gradient augmente de manière significative (Figure 14b).

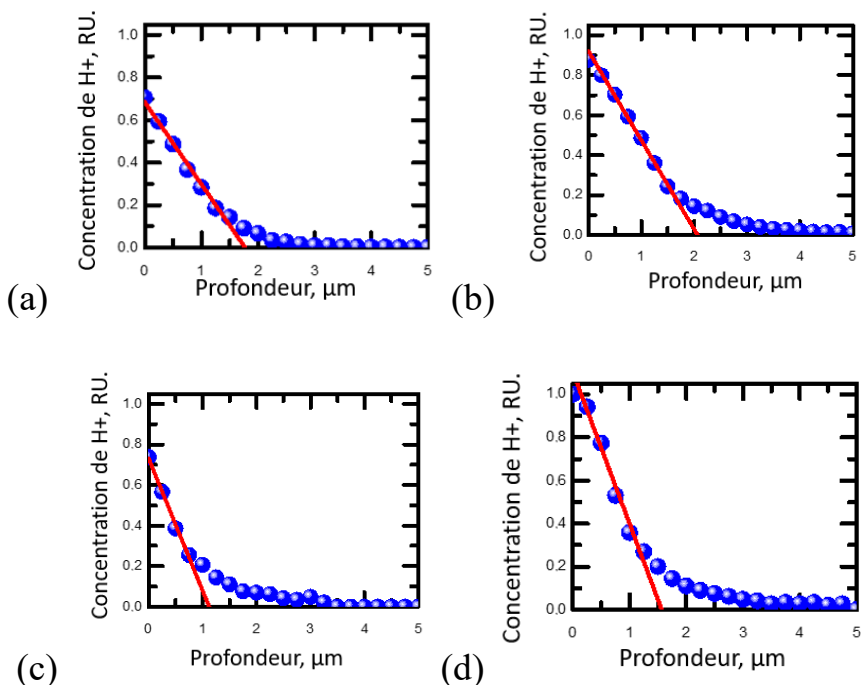


Figure 13 - Dépendance de la concentration en ions  $H^+$  en fonction de la profondeur près de la surface polaire Z pour le temps d'échange protonique : (a) - 12 h, (b) - 24 h, (c) - 36 h et (d) - 48 h à 300°C avec une proportion de benzoate de lithium de 3,0 %.

La dépendance de la magnitude du champ dans lequel la commutation est initiée par rapport à la magnitude du gradient de composition a été analysée. Il a été supposé que la commutation se produisait par la somme du champ appliqué et du champ interne de cohérence, qui était proportionnel au gradient de concentration des ions  $H^+$ .

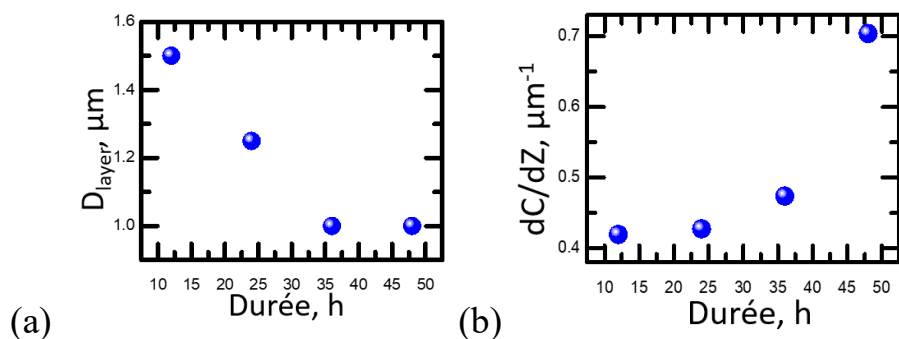


Figure 14 - Dépendances par rapport à la durée de l'échange protonique : (a) – de l'épaisseur de la couche de gradient et (b) - du gradient de la concentration relative d'ions  $H^+$ . Température de 300°C, fraction de benzoate de lithium 3,0%.

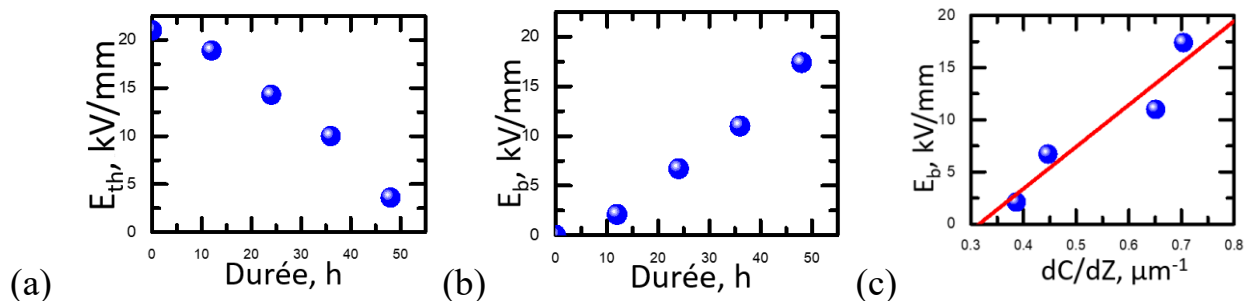


Figure 15 – Dépendances par rapport à la durée de l'échange protonique : (a) – du champ initial de commutation et (b) – du champ interne de cohérence. (c) - Dépendance du champ interne de cohérence par rapport au gradient de concentration des ions  $H^+$  dans la couche superficielle. Température de 300°C, fraction de benzoate de lithium de 3,0%.

Il est démontré (Figure 15b) que dans les conditions expérimentales, le champ interne de cohérence  $E_b$  augmente linéairement avec la durée de l'échange protonique et atteint une valeur de 17 kV/mm, ce qui conduit à une diminution du

champ de seuil à 4 kV/mm. L'hypothèse selon laquelle l'intensité du champ interne de cohérence est proportionnelle au gradient de concentration des ions H<sup>+</sup> est ainsi confirmée expérimentalement (Figure 15c).

**Le quatrième chapitre** étudie l'évolution de la structure de domaine dans les cristaux SPE CLN et la création de structures de domaine périodiques lors de la commutation locale à l'aide de la sonde SPM.

Des plaques SPE CLN d'une épaisseur de 0,5 mm, coupées perpendiculairement à l'axe polaire et polies jusqu'à une qualité optique, ont été utilisées pour commuter la polarisation. Un échange protonique doux a été effectué dans les plaques pendant 12, 24, 36, 48 et 72 heures à 300°C et à une concentration de benzoate de lithium de 3,0 %. Des commutations ponctuelles et à balayage linéaire ont été utilisées.

Pendant la commutation ponctuelle, une impulsion de tension a été appliquée à la sonde SPM, qui était en contact avec la surface de l'échantillon. Avant la fin de l'impulsion, la sonde a été retirée de la surface. L'amplitude de l'impulsion allait jusqu'à 300 V avec des durées allant de 1 ms à 100 s. Il a été procédé à l'enregistrement de chaînes de domaines isolés avec différentes distances entre les points d'application de la tension.

Il a été constaté qu'aucune commutation locale n'a été observée dans les échantillons dont la durée d'échange protonique était inférieure à 48 heures dans toute la gamme de tensions et de durées. Toutes les études ultérieures ont été réalisées sur des échantillons dont la durée d'échange protonique était de 48 et 72 heures.

Les dépendances du diamètre effectif des domaines ponctuels par rapport à la durée et à l'amplitude de l'impulsion de tension ont été analysées (Figure 16a). La dépendance obtenue du diamètre par rapport à la tension appliquée a été approximée par l'équation [21]:

$$r(U_{tip}) = \sqrt{a(\frac{U_{tip}}{E_{th}})^{2/3} - R_{tip}^2} \quad (5)$$

où  $a = \sqrt[3]{\frac{CR_{tip}}{2\pi\varepsilon_0(1+\varepsilon)}}$ ,  $U_{tip}$  – tension appliquée,  $R_{tip}$  – rayon de courbure de la sonde,  $E_{th}$  – champ de seuil,  $C$  – capacité de la sonde,  $\varepsilon_0$  – constante diélectrique du vide,  $\varepsilon$  – constante diélectrique de l'échantillon.

La tension de seuil résultante pour une durée d'impulsion d'une seconde est d'environ 50 V.

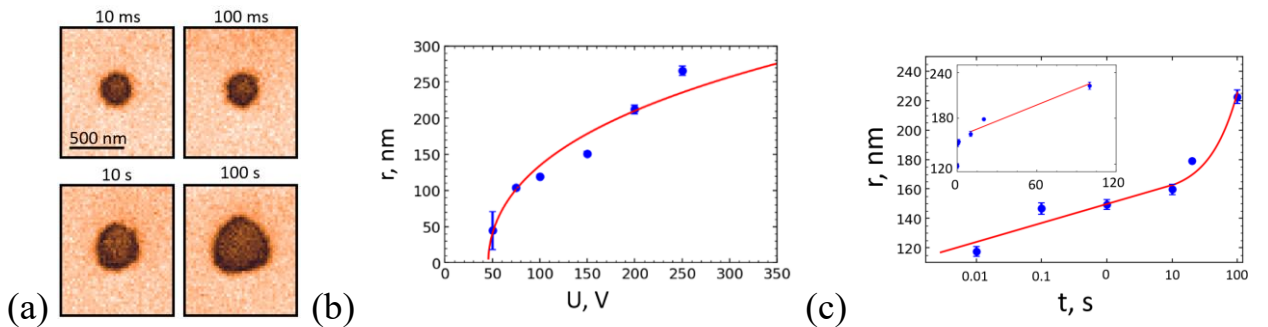


Figure 16. (a) Images PFM de domaines isolés obtenus par commutation ponctuelle à une tension de 200 V et différentes durées d'impulsion. Dépendances du rayon effectif des domaines: (b) - par rapport à la tension appliquée à une durée d'impulsion de 1 s, (c) - par rapport à la durée d'impulsion à une tension de 200 V. Durée de l'échange protonique de 72 heures, température de 300°C, fraction de benzoate de lithium de 3,0 %.

La dépendance logarithmique du diamètre du domaine par rapport à la durée de l'impulsion a été observée pour les domaines circulaires avec des durées d'impulsion inférieures à 10 s, comme c'est traditionnellement le cas pour la commutation locale dans les ferroélectriques uniaxiaux (Figure 16b). La dépendance du diamètre des domaines est devenue linéaire pour des durées d'impulsion supérieures à 10 s (Figure 16c dans l'encadré). La caractéristique observée peut être attribuée à la transition de la nucléation stochastique à la nucléation déterministe [22].

La dépendance de la période de la taille des domaines ponctuels dans le circuit a été étudiée. Il a été démontré que la forme circulaire des domaines était déformée

à des distances entre les centres d'application de la tension inférieures à 500 nm et que le diamètre des domaines diminuait avec la période (Figure 17a). La diminution de la taille est due à deux effets: (1) une diminution du champ de commutation du domaine en raison de la contribution du champ dépolarisant créé par le domaine précédent dans la chaîne, (2) une commutation inversée partielle du domaine commuté par le champ dépolarisant du domaine créé. Le premier effet est une réduction de la taille des domaines de la chaîne par rapport au premier domaine, et le second est une distorsion de la forme circulaire des domaines (Figure 17b). Lorsque la période est inférieure à 300 nm, les domaines fusionnent pour former un domaine lamellaire, d'environ 150 nm de large, qui est indépendant de la période (Figure 17c).

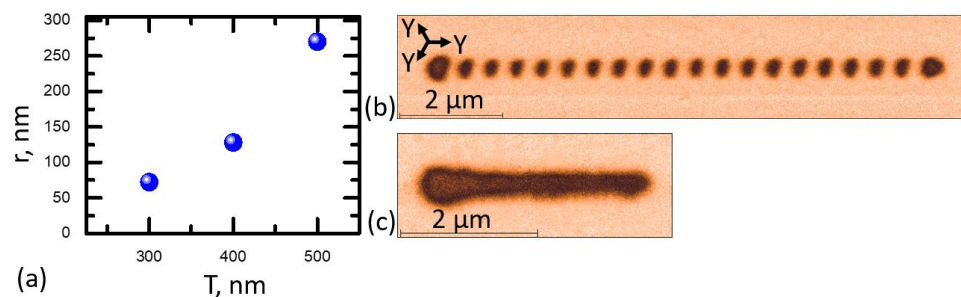


Figure 17. (a) - Dépendance du diamètre effectif du domaine par rapport à la période entre les domaines, PFM, chaînes de domaines ponctuels avec différentes périodes, nm: (b) - 500, (c) - 150. Durée de l'échange protonique de 72 heures, température de 300°C, fraction de benzoate de lithium de 3,0 %.

Les domaines lamellaires ont été créés par balayage le long de la direction cristallographique Y (Figure 18b-c). De plus, les domaines lamellaires ont été formés à des tensions supérieures à 150V (Figure 18b-d).

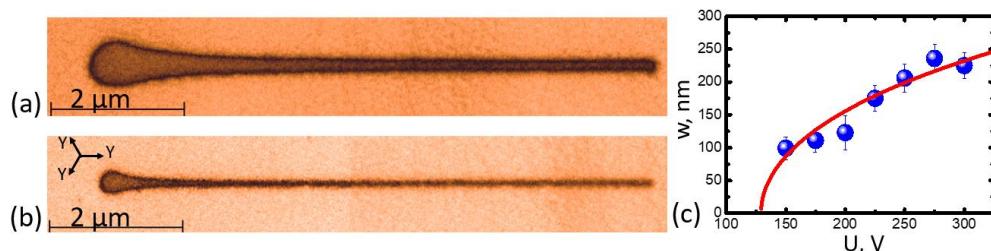


Figure 18 Images PFM de domaines lamellaires obtenus par commutation de balayage à différentes tensions, V: (a) - 150, (b). - 270. (c) Dépendance de la largeur du domaine lamellaire

par rapport à la tension. Vitesse de balayage de 1  $\mu\text{m/s}$ . Durée de l'échange protonique de 72 heures, température de 300°C, fraction de benzoate de lithium de 3,0%.

La dépendance de la largeur en régime permanent du domaine lamellaire par rapport à la tension a été analysée. La dépendance obtenue a été approximée par l'équation (5). La valeur de seuil était de 130 V et la largeur maximale atteignait 250 nm. Il a été constaté l'absence de changement notable dans la taille de la structure du domaine lamellaire créé, en dépit d'une visualisation répétée pendant une heure.

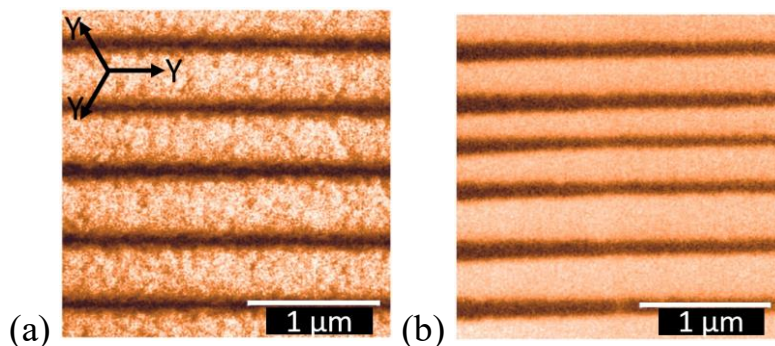


Figure 19. Images PFM de structures de domaine régulières créées par commutation de balayage, période de 500 nm. Durée de l'échange protonique (a) - 48 h, (b) - 72 h, à 300°C avec une fraction de benzoate de lithium de 3,0%.

Chaque domaine lamellaire a été balayé deux fois, de gauche à droite et de droite à gauche, pour créer des RDS. Il n'a pas été possible, à température ambiante, d'obtenir des RDS d'une période submicronique, en raison de l'interaction des domaines étudiés précédemment dans le cadre de la commutation ponctuelle. Pour réduire l'interaction, la commutation a été effectuée à des températures élevées, ce qui a accéléré le écrantage volumique et réduit le champ de seuil. Une RDS stable avec une période de 500 nm est obtenue par un balayage de 200 V à 85°C (Figure 19).

**Le cinquième chapitre** est consacré à l'étude de la génération de seconde harmonique dans les échantillons de MgOCLN avec une RDS générée par balayage par faisceau d'électrons focalisés.

Les images optiques de la structure de domaine créée sur les deux surfaces polaires sont présentées dans la Figure 20. On constate que la structure n'est pas réticulée.

La mesure de la dépendance de la puissance SHG par rapport à la longueur d'onde de pompage (Figure 21a) a montré que l'efficacité de conversion maximale est observée à 744 - 747 nm. La largeur totale du pic principal à mi-hauteur est de 4 nm, ce qui indique une grande sensibilité du processus SHG à la longueur d'onde de pompage. L'efficacité SHG normalisée dans la structure de domaine régulière générée avec une longueur de 1,5 mm était de 0,3 %/(W·cm).

La dépendance de la puissance SHG à la position du foyer de l'émission de pompage lors du déplacement le long de la coordonnée Z a montré que la profondeur de la RDS à laquelle la génération effective de seconde harmonique se produit était d'environ 300  $\mu\text{m}$  (Figure 21b).

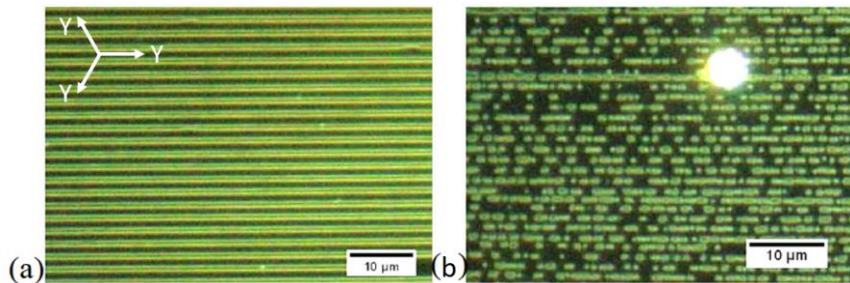


Figure 20. Structure de domaine régulière avec une période de 2  $\mu\text{m}$  sur les surfaces polaires (a) - Z- et (b) - Z+. Identifiée par gravure chimique sélective. Microscopie optique, champ sombre.

La température de quasi-accord de phase pour la longueur d'onde de pompage de 747 nm était de 32°C (Figure 21 c), ce qui est proche de la valeur calculée de 47°C obtenue en utilisant l'équation de Sellmeier [23]. L'efficacité normalisée de génération de seconde harmonique dans l'élément de 1,5 mm de long, y compris les pertes par réflexion, était de 0,4 %/(W·cm).

Une rotation du cristal avec une RDS de 5 degrés par rapport à l'axe Z, correspondant à une augmentation effective de la période de la structure de 8 nm, a entraîné une augmentation significative de la puissance (Figure 21d).

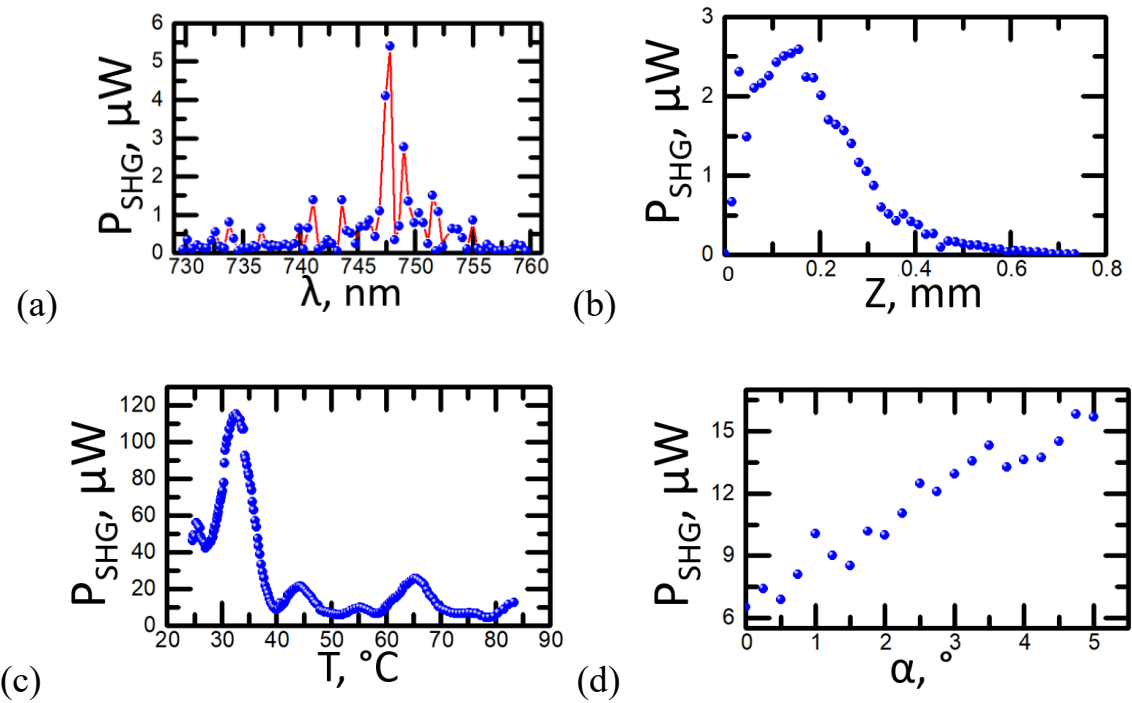


Figure 21. Dépendance de la puissance de SHG par rapport à: (a) la longueur d'onde de pompage, (b) - la coordonnée  $Z$  du faisceau de pompage, (c) - la température, (d) - l'angle de rotation de l'échantillon par rapport à l'axe  $Z$ . La longueur d'onde de pompage dans (b-d) est de 747 nm.

Ainsi, il a été possible pour la première fois de produire une émission d'une longueur d'onde de 373 nm en utilisant la méthode de SHG dans un cristal de niobate de lithium dopé au magnésium avec une RDS de 2  $\mu\text{m}$ , créée par balayage avec un faisceau d'électrons focalisés.

## PRINCIPAUX RÉSULTATS ET CONCLUSIONS DE L'ÉTUDE

- Il a été étudié pour la première fois la croissance anormale de domaines lamellaires sur la surface polaire  $Z$  pendant la commutation de polarisation dans des monocristaux de niobate de lithium modifiés par un échange protonique doux.
- Il a été trouvé que les champs de seuil de formation de domaines anormalement bas sur la surface polaire  $Z$  dépendaient de la durée du processus d'échange protonique.
- Il a été détecté l'effet de la formation de structures de domaine quasi-périodiques pendant la croissance de domaines lamellaires à partir d'une paroi

de domaine planaire.

4. La diminution anormale observée des champs de seuil de la croissance des domaines lamellaires à la suite d'un échange protonique doux est attribuée à la formation d'un champ interne de cohérence causé par la présence d'un gradient de composition dans la couche superficielle.
5. Il est démontré que la valeur du gradient de composition dans la couche superficielle croît avec l'augmentation de la durée de l'échange protonique, ce qui conduit à une diminution du champ de seuil.
6. Il est démontré qu'il est possible de créer une structure de domaine régulière et stable avec une période de 500 nm en commutant localement la polarisation à l'aide d'un microscope sonde à balayage.
7. Il a été obtenu pour la première fois une émission de 374 nm de longueur d'onde par génération de seconde harmonique dans un cristal de niobate de lithium dopé au magnésium avec une structure de domaine régulière d'une période de 2  $\mu\text{m}$  créée par balayage à l'aide d'un faisceau d'électrons focalisé.

### **Perspectives pour le développement futur du sujet**

Les résultats obtenus au cours de la recherche seront utilisés pour poursuivre le développement de méthodes d'ingénierie de domaine pour créer des structures de domaine régulières dans les guides d'ondes optiques. Des méthodes seront développées pour créer des guides d'ondes optiques avec une structure de domaine régulière pour la conversion de longueur d'onde en utilisant la quasi-adaptation de phase. Des guides d'ondes optiques fabriqués par la méthode d'échange protonique dans des cristaux de niobate de lithium avec une structure de domaine régulière précise seront utilisés dans des dispositifs de communication quantique.

## RÉFÉRENCES

1. High-frequency resonance in acoustic superlattice of LiNbO<sub>3</sub> crystals/ Y. Zhu, et al. // Appl. Phys. Lett. – 1988. – Vol. 53. – P. 2278–2280.
2. Khan A.I. The future of ferroelectric field-effect transistor technology / A.I. Khan, A. Keshavarzi, S. Datta // Nat. Electron. – 2020. – Vol. 3. – P. 588–597.
3. Hu X. Nonlinear beam shaping in domain engineered ferroelectric crystals / X. Hu, Y. Zhang S. Zhu // Adv. Mat. – 2020. – Vol. 32 – P. 1903775.
4. Nanodomain engineering for programmable ferroelectric devices / A. Lipatov et al. // Nano Lett. – 2019. – Vol. 19. – P. 3194.
5. Kores C C. Quasi-phase matching waveguides on lithium niobate and KTP for nonlinear frequency conversion: A comparison / C. C. Kores, C. Canalias, F. Laurell // APL Photonics. – Vol. 6. – 2021. – P. 091102.
6. Bazzan M. Optical waveguides in lithium niobate: Recent developments and applications. / M. Bazzan, C. Sada // App. Phys. Rev. – Vol. 2:4. – 2015. – P. 040603.
7. Soft-proton-exchange tapers for low insertion-loss LiNbO<sub>3</sub> devices / D. Castaldini, et al. // IEEE J. Light. Technol. – Vol. 25. – 2007. – P. 1588–1593.
8. Soft proton exchange on periodically poled LiNbO<sub>3</sub>: A simple waveguide fabrication process for highly efficient nonlinear interactions / L. Chanvillard et al. // Appl. Phys. Lett. – Vol. 76:9. – 2000. – P. 1089–1091.
9. Hum, D. S. Quasi-phasematching / D. S. Hum, M. M. Fejer // Comptes Rendus Phys. – 2007. – Vol. 8:2. – P. 180–198.
10. Reduction of lattice defects in proton-exchanged lithium niobate waveguides / H. G. Muller et al. // J. App. Phys. – 2011. – Vol. 110. – P. 033539.
11. Pershin S. M. Raman spectroscopy of the OH group vibrations in structural complexes of liquid water / S. M. Pershin // Opt. Spectrosc. – 2005. – Vol. 98. – P. 543–554.
12. In situ investigation of formation of self-assembled nanodomain structure in lithium niobate after pulse laser irradiation / V. Ya. Shur, et al. // Appl. Phys. Lett. – 2011. – Vol. 99. – P. 082901.
13. Dimensionality increase of ferroelectric domain shape by pulse laser irradiation, / V.Ya. Shur, M.S. et al. //Acta Mater. – 2021. – Vol. 219. – P. 117270.
14. Li, C.H. Minimum cross entropy thresholding / C.H. Li and C.K. Lee // Pattern Recognition. – Vol. 26. – 1993. – P. 617.
15. Kolmogorov A.N. On the statistical theory of crystallization of metals / A.N. Kolmogorov. // Izvestiya Rossiiskoi Akademii Nauk. Seriya Matematicheskaya. – 1937. – Vol. 3. – P. 355–359.
16. Avrami M. Kinetics of phase change. I General theory. / M. Avrami // J. Chem. Phys. – 1939. – Vol. 7. – P. 1103-1112.
17. Shur V. Kinetics of phase transformations in real finite systems: Application to switching in ferroelectrics / V. Shur, E. Rumyantsev, S. Makarov // J. Appl. Phys. – 1998. – Vol. 84:1. – P. 445.
18. Abnormal domain growth during polarization reversal in lithium niobate crystal modified by proton exchange / E. Savelyev et al. // Cryst. – 2023. – Vol. 13. – P. 72. – 82.

19. Investigation of jerky domain wall motion in lithium niobate / I.S. Baturin, et al. // Ferroelectrics. – 2008. – Vol. 374. – P. 136–143.
20. Domain structure of lead germanate, / V.Y. Shur, et al. // Ferroelectrics. – 1989. – Vol. 98. – P. 29–49.
21. Shur V.Ya. Arising and evolution of the domain structure in ferroics / V.Ya. Shur, E.L. Rumyantsev // J. Korean Phys. Soc. – 1998. – Vol. 32. – P. 727–732.
22. Domain structure formation by local switching in the ion sliced lithium niobate thin films // B. N. Slautin et al. / App. Phys. Lett. – 2020. – Vol. 116. – P. 152904
23. Jundt D.H. Temperature-dependent Sellmeier equation for the index of refraction, ne, in congruent lithium niobate / D.H. Jundt // Opt. Lett. – 1997. – Vol. 22:20. – P. 1553–1555.

### **LISTE DES PUBLICATIONS SUR LE SUJET DE LA THÈSE**

1. Savelyev E. D. Second harmonic generation in periodically poled MgO:LN crystal with 2 μm period created by e-beam irradiation / **E. D. Savelyev**, A. R. Akhmatkhanov, D. S. Chezganov, E. O. Vlasov, E. A. Pashnina, V. Ya. Shur, H. Tronche, F. Doutre, T. Lunghi & P. Baldi // Ferroelectrics. – 2021. – Vol. 576. – P. 50-54, DOI: 10.1080/00150193.2021.188825
2. Savelyev E. D. Domain growth in LiNbO<sub>3</sub> with surface layer modified by soft proton exchange / **E. D. Savelyev**, A. R. Akhmatkhanov, E. D. Greshnyakov, A. S. Abramov, H. Tronche, F. Doutre, T. Lunghi, P. Baldi, M. M. Neradovskiy, V. Ya. Shur // Ferroelectrics. – 2022. – Vol. 592. – P. 64-71. DOI: 10.1080/00150193.2022.2052247
3. Savelyev E. Abnormal domain growth during polarization reversal in lithium niobate crystal modified by proton exchange / **E. Savelyev**, A. Akhmatkhanov, M. Kosobokov, H. Tronche, F. Doutre, T. Lunghi, P. Baldi, V. Shur // Crystals. – 2023. – Vol. 13. – P. 72. DOI: 10.3390/cryst13010072

# Introduction

## Research rationale and its research mastery

Ferroelectric crystals are widely used in acoustics [1], microelectronics [2] and optics [3]. Domain engineering [4] has been developing rapidly in recent years – a field of knowledge that studies methods of creation of domain structure (DS) of the specified geometry in ferroelectrics for practical use.

One of the most widely used ferroelectric crystals is Lithium Niobate ( $\text{LiNbO}_3$ ). The well-developed technology of Czochralski process makes it possible to obtain big size high-quality congruent lithium niobate (CLN) single crystals. CLN possesses high values of piezoelectric and non-linear optical coefficients [5], as well as a high phase transition temperature which make it possible to create different devices for opto-acoustics, non-linear optics, and integrated optics [6].

Optical waveguides in the CLN crystals are created for applications in the telecommunications and integrated optics. One of the most popular methods of creating optical waveguides in CLN is proton exchange (PE) [7]. In this case, the change of refraction index in the near-surface layer of a CLN plate is realized by the replacement of lithium ions with protons. Benzoic acid is used usually as a source of protons. Lithium benzoate is added into benzoic acid to implement soft proton exchange (SPE) which leads to the deceleration of the exchange process and the creation of waveguides with the composition gradient [8].

The creation of periodic domain structures (PDS) in CLN single crystals makes it possible to use the effect of the quasi-phasematching [9] to implement the record efficiency of second harmonic generation (SHG) and optical parametric oscillation. The most widespread method of creating PDS is the application of an external electric field using the periodical electrodes created by photolithography. Recently, new methods of PDS creation have been developed: by scanning with the focused beam of electrons or ions, as well as by applying the field with a conducting probe of a scanning probe microscope. It should be noted that the creation of optical waveguides with PDS for wavelength conversion has an important practical

application and requires deep study of the domain structure kinetics in PE CLN crystals. It is also noteworthy, that the low conductivity of a modified near-surface layer of PE CLN [10] hampers screening of depolarization field during polarization reversal. Herewith, the evolution of the domain structure represents a highly nonequilibrium process that is considered as the first-order phase transition analogue. Creation of optical waveguides by the PE method leads to forming the composition gradient in the near-surface layer that creates a “built-in” electric field that has a significant impact on the domain structure kinetics. Besides, the near-surface layer represents an artificial dielectric gap that reduces the effectiveness of external screening thus leading to screening retardation of the depolarization field. The study of the features of the domain structure evolution during polarization reversal under the conditions of the incomplete screening of the depolarization field and the presence of the composition gradient is an important fundamental problem of the physics of ferroelectrics.

Specific aims of the work: to study the formation of a periodic domain structure and the conversion of the laser radiation wavelength in modified lithium niobate single crystals.

The following basic problems were formulated to achieve the specific aims:

1. To reveal and explain the peculiarities of the anomalous growth of stripe domains on the polar surface during polarization reversal in lithium niobate single crystals modified by the soft proton exchange method.
2. To establish criteria for a controlled change in the spatial distribution of the composition in the surface layer to control the range of fields in which the anomalous kinetics of the domain structure is observed in modified lithium niobate single crystals.
3. To develop methods of creating quasi-periodic and periodic stripe domain structures in modified lithium niobate single crystals.
4. To implement second-harmonic generation in the near UV in single crystals of magnesium-doped lithium niobate with the periodic domain structure created by focused electron beam scanning.

Studied objects:

1. The studied samples represent 0.5-mm-thick CLN plates cut perpendicular to the polar axis and polished to the optical quality. Soft proton exchange with the duration from 12 to 72 hours in benzoic acid with addition of 3.0% of lithium benzoate at the temperature of 300°C has also been performed in the mentioned samples.

2. Plates of congruent Mg-doped lithium niobate with PDS created by focused electron beam irradiation of a Z -polar surface coated with a layer of photoresist were used for second-harmonic generation studies.

Academic novelty of the work:

1. Study of the new effect of the formation and anisotropic growth of stripe domains on the polar surface of a uniaxial ferroelectric with a modified surface layer in the uniform electric field.

2. Study of the new effect of the anomalous decrease of the threshold fields of the formation and growth of stripe domains on the polar surface of a uniaxial ferroelectric with a modified surface layer due to the composition gradient.

3. The formation of quasi-periodic stripe domain structures growing from the planar domain wall in modified single crystals of a uniaxial ferroelectric has been demonstrated for the first time.

Theoretical relevance of the conducted studies:

1. The research has demonstrated the necessity of considering the influence of the composition gradient on the threshold fields of the domain formation and growth in crystals with spatially heterogenous composition.

2. It has been shown that the formation of a stripe domain structure in a uniaxial ferroelectric when switching in a growing field can be described by a modified Kolmogorov-Avrami model.

Practical relevance of the conducted studies

1. The studied anisotropic growth of stripe domains opens possibilities for manufacturing PDS in waveguides created in lithium niobate single crystals by the soft proton exchange method.

2. Controllable significant decrease of the threshold fields by increasing the duration of the proton exchange is of considerable interest to developing the methods of domain engineering in integral optics.

3. Obtaining the laser light with 374 nm wavelength by the second-harmonic generation in CLN single crystals with PDS with a period of 2  $\mu\text{m}$  created by focused electron beam scanning is of considerable interest for the UV generation.

Methodology and methods of the study:

Systematic experimental studies of the DS have been conducted with the use of modern high-precision analytical equipment. *In situ* domain imaging has been done by optical microscopy with the use of a high-speed camera. The spatial distribution of  $\text{H}^+$  ions in the studied plates has been measured by the confocal Raman microscopy (CRM). The non-destructive domain imaging at the surface has been performed by piezoelectric force microscopy (PFM). The domain imaging in the bulk has been performed with the use of CRM and Cherenkov-type second-harmonic generation microscopy (SHGM). The isolated domains and DS were created by local polarization reversal using a probe of a scanning probe microscope.

Quality of the obtained results is ensured using the checked and calibrated measuring equipment, certified measuring techniques, reliable experimental statistics, implementation of independent experimental data processing technique, consistency with the results of other authors and coherence with the known physical models. The reliability of the estimates is ensured by assumption validity as well as by the coherence with the experimental results.

Provisions submitted for defense:

1 The anomalous growth of stripe domains at the polar surface during polarization reversal in CLN single crystals modified by the soft proton exchange method is conditioned by the inefficient screening of a depolarizing field caused by the presence of a surface dielectric gap.

2. The anomalous decrease of a threshold fields of nucleation and growth of stripe domains is caused by formation of a bound internal field in the near-surface layer proportional to the composition gradient created by soft proton exchange.

3. The formation of quasi-periodic structure of stripe domains grown from a planar domain wall is caused by the electrostatic interaction between stripe domains and charged domain walls.

4. The creation of a stable PDS with the period of 500 nm during local polarization reversal by a probe of a scanning probe microscope with higher temperature is conditioned by the growth of the screening efficiency and the decrease of the threshold fields.

5. The second-harmonic generation with wavelength of 374 nm in magnesium doped CLN with the PDS created by a focused electron beam with the normalized effectiveness of 0.4% (W cm) is due to the good reproducibility of the structure period.

#### Evaluation of results.

The main results of the work were presented at six Russian and international conferences and symposiums: 1) International conference "Research of ferroelectric materials by Russian scientists. Centenary of the discovery of ferroelectricity" (Ekaterinburg, 2020), 2) XXII All-russian conference on ferroelectric physics (VKS-XXII) (Ekaterinburg, 2021), 3) International conference "Modern Nanotechnologies" (IWMN-2022) (Ekaterinburg, 2022), 4) All-russian scientific conference with international participation "Yenisei Photonics - 2022" (Krasnoyarsk, 2022), 5) International symposium on applications of ferroelectrics (ISAF-PFM-ECAPD-2022) (Tours, France, 2022). 6) International conference "Materials Science and Nanotechnology" (MNC-2023) (Ekaterinburg, 2023)

#### Publications and individual contribution of the author.

The main results have been published in 9 publications, including three articles in peer-reviewed scientific journals included in the international citation databases Scopus and WoS, in six abstracts of international and All-Russian conferences and one computer program. The dissertation work was conducted using

the equipment of the Ural Center for Collective Use "Modern Nanotechnologies" of the Institute of Natural Sciences and Mathematics of the Ural Federal University in the framework of research conducted with the support of the Russian Foundation for Basic Research (grant 20-32-90192 Graduate students).

The main results were obtained personally by the author or with his active participation. The choice of the research direction, discussion of the results and formulation of the tasks were carried out jointly with the scientific supervisors, Ph. D., Professor P. Baldi, Dr. Habil, Professor V. Y. Shur and Ph. D. senior staff scientist A. R. Akhmatkhanov. The production of samples, switching of polarization in a homogeneous field, domain imaging by optical microscopy and CRM methods, the study of DS parameters, analysis and processing of the results were carried out by the author personally. Local polarization reversal and domain imaging by the piezoresponse force microscopy (PFM) method were carried out jointly with Ph. D., junior staff scientist B.N. Slautin, junior staff scientist L.V. Gimadeeva and junior staff scientist A.S. Abramov. Domain imaging by the SHG was carried out jointly with staff scientist M. S. Nebogatikov and Ph. D., junior staff scientist A.S. Slautina.

#### Structure and the volume of the dissertation.

The dissertation work consists of the introduction, five chapters, the conclusion, a list of abbreviations and symbols and a list of references. The total volume of the work is 138 pages, including 65 figures, one table and a list of references containing 175 titles.

# Literature review

## 1.1 Domain structure of uniaxial ferroelectrics

### 1.1.1 Ferroelectrics. Basic concepts

A ferroelectric is a dielectric that has, in a certain temperature range, a spontaneous polarization oriented in two or more directions, which can be changed by applying an external electric field.

In uniaxial ferroelectrics, the presence of spontaneous polarization leads to the appearance of bound charges on polar surfaces, which create a depolarizing field that tends to change the direction of spontaneous polarization and leads to the creation of a domain structure. The field existing in the crystal is compensated by several screening mechanisms.

The polar component of the spatially non-uniform and time dependent local electric field ( $E_{loc.z}$ ) leads to evolution of the ferroelectric domain structure. This component is the sum of the following parts: (1) external field ( $E_{ex.z}$ ) generated by the application through the electrodes by an external source, (2) depolarizing field ( $E_{dep.z}$ ) generated by bound charges at the polar surfaces, (3) external screening field ( $E_{scr.z}$ ) due to the rapid charge redistribution on the electrodes, (4) bulk screening field ( $E_{b.z}$ ) due to several relatively slow processes (Figure 1.1b) [11,12].

$$E_{loc.z}(r, t) = E_{ex.z}(r, t) - [E_{dep.z}(r, t) - E_{scr.z}(r, t)] - E_{b.z}(r, t) \quad (1.1)$$

$$E_{loc.z}(r, t) = E_{ex.z}(r, t) - E_{rd.z}(r, t) - E_{b.z}(r, t) \quad (1.2)$$

where  $E_{rd.z}(r, t) = E_{dep.z}(r, t) - E_{scr.z}(r, t)$  is the residual depolarizing field.

The existence of a residual depolarizing field is caused by incomplete compensation of the depolarizing field by external screening due to the existence of the intrinsic or artificial dielectric layers at the polar surfaces. The screening of the depolarizing field determines the evolution of the domain structure during polarization reversal.

### 1.1.2 Evolution of the domain structure during polarization reversal

When the high enough value of an external electric field is applied to a single-domain ferroelectric crystal, five main stages in the domain structure evolution can be distinguished: (a) the appearance of new domains, (b) domain growth in the polar direction, (c) sideways domain growth, (d) domain coalescence, and (e) spontaneous backswitching after external field switch off [11,13] (Figure 1.1).

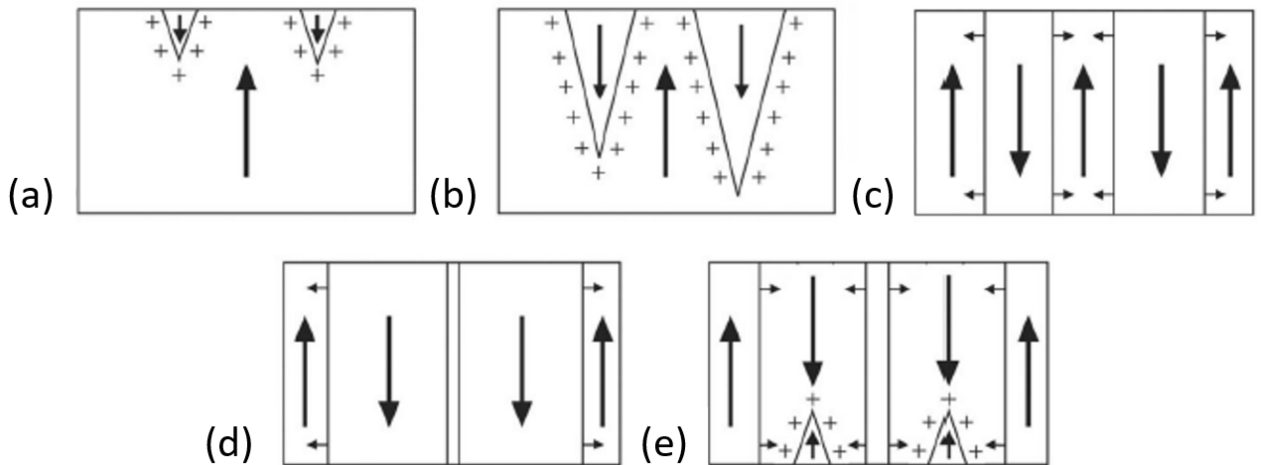


Figure 1.1 - The main stages of the evolution of the domain structure during polarization reversal: (a) the formation of new domains, (b) growth in the polar direction, (c) sideways growth, (d) domain coalescence, (e) spontaneous backswitching after external field switch off [14].

The study of the formation of new domains during switching from a single-domain state is extremely difficult since it requires imaging of the appeared isolated needle-like nanodomains with a charged domain wall (Figure 1.1a). It must be understood that the only way to obtain a single-domain crystal is cooling in a constant electric field through the ferroelectric phase transition. Usually, in the study of domain kinetics under the action of alternative field pulses the residual nanodomains are observed [15].

During forward growth the needle-like domains grow rapidly in a polar direction (Figure 1.1b). Direct observation of forward growth is experimentally difficult. Recent studies of domain growth on a nonpolar cut of uniaxial crystal under local polarization reversal allows to reveal that the forward growth represents the

step generation at the domain wall at the surface and motion of the charged kinks in polar direction [16].

The sideways growth stage, which is the wall motion in the direction perpendicular to the polar direction, is the best studied by *in situ* optical methods with high temporal resolution (Figure 1.1c). The shape of growing isolated domains depends on the switching conditions [17–19]. Changes in the applied field and temperature, modification of the surface layer [20–22], and type of electrodes [23] make it possible to create various domain shapes, which are determined not only by the crystal symmetry, but also by the growth kinetics.

Coalescence is a domain merging when the polarization reversal is close to completion (Figure 1.1d). The retardation or stopping of approaching domain walls caused by electrostatic interaction leads to the existence of residual isolated domains [20]. Moreover, the merging of isolated domains in the shape of convex polygons leads to ultrafast restoration of the wall orientation. The obtained shape stability effect is due to giant dependence of the domain wall velocity on orientation and formation of short-lived superfast domain walls [14].

After external electric field switch-off the spontaneous backswitching is observed usually. This process leads to partial or complete restoration of the original domain structure by arising of domains with the initial direction of spontaneous polarization and growth of the residual domains (Figure 1.1e) [24].

### 1.1.3 Screening of depolarizing fields

Depolarizing fields in ferroelectrics can be compensated by various external and bulk screening mechanisms.

External screening is possible due to the redistribution of charges on polar surfaces.

In samples with a free polar surface not covered with electrodes, screening occurs due to adsorption of ions from the external environment or surface breakdown, and in vacuum due to electron emission (Figure 1.2).

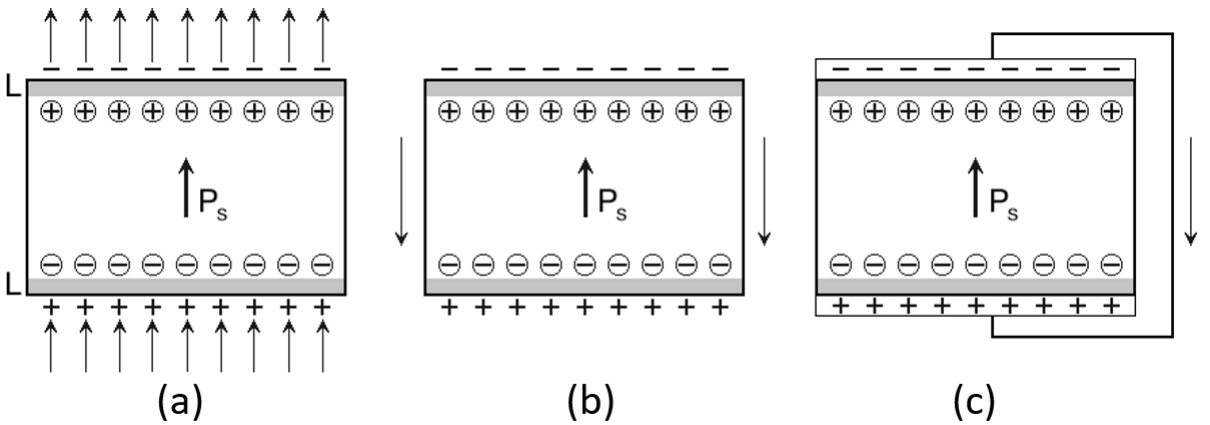


Figure 1.2 - Schematic representation of the mechanisms of external screening: (a) breakdown in the environment or electron emission, (b) surface conductivity along the side faces of the sample, (c) charge redistribution on the electrodes.

In a ferroelectric capacitor with solid electrodes on polar surfaces, screening is accompanied by a current in the external circuit.

All the considered mechanisms do not allow to screen completely the depolarizing field due to the existence in any ferroelectric of intrinsic or artificial surface dielectric layer [25] (Figure 1.3). The spatial separation of bound and screening charges leads to the existence of a residual depolarizing field, which can be screened by slow bulk screening processes.

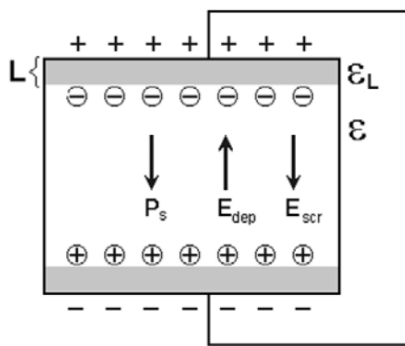


Figure 1.3 - Distribution of fields in a ferroelectric capacitor with a dielectric layer.

Bulk screening can be caused by bulk conductivity, reorientation of dipole defects, or injection of charge carriers from electrodes through a dielectric gap (Figure 1.4).

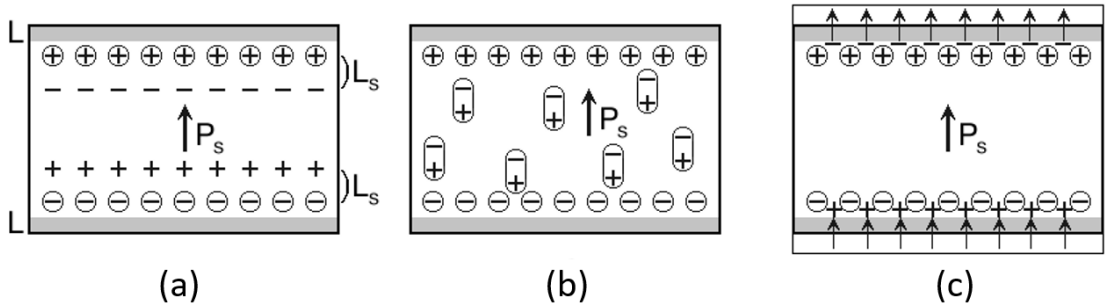


Figure 1.4 - Schematic representation of the mechanisms of internal screening: (a) charge redistribution in the volume, (b) reorientation of dipole defects, (c) injection of charge carriers through the surface dielectric gap

The bulk conductivity in ferroelectrics depends on temperature and can have an electron-hole and ion character [26]. In LN and related crystals, lithium ions diffuse at high temperatures in the channels formed by oxygen octahedra in accordance with the polar direction.

**Reorientation of dipole defects.** In real ferroelectrics, there are dipole defect clusters [15,27], which in LN consist of four lithium vacancies and one Nb ion in place of lithium:  $[\text{Nb}4+\text{Li}] = 4[\text{V}-\text{Li}]$  [28] (Figure 1.5).

After polarization reversal, the defective cluster changes its orientation by thermal activation to a more favorable one for the new direction of spontaneous polarization [28] (Figure 1.5).

Charge carrier injection is the process of tunneling of charge carriers from an external electrode into a ferroelectric crystal induced by a depolarizing field in the dielectric gap [29]. The injected charges participate in the bulk screening. Injection is observed only for solid electrodes and is impossible for electrodes made of liquid electrolyte.

Bulk screening provided by all the above mechanisms. Several relaxation times can be observed due to the competition of screening mechanisms.

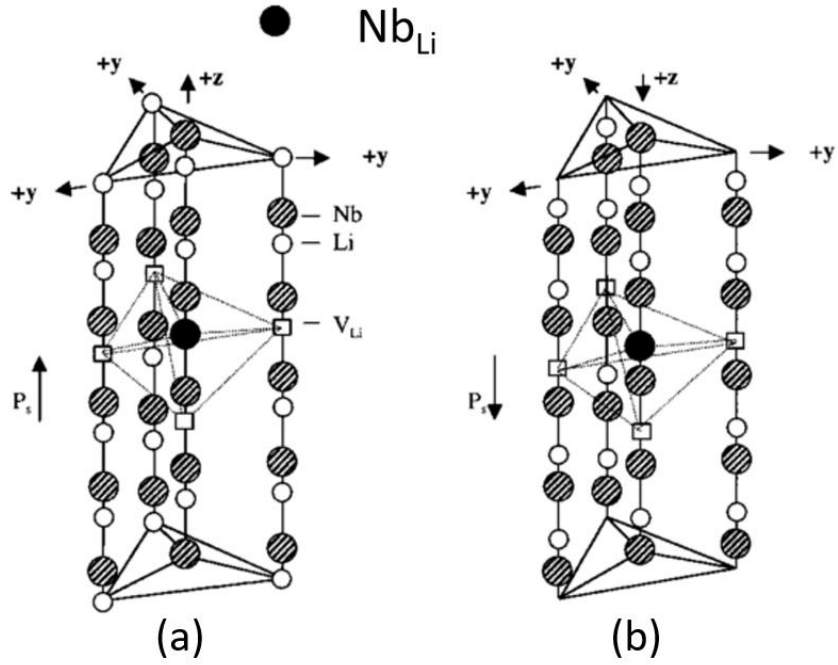


Figure 1.5 - Scheme of configurations of dipole defects in CLN, corresponding to the directions of polarization (a)  $+P_s$  and (b)  $-P_s$  [28]

External screening processes have significantly shorter relaxation times than the bulk screening ones. The characteristic times of these processes vary from milliseconds to months. The switching cycle, as a rule, takes much less time than is necessary for the bulk screening process, so the bulk screening field does not have time to change significantly during such a cycle.

#### **1.1.4 Kinetic approach to describe the evolution of the domain structure.**

Within the framework of the kinetic approach, the evolution of the domain structure is considered as an example of a first-order solid-solid phase transition determined by nucleation processes [30]. In this case, the analogy between the growth of domains and crystals is considered. With this approach, the domain wall is considered as a phase boundary, and the domains as phase volumes. The evolution of the domain structure in the field is the result of the generation of one-, two- and three-dimensional nuclei with an advantageous orientation of spontaneous polarization (Figure 1.6).

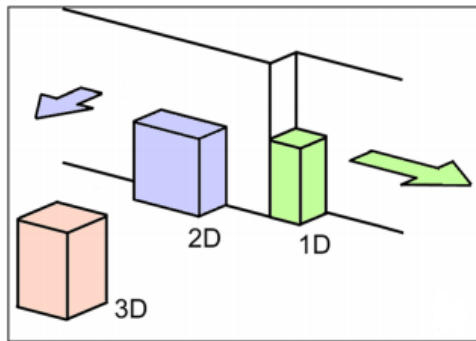


Figure 1.6 - Schematic representation of the processes of nucleation 1D, 2D and 3D [12]

The kinetic approach is well suited to explain the complex shape of domains and domain structures [11,17]. The motion of the domain wall occurs due to the generation of unit cell-thick steps (pairs of kinks) on it by 2D nucleation (Figure 1.7a). 1D nucleation is the process of kink motion along the wall. The probability of nucleation is determined by the local excess over the threshold of the polar component of the field averaged over the size of the nucleus [12]:

$$\Delta E_{loc.z}(r, t) = E_{loc.z}(r, t) - E_{th} \quad (1.3)$$

Field dependence of the step generation rate:

$$dn_s/dt(E) = k (E_{loc} - E_{th.st}) \quad (1.4)$$

where  $n_s$  is the concentration of steps.

Field dependence of the kink velocity:

$$v_k(E) = \mu_k (E_{loc} - E_{th.k}) \quad (1.5)$$

where  $\mu_k$  is the kink mobility.

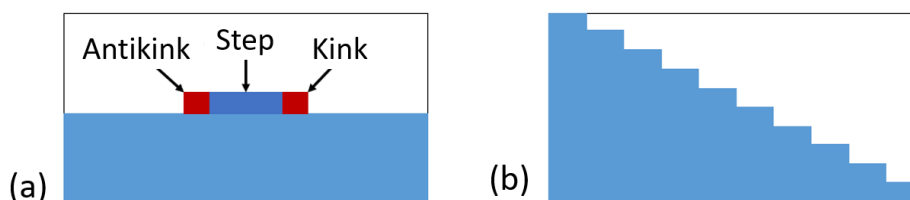


Figure 1.7 - (a) The domain wall motion due to the steps generation and kink motion, (b) "flat" domain wall deviated from the main crystallographic direction.

### 1.1.5 Kinetics of the domain structure under highly nonequilibrium switching conditions

The influence of the bulk screening retardation on the evolution of the domain structure was considered using the example of the shift of a flat domain wall from a completely screened state in a flat ferroelectric capacitor with a dielectric gap (Figure 1.8) [31]. The step formation probability has a stochastic character and is equally probable over the whole domain wall.

The spatial distribution of the bulk screening field does not occur during domain wall shift if the bulk screening process proceeds slowly. The position of the charges that screened its initial position and the change in the sign of the bound charges leads to a decrease of the switching field. As a result, behind the domain wall near the electrode, a trail of bound and screening charges with a density of  $2P_S$  is formed. The field created by the charges is screened by the current in the external circuit, however, the presence of a dielectric gap leads to only partial rapid screening of the field.

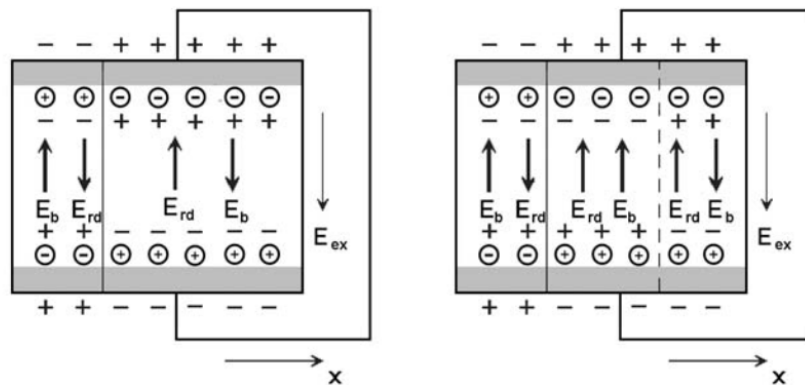


Figure 1.8 - Scheme of changes in the distribution of fields and charges when a flat domain wall shifts from a screened state. On the left - the wall in the initial state, on the right - after the shift [32]

When calculating the retardation effect of  $E_{rd}$ , we can restrict ourselves to considering a flat strip capacitor, the width is equal to the domain wall shift  $\Delta x$ , and the charge density  $\sigma_b$  is reduced compared to  $P_S$  due to external screening [33]:

$$\sigma_b = \frac{L}{d} \frac{\varepsilon}{\varepsilon_L} P_S (1 + k) \quad (1.6)$$

where  $k$  is the degree of screening ( $-1 < k < 1$ ).

With this consideration, the value of the polar component of the residual depolarizing field  $E_{rd.z}(\Delta x)$ , averaged over the thickness of the sample, is given by the formula [34,33]:

$$E_{rd.z}(\Delta x) = \frac{2\sigma_b}{\varepsilon\varepsilon_0} F\left(\frac{\Delta x}{d}\right), \quad (1.7)$$

$$\text{where } F(A) = \frac{1}{\pi} [2 \operatorname{arctg}(A) + A \cdot \ln(1 + A^{-2})] \quad (1.8)$$

If we assume that the instantaneous velocity of the domain wall is proportional to the excess of the switching field above the threshold, then the motion will slow down with increasing shear [34]:

$$v(E) = \mu (E_{loc.z} - E_{th.z}) \quad (1.9)$$

The wall will stop at  $E_{loc.z} - E_{th.z} = 0$ , and after the external field is turned off, a complete backswitching will occur, under the action of  $E_{rd}$  and the uncompensated field of screening charges that did not have time to realign.



Figure. 1.9 - Correlated nucleation - the formation of a domain chain during switching from a polydomain state in lead germanate in a strong field [35].

In the case of inefficient screening, discrete switching can be observed due to the formation and growth of an ensemble of isolated domains arising because of correlated nucleation. This effect was first observed during switching in a uniform field in plates of a uniaxial ferroelectric lead germanate (PGO) [36]. It was shown that a chain of isolated domains with a diameter of less than 10  $\mu\text{m}$  appeared in front of the moving domain wall (Figure 1.9). Correlated nucleation was also observed in CLN (Figure 1.10).

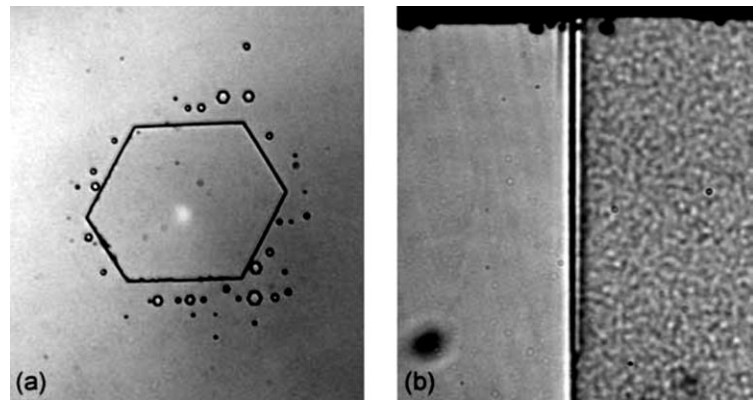


Figure 1.10 - Formation of isolated domains during the growth of a hexagonal domain in CLN. (a) Z+ surface, (b) Y section [32].

Polarization reversal under the action of a series of pulses was accompanied by repeated successive formation of chains of non-through needle-like domains surrounding the original domain, which led to the formation of a "wide domain wall" (Figure 1.11). The density of isolated domains reached  $10^6 \text{ cm}^{-2}$ . The appeared chains of domains were oriented along the Y-crystallographic directions [36].

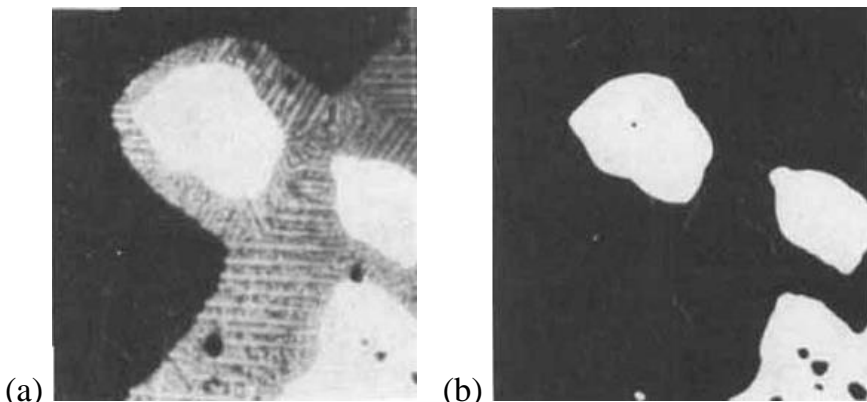


Figure 1.11 - (a) Self-organized structure of isolated domains that appeared in PGO when switching by a series of field pulses from (b) a polydomain state [36].

Computer modeling revealed that the field maximum arising in front of the domain wall at a small depth from the surface at a distance close to the thickness of the dielectric gap  $L$  appears shifts  $r_s$  when a residual depolarizing field trail shifts behind the shifting domain wall (Figure 1.12).

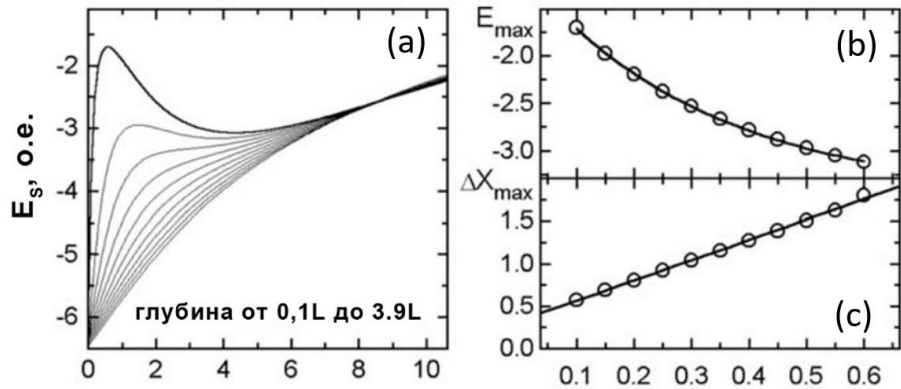


Figure 1.12 – (a) Results of computer simulation of the spatial distribution of the local value of the electric field  $E_{loc}$  near the stripe domain at different depths from the surface. Depth dependence of (b) the magnitude of the  $E_{loc}$  maximum and (c) the distance from the domain wall to the position of the maximum. Distances and depths are normalized to the thickness of the dielectric gap [32].

Thus, the motion of the domain wall turns into a discrete process of formation of chains of domains in front of the wall.

The existence of an artificial dielectric gap reduces the effectiveness of external screening. In this case, strongly nonequilibrium conditions for polarization reversal are realized, under which the kinetics of the domain structure changes qualitatively.

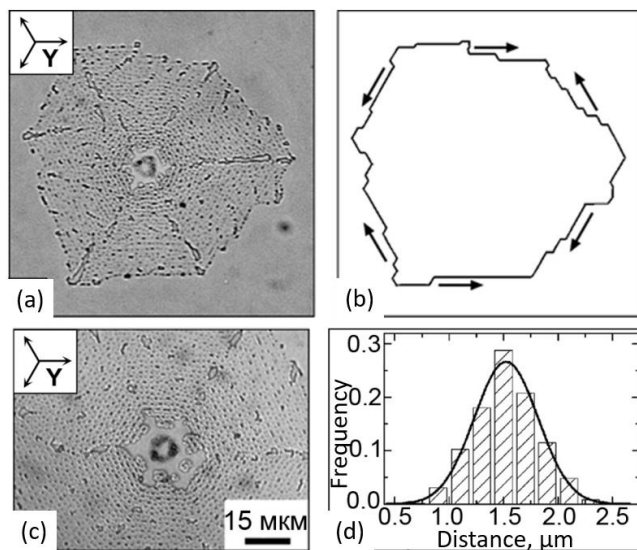


Figure 1.13 - Net-like domain structure formed when switching in a uniform field in stoichiometric lithium tantalate with an artificial dielectric layer. (a), (c) Optical images after selective etching.

(b) Schematic representation of the ensemble boundary. (d) Histogram of distribution of distances between neighboring domains

It was experimentally demonstrated that in plates of stoichiometric lithium tantalate SLT, when switching polarization, the dielectric layer (photoresist 2  $\mu\text{m}$  thick) plays an important role. Experiments have shown that in a uniform electric field, the motion of the domain wall is replaced by discrete switching, which leads to the formation of a net-like domain structure (Figure 1.13).

At the initial stage, a hexagonal domain was formed around the hole in the dielectric layer. Subsequent switching was carried out due to the formation and growth of a quasi-regular self-organized structure (ensemble) consisting of isolated needle-like nanodomains.

The growth of the ensemble followed all stages of the growth of a macroscopic isolated domain. In this case, the boundary of the ensemble played the role of a domain wall. The formation and growth along the boundary of the ensemble of isolated domains corresponded to the growth of steps. By analogy with the growth of an isolated domain, the boundary of the switching region had a hexagonal shape, the edges were oriented along the Y-crystallographic directions. Statistical analysis of images showed that the average distance between isolated domains is of the same order as the thickness of the dielectric layer (Figure 1.13d).

Correlated nucleation was also observed during switching in a uniform field in CLN crystals, in which a uniform modified layer (without a composition gradient) was created by proton exchange (Figure 1.14) [21]. Registration of instantaneous images in real time made it possible to reveal the existence of a strip filled with nanodomains in front of the moving domain wall. The growth of the domain in this case was carried out due to the appearance of a new chain of nanodomains in front of the strip and the merging of nanodomains with the moving domain wall.

Several scenarios for the evolution of the domain structure depending on the layer thickness and the excess of the field above the threshold were revealed: (1) the growth of hexagonal domains, (2) the anisotropic growth of a wide domain wall, and

(3) the growth of domain rays (strip domains) along selected crystallographic directions ( $Y+$ ), with the subsequent formation of a self-organized quasi-regular structure [37]. It was also found that the growth of domain rays begins in  $Y-$  crystallographic directions and leads to the formation of a net structure (Figure 1.14).

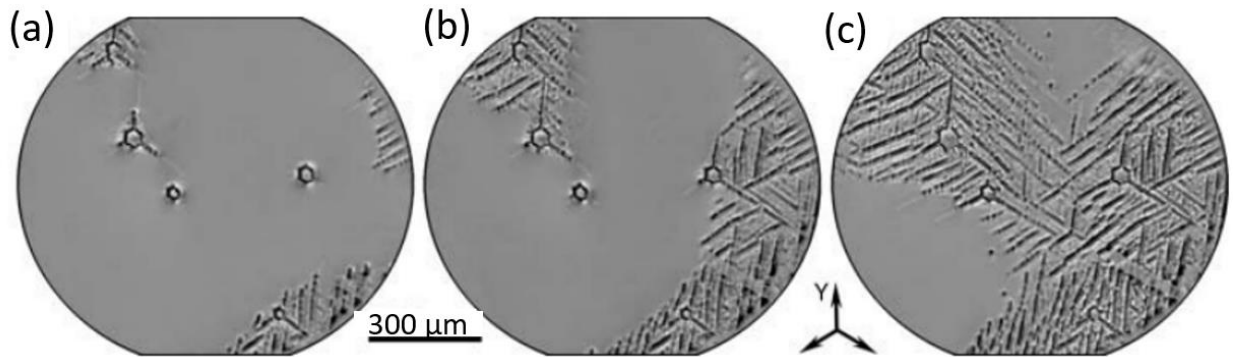


Figure 1.14 - Evolution of the domain structure *in situ* optical microscopy. CLN with a surface layer modified by the proton exchange method, layer thickness  $3.4 \mu\text{m}$  Exceeding the threshold of  $1.4 \text{ kV/mm}$ . Time from the start of switching: (a) 11.5 s, (b) 13.1 s, (c) 15.5 s [37].

## 1.2 Domain imaging methods

A change in the direction of polarization of LN crystals under the application of an external electric field is obviously accompanied by a change in their domain structure. Thus, the study of the kinetics of the domain structure is a detailed study of the processes of switching the polarization of ferroelectrics. Domain structure research methods can be divided into two main groups:

1. Integral methods measure characteristics such as hysteresis loops, switching current and charge, pyro signal, piezo signal, light scattering. Even at very high switching speeds, this approach allows research. The need to involve additional model representations and the complexity of interpretation are among the shortcomings of integral methods.

2. Imaging methods are superior in their capabilities to integral methods, since they allow you to directly extract information about the evolution of the DS. However, many of these methods, for example, optical ones, are applicable only to a limited set of ferroelectrics and, moreover, are inapplicable to the study of fast processes.

### **1.2.1 Selective chemical etching**

Selective chemical etching, pioneered by Hutton and Merz [38] to visualize DS in barium titanate, is a very easy to use and popular technique. The method is based on the difference in the etching rate of surfaces with different directions of spontaneous polarization. The DS relief revealed by etching can be further visualized by optical, scanning electron, or probe microscopy.

Hydrofluoric acid (HF) or a mixture of hydrofluoric and nitric acids (HNO<sub>3</sub>) [39] is commonly used for selective chemical etching of LN. This approach is used to detect DS both on polar (Z-cut) and non-polar (Y-cut) surfaces. The etching rates of Z- and Y- cuts are more than two orders of magnitude higher than those of Z+ and Y+ cuts [40]. When observed in reflected light, a relief is observed on the surface after etching, which corresponds to the static surface domain structure at the time of etching.

It should be noted that the etching products, which are nonuniformly distributed over the surface, hinder the etching process. In addition, etching itself can lead to a change in the shape of the detected domains [41]. During prolonged etching, the shape of the domains can be significantly distorted due to etching of the side surfaces, up to the complete disappearance of the domain; therefore, it is not possible to study nanodomain structures in LN crystals by this method.

Other disadvantages of the method include the need to remove the solid electrodes from the sample surface (this problem can be solved by using a liquid electrolyte as electrodes), the impossibility of observing changes in the DS occurring in the interval between the end of the field pulse and etching (for example, spontaneous backswitching when the external fields). Since etching is a procedure that destroys the sample surface, it makes it impossible to switch the sample again under the same conditions as before etching.

### **1.2.2 Optical imaging**

Direct imaging of the domain structure using a polarizing optical microscope is the simplest way to study the features of the evolution of the domain structure

during polarization reversal in ferroelectric under the action of an external electric field [13,42–44]. Within the limits of its applicability, the method makes it possible to obtain a sufficiently high spatial resolution (up to 0.5  $\mu\text{m}$ ), and the use of various methods of fast image recording (high-speed photography or video recording, as well as stroboscopic illumination [45]) provides the high temporal resolution (up to 10 ns [17, 46]), necessary for the investigation of fast processes. Quantitative information about the DS dynamics during the switching process (the velocity of domain walls, the number, size, and shape of individual domains) is extracted by statistical processing of the obtained images.

A necessary condition for the imaging of DWs using optical microscopy is to obtain the optical contrast of domains or the contrast of domain walls. In LN crystals, which have a strongly pronounced electro-optical effect [40,47-50], a 180-degree DS can be visualized by applying an electric field along the polar axis of the crystal. Then for light propagating along the polar axis, the electro-optical effect causes a change in the refractive index. The jump in the refractive index on the domain walls is because the sign of the change is different in domains with different directions of spontaneous polarization. Such an effect makes it possible to observe the contrast of domain walls in crossed polarizers [47, 51]. An external electric field applied to the sample not only switches the DS, but also serves to visualize the DS in the process of switching. The internal residual depolarizing fields formed by the charged domain walls in LN also give the contrast of the domain walls even in the absence of an external electric field.

### 1.2.3 Scanning electron microscopy

The method of scanning electron microscopy (SEM) can be used both for imaging of DS revealed by selective chemical etching and for direct study of DS without additional surface modification to reveal domains [52–59]. The use of a transmission electron microscope makes it possible to study DS with extremely high spatial and temporal resolution [53, 57–58]. The main disadvantage of using

transmission electron microscopy is its applicability only to ultrathin samples (on the order of 100 nm).

Another method for DS imaging is based on the detection of secondary electrons excited by a scanning electron beam of a scanning electron microscope. There is a dependence of the emission of secondary electrons on the surface relief of the ferroelectric under study [52, 55, 56, 58]. The main problem of the method is related to the fact that irradiation with an electron beam leads to charging of the crystal surface. The consequence of this is the distortion of the electric potential of the surface, and the creation of electric fields that can lead to a rearrangement of the DS. The deposition of a very thin (tens of nanometers) metal or semiconductor layer on the crystal surface solves the problem of excess charge [52]. The conductive layer must be thin enough to allow the electrons to be scanned into the surface layer of the ferroelectric.

The experimental parameters (accelerating voltage, electron beam current density, angle of incidence, scanning speed) can be chosen in such a way that the difference between the currents of electrons bombarding the surface and reflected and secondary electrons leaving the ferroelectric surface is compensated by bulk conductivity [52]. In this case, the surface remains unchanged, and the domain contrast is observed in the DS image. With a slight deviation from this equilibrium, a contrast of domain walls shifts in the image [52, 60]. It is possible to cause a switching of the spontaneous polarization of a ferroelectric with a significant deviation from equilibrium. The method has a high spatial resolution (less than 1  $\mu\text{m}$ ), however, the possibility of studying fast processes is limited.

#### **1.2.4 Scanning probe microscopy**

Scanning probe microscopy (SPM) has an extremely high spatial resolution - nanometer resolution in the scanning plane and subnanometer resolution along the vertical axis, as well as a variety of operating modes that allow recording the distribution of domains on the surface of ferroelectrics.

The high spatial resolution of the technique is achieved using special sensors - cantilevers, which are microbeams fixed at one end and with a microneedle (probe) at the other end. The use of piezoceramics, which make it possible to accurately position the probe over the sample, and the radius of the probe's curvature of the order of nanometers, provide high spatial resolution.

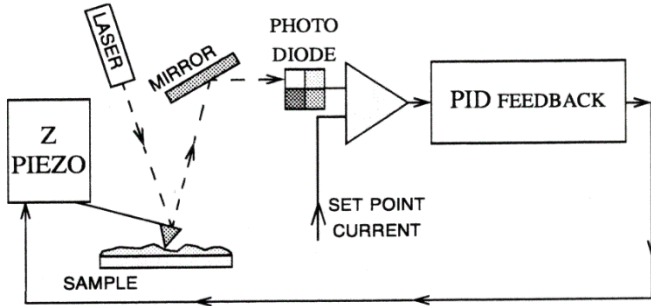


Figure 1. 15 - Block diagram of the SPM microscope

The high resolution along the vertical axis is explained by the fact that even small variations in the interaction between the probe and the sample surface led to bending of the cantilever, which is detected by the deflection of the laser beam reflected from the end of the cantilever on which the probe is attached. The use in the feedback system (Figure 1.15) allows the use of a constant signal (constant force) mode, in which the vertical displacement of the cantilever is registered, and the bend is maintained in a fixed state. When operating in the constant current mode, the cantilever bending does not move vertically, and the amount of its bending is recorded when interacting with the sample surface.

Atomic force microscopy (AFM), which registers short-range forces (for example, van der Waals forces) during relief measurements, is the main mode of SPM operation. AFM makes it possible to reveal 90° DS in multiaxial ferroelectrics and to visualize DS after selective chemical etching. In the latter case, the presence of 90° domain walls leads to different slopes of the surface on opposite sides of the walls. This technique has been successfully used to study static DS in lead titanate ( $\text{PbTiO}_3$ , PT) [61, 62] and BT [63].

In the study of ferroelectrics, piezoelectric response force microscopy (PFM) [64] is the most universal technique. PFM makes it possible to observe the DS and

the spatial distribution of polarization even in the case of complete screening of bound charges. During scanning of the sample surface by the PFM method, mechanical vibrations obtained due to the inverse piezoelectric effect are recorded at the purity of the applied field. The field is applied between the probe pressed against the surface of the sample and the lower electrode. Obviously, in antiparallel domains, oscillations occur in antiphase, since the signs of the piezoelectric coefficients are determined by the  $P_s$  direction. In the general case, surface oscillations can occur both in the vertical section (change in thickness) and in the transverse direction (measurement of the geometric dimensions of the sample in the scanning plane). Registration of the vertical deflection of the cantilever and its twisting (amplitude and phase at the frequency of the applied field) makes it possible to reconstruct the spatial distribution of all three polarization projections near the surface. Along with its versatility, the method has a high spatial resolution (of the order of 10 nm), which makes it widely used to study the static DS of ferroelectrics.

Using SPM, one can not only visualize the DS, but also perform local polarization reversal with subsequent control of the formed DS [65, 66]. By applying a field of the opposite sign, it is possible to erase the nanodomains [66] obtained by local switching, since the switching is reversible. Such reversible local switching can be used to record information at a density greater than 10 Gb/cm<sup>2</sup>.

### 1.2.5 Confocal Raman microscopy

The recording of Raman spectra sensitive to mechanical stresses [67, 68] is used to visualize domain walls in ferroelectrics, since micron-sized regions of mechanical stresses have been found near domain walls [76].

The authors of [70] observed domains using the CRM technique with the application of an external electric field. On the other hand, in [71], in a regular domain structure in LN doped with Er, at a temperature of 120°C, an insignificant change in the Raman scattering spectrum near domain walls in the region of 600 cm<sup>-1</sup> was observed; the authors concluded that this method is inefficient for

visualizing domains . There was also a publication [72] reporting a shift of the spectrum line in the  $580 \text{ cm}^{-1}$  regions by  $1.5 \text{ cm}^{-1}$ .

Papers [73, 74, 77] demonstrated a significant variation in the intensity of several Raman scattering lines near the domain wall in PDS in CLN. Using the effect of changing the line intensity, one can construct two-dimensional and three-dimensional maps of domain walls both on the crystal surface and in the bulk of the CLN [62, 76].

### 1.2.6 Second harmonic generation microscopy

Imaging of domains in ferroelectrics by second harmonic generation microscopy (SHGM) is based on measuring the intensity of the second harmonic signal obtained by irradiation with a focused pump beam [77]. In this case, the generation of the second harmonic signal occurs non-collinear to the pump radiation (Figure 1.16a), therefore it is called Cherenkov-type second harmonic generation [78]. When using unpolarized pump radiation in a biaxial optical crystal, in the general case, second harmonic generation is observed at the ordinary and extraordinary waves (Figure 1.16b).

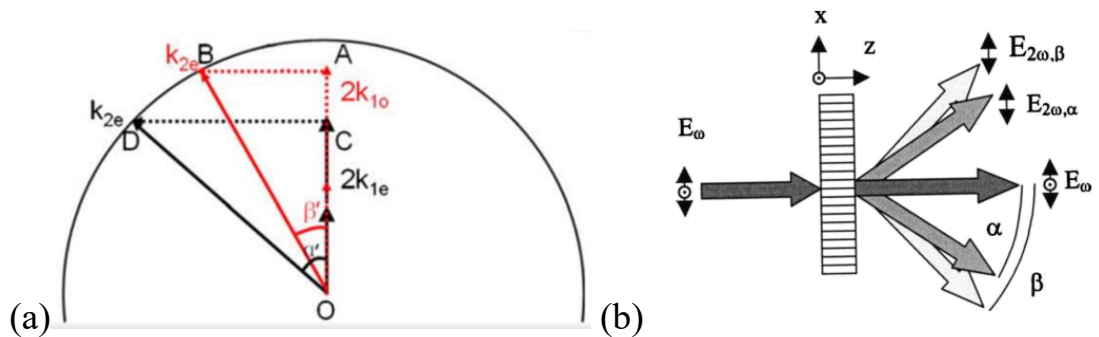


Figure 1.16 – (a) Vector scheme of phase matching in the generation of the second harmonic on the domain wall. (b) Scheme of second-harmonic signal generation during the passage of pump radiation through a ferroelectric with a regular domain structure

As a rule, a pulsed (nanosecond or femtosecond) pump laser emitting in the near-IR range is used as pump radiation [78]. The second harmonic signal is detected using a photomultiplier tube. The second harmonic signal and the pump wave are separated using a spatial mask (Figure 1.17).

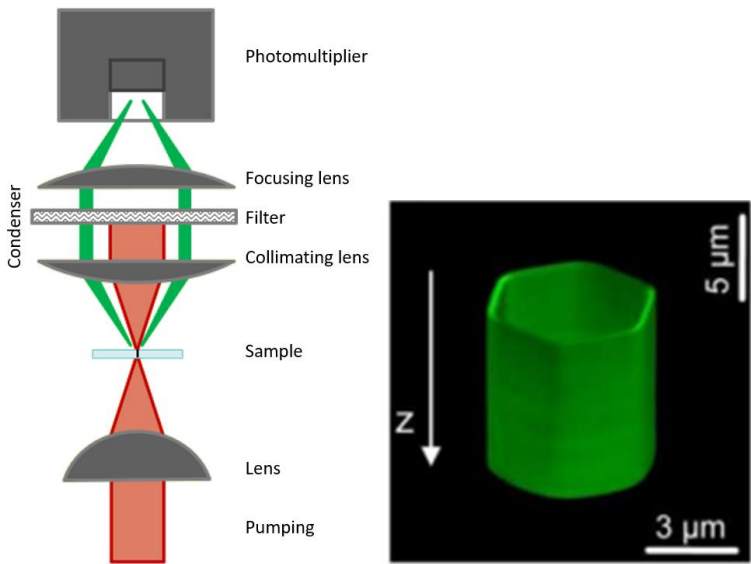


Figure 1.17 - (a) Scheme of the installation for imaging of the domain structure by the MGVG method. (b) 3D SHG image of a hexagonal domain in CLN

Imaging of the domain structure in the volume of the crystal is carried out by scanning the volume of the sample with a focused pump beam with simultaneous detection of the second harmonic signal (Figure 1.17a).

### 1.3 Lithium niobate.

#### 1.3.1 Basic physical properties

Lithium niobate LiNbO<sub>3</sub>, due to its unique properties, has secured wide use, it is one of the most studied ferroelectrics.

Under normal conditions, at room temperature, in LN can observed a rhombohedral (trigonal) structure and space symmetry group R3c (point group 3m). In the paraelectric phase, LN has a space group symmetry  $R\bar{3}c$ , the transition occurs at a temperature above the Curie point  $T_c = 1483K$ , it is worth noting that the melting point is 1533K. Disordered oxygen octahedra located one above the other with a slight rotation and having one common face make up the LN crystal lattice. O<sup>+</sup> ions are collected in hexagonal close-packed in a plane perpendicular to the polar axis. Alternating ions of lithium, niobium and vacancies fill the distance between the oxygen planes (Figure 1.18b). The observed spontaneous polarization in LN is  $P_s=71 \mu C/cm^2$  at room temperature [79] and occurs due to displacements of Li<sup>+</sup> and Nb<sup>+</sup> ions relative to oxygen octahedra. When passing through the Curie temperature,

in the paraelectric phase, lithium ions shift in the plane of oxygen octahedra, and niobium ions move to a central position between oxygen planes (Figure 1.18a) [80-82].

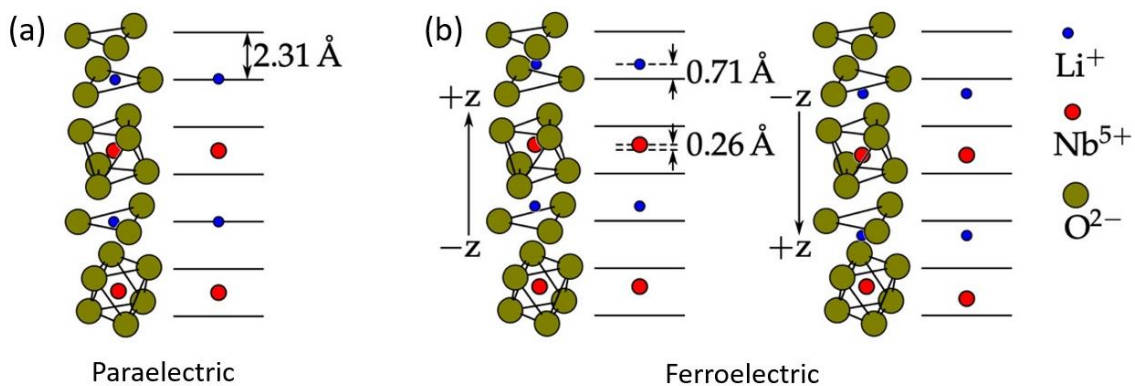


Figure 1.18 – LN structure in (a) paraelectric and (b) ferroelectric phases [84]

Despite the presence of a rhombohedral LN structure, it is easier to describe the properties of niobate using a rectangular coordinate system with x, y, z axes. By choosing the z-axis parallel to the c crystal axis (polar axis). The x-axis is chosen in such a way that one of the three transfer vectors of the hexagonal unit cell is parallel to it. And the y-axis made up the right triple with x and z vectors. The planes perpendicular to the x, y, z axes, corresponding to the Miller indices  $(2\bar{1}10)$ ,  $(1\bar{1}00)$ , and  $(0001)$ , are called the X, Y, Z cuts of the crystal [81].

LN has a unique set of properties. High pyroelectric, piezoelectric, electro-optical, acousto-optical, and photoelastic coefficients are characteristic of LN [1,56]. Under the action of a high-density light flux in LN, a photorefractive effect can be observed, the refractive index [84, 85] changes locally. The photorefractive effect is due to the linear electro-optical effect and the volumetric photovoltaic effect. LN is transparent in the wavelength range from 350 nm to 5.2  $\mu$ m [84], which makes it extremely important for optical applications.

### 1.3.2 Domain structure of lithium niobate

Systematic and large-scale experiments with LN have made it possible to reveal a variety of metastable domain shapes [87, 88], while so far only hexagonal

domains associated with the symmetry C<sub>3v</sub> of the crystal have been theoretically explained [22, 23, 86].

Field dependence of the domain shape.

The change in the shape of the growing domains is caused by the spatial inhomogeneity of the local field on the domain wall, which, in turn, is due to the screening retardation effect. For a hexagonal domain, the angular dependence  $E_{rd,z}(\phi)$  was calculated, it is shown in Figure 1.19b. The  $E_{loc,z}$  maxima are localized at the vertices of the domain (Figure 1.19d), which makes it possible to explain the effect of deterministic nucleation - the generation of steps at the vertices and the anisotropic motion of kinks (Figure 1.19a) [89, 90]. Flat domain walls deviated from the Y-crystallographic direction (Figure 1.7b) (Figure 1.19a) are formed due to the uniform spatial distribution of kinks and the effect of deterministic nucleation.

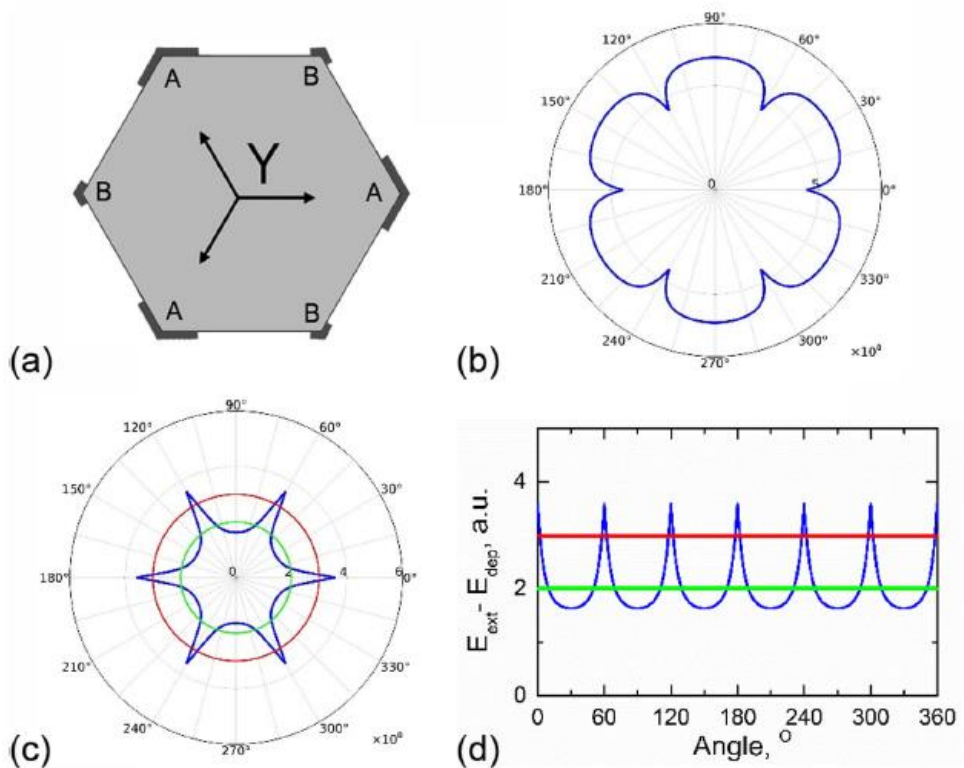


Figure 1.19 - (a) Scheme of the growth of a hexagonal domain with deterministic nucleation with generation of steps at the vertices and anisotropic motion of kinks. The calculated angular dependences of (b) the residual depolarizing field and (c, d) the local field are blue lines. Threshold fields: red line for step generation, green line for kink motion [91]

The fields for the motion of kinks  $E_{th,k}$  and the generation of steps  $E_{th,st}$ , as well as the ratio between the maximum field  $E_{max}$  and minimum field  $E_{min}$  determine the qualitative change in the shape of the domain with an increase in the external field.

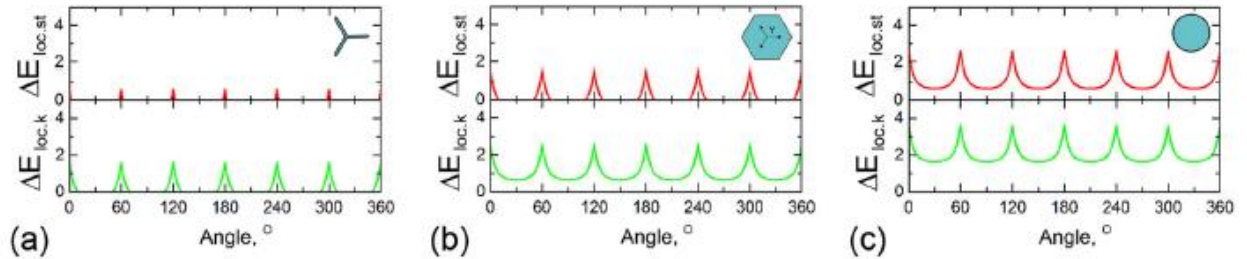


Figure 1.20 – Angular dependences of the excess of the local field over the threshold values for the motion of the kink  $\Delta E_{loc,k}$  and the generation of steps  $\Delta E_{loc,st}$  in domains of various shapes: (a) dodecagons, (b) hexagons, (c) round

There are three types of angular dependencies: (Figure 1.20). (1) Limited regions of step generation and kink motion lead to the formation of dodecagon-shaped domains (Figure 1.20a). (2) The limitation of the step generation area and the possibility of kinks moving along the whole wall led to the formation of polygonal domains (Figure 1.20b). (3) the formation of round domains is possible due to the generation of steps and the motion of kinks along the whole length of the wall (Figure 1.20c).

Dodecagon-shaped domains, a concave irregular polygon with three arms (flat-walled stripe domains) and twelve corners (Figure 1.21), appear when kink motion is restricted to narrow regions close to the apexes at  $E_{th,k} > E_{min}$  (Figure 1.21a). An increase in the external field leads to an increase in the width of the stripe domains.

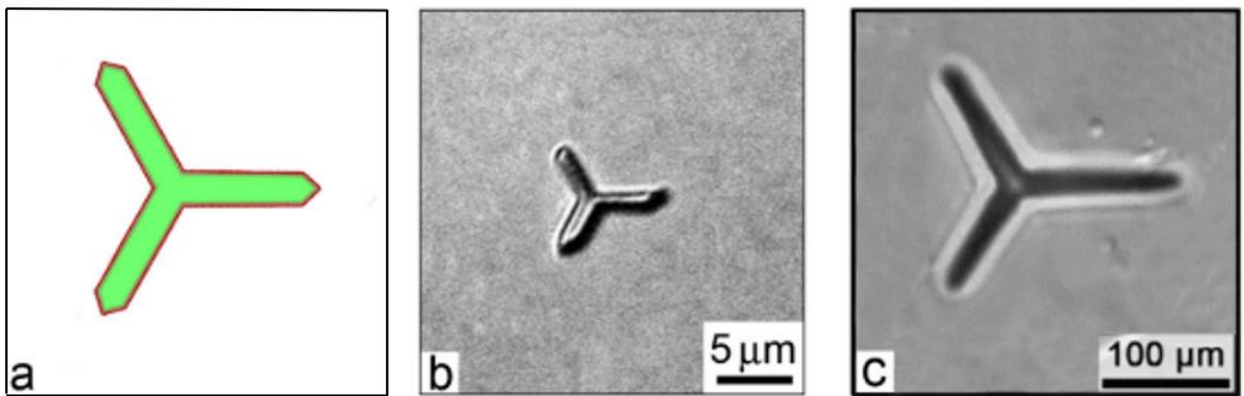


Figure 1.21 - Dodecagon domains: (a) scheme, (b, c) optical images in CLN with a surface dielectric layer

### 1.3.3 Evolution of the domain structure under pulsed IR laser irradiation

Pulsed irradiation of LN with IR laser radiation with a wavelength of  $\lambda = 10.6 \mu\text{m}$  leads to the formation of self-similar (fractal) structures consisting of domain beams (strip domains) of submicron width [92].

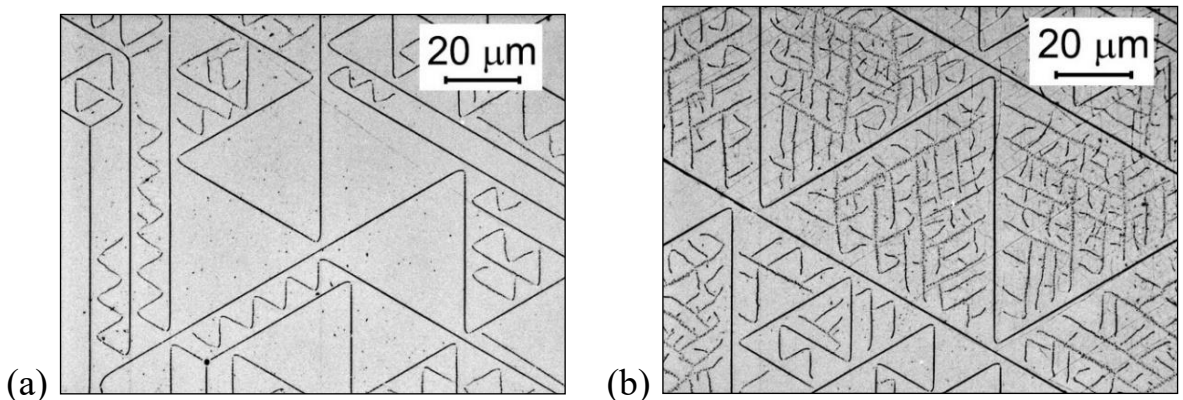


Figure 1.22 - Self-similar domain structures formed because of pulsed irradiation with an IR laser: (a) without branching and (b) with intense branching. optical microscopy

Most of the irradiated zone of the irradiated zone is usually occupied by self-similar structures. They are ensembles consisting of equilateral triangles and regular zigzags formed in the process of interaction of domain rays growing in different Y directions (Figure 1.22a). When "reflection" occurs, the beam growth changes by  $120^\circ$  (Figure 1.23), this behavior is due to electrostatic interaction. For this interaction, an important feature can be distinguished, the beams did not intersect, and a common characteristic of the entire irradiated zone was a certain distance at which the beams were "reflected".

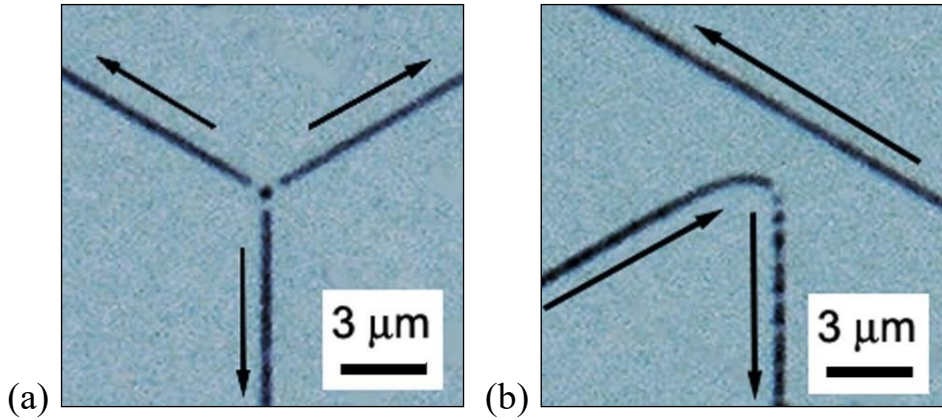


Figure 1.23 - (a) A triplet formed during the growth of rays from an isolated nanodomain inside the irradiation zone. (b) Reflection (discrete change in growth direction). Arrows indicate the direction of ray growth. optical microscopy

In [60], thanks to *in situ* visualization, the kinetics of the domain structure was studied in detail when irradiated with a laser with a long wavelength  $\lambda = 10.6 \mu\text{m}$  (Figure 1.24). It was shown that the evolution of DS is the growth of nanodomain chains leading to the formation of self-ordered quasi-regular structures (Figure 1.24). It was also shown that cooling of the samples leads to the beginning of switching after the end of laser heating. Three stages were distinguished in the kinetics of anisotropic nanodomain chains: nucleation, growth of domain chains, and chain branching. The demonstrated scenario of the evolution of the domain structure was explained as follows: the driving force was the pyroelectric field that appeared because of sample cooling, and the absence of electrodes and an external circuit deprived the sample of the possibility of effective screening. Inefficient screening and high speed characterized the process as strongly non-equilibrium.

Also, inside the irradiated area, the growth of domain rays from an isolated nanodomain in three equivalent Y directions, the formation of triplets was observed (Figure 1.24a).

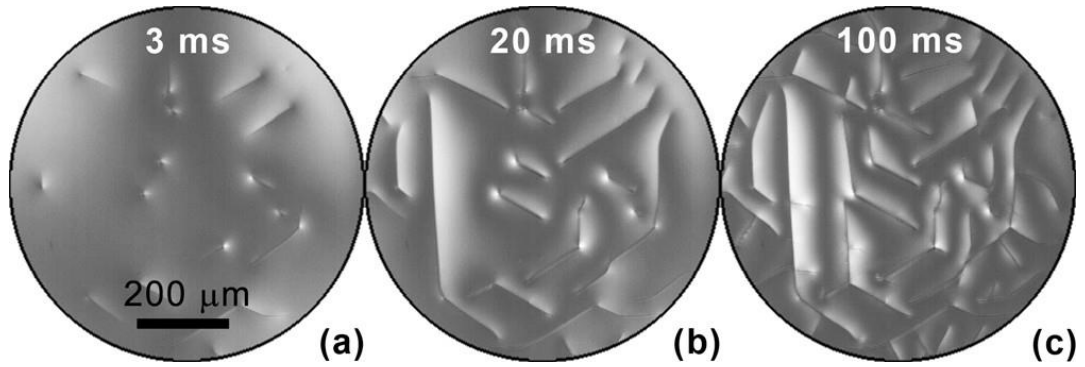


Figure 1.24 – *In situ* rendered instantaneous images of the domain structure. Three stages of domain structure evolution: (a) nucleation, (b) growth, (c) branching. Optical microscopy in crossed polarizers [93]

The anomalous scenario of domain structure evolution observed in the described experiments was explained within the framework of the kinetic approach. It should be noted that, in this case, no external electric field was applied to the sample and there were no electrodes on the surface of the sample; thus, switching of spontaneous polarization was realized under conditions of low efficiency of external screening. The appearance of new domains leads to the appearance of an uncompensated depolarizing field of bound charges, which causes an unusual self-organized behavior of nanodomain structures.

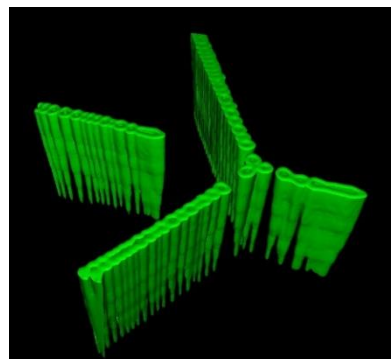


Figure 1.25 - Three-dimensional SHGM image of a ridge domain in CLN that appeared after irradiation with a laser pulse.

Further studies showed that irradiation of a single-domain sample with the first laser pulse leads to the appearance of stable narrow one-dimensional (1D) stripe domains with a width of about a micron on the surface in the entire irradiated zone

(Figure 1.24). A three-dimensional image of a stripe domain in the bulk, obtained with the help of SHG, made it possible to reveal the comb shape of these domains with charged domain walls (CDWs) [94]. The depth of germination of domains is from 30 to 70  $\mu\text{m}$  (Figure 1.25). The length of the teeth is from 5 to 7  $\mu\text{m}$  (from 0.1 to 0.2 of the total domain depth), the period of the teeth is about 1  $\mu\text{m}$ .

### 1.3.4 Shape stability effect

For the growth of hexagonal domains in CLN, the effect of shape stability is observed, which is an ultra-fast restoration of the hexagonal shape of the domain resulting from the merging of two domains (Figure 1.26). In this case, the convex shape and the orientation of the domain walls along the Y direction are restored.

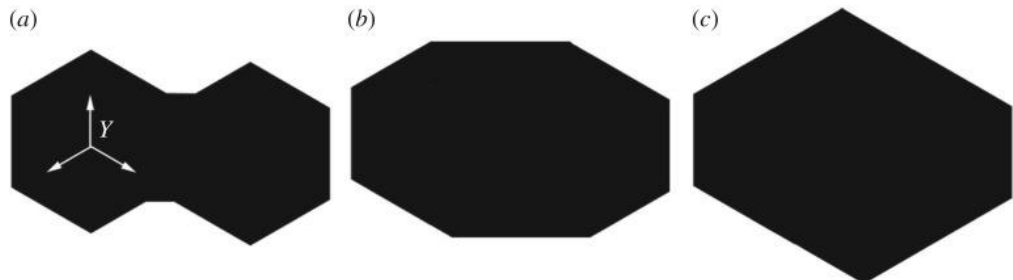


Figure 1.26 - Schematic representation of the main stages of the shape stability effect. [95]

Three stages can be distinguished in the shape recovery process: (1) after merging, a polygon with two concave corners (10 Y walls and 2 X walls) appears, (2) rapid overgrowth of concave corners, which leads to the formation of a domain with only convex corners (6 Y walls and 2 X walls), (3) restoration of the hexagonal shape (6 Y walls).

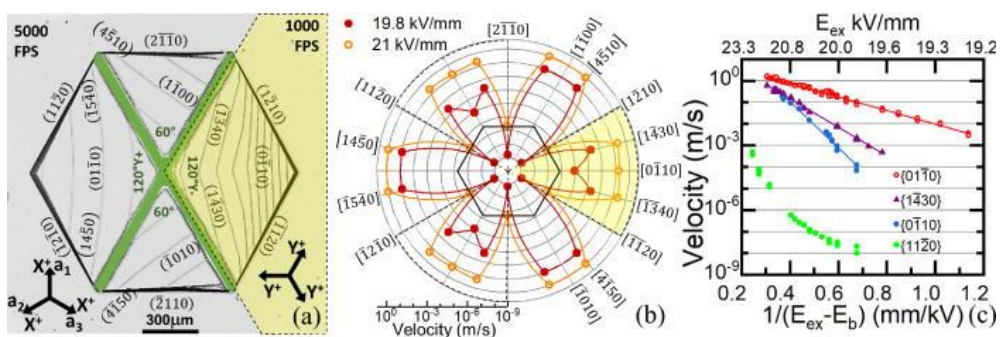


Figure 1.27 - The sequence of positions of domain walls (kinetic map) during the growth of the X-shaped domain highlighted in green.  $E_{ex} = 20.7 \text{ kV/mm}$ ; video frame rate is 5000 frames

per second. (b) Wolfe diagram. (c) Field dependence of the velocities of domain walls of various orientations. CLN

The orientation dependence of the domain wall velocity was experimentally measured in CLN [96]. The constructed angular velocity dependence (Wulff diagram) (Figure 1.27) showed that the velocity of the fastest domain wall exceeds the velocity of the hexagonal domain wall (Y-oriented) by more than three orders of magnitude. Ultrafast domain walls are formed because of domain fusion and are short-lived. It should be noted that the shape retention effect is not observed when switching at temperatures above.

## 1.4 Regular domain structures

Forty years ago, the idea of creating stable and regular domain structures for optimizing the properties of ferroelectric crystals first appeared [97]. It was proposed to change the piezoelectric properties of ferroelectrics by creating stable domain structures. They argued that a domain structure of a given geometry would make it possible to control the spectrum of resonant frequencies and realize very high frequency regimes [97].

Currently, domain engineering methods are successfully used to create laser frequency converters with record efficiency [98].

### 1.4.1 Quasi phase matching

The development of nonlinear optics is associated with the creation of lasers - powerful sources of coherent radiation. It is known that in the case of falling into an electric field, polarization occurs in dialectics. The polarization  $P(t)$  depends linearly on the field strength if the field is weak. But the application of a strong field causes nonlinear effects, which are associated with the dependence of the polarization of higher degrees of intensity. In the general case, by expanding the polarization in terms of the strength of the external field, one can observe:

$$P = \epsilon_0(\chi^{(1)}E + \chi^{(2)}E^2 + \chi^{(3)}E^3 \dots) \quad (1.10)$$

where  $\chi(i)$  are the susceptibilities describing the nonlinear effects of the i-th order.

The response of the medium, which is proportional to the doubled frequency  $\omega$ , can be observed due to the presence of a non-zero second-degree susceptibility  $\chi^{(2)}$ ,  $E(t) \sim \cos(\omega t)$ , in other words, at each point of the crystal one can observe the formation of photons with doubled energy and twice the absorbed frequency (SHG, second harmonic generation) [99]. When light passes through a nonlinear medium, one can observe the interaction of photons with each other (parametric generation of light), a change in the frequency of light. Such effects are widely used in sources of coherent radiation with a tunable wavelength, for example, to generate radiation with frequencies different from the frequency of the pump wave [100], to generate photons with desired properties [101], to control the amplitude and phase [102, 103], etc. To implement a nonlinear optical effect, it is fundamental to fulfill the phase-matching condition [99]. For example, for SHG, when light passes through a nonlinear medium of length  $L$  parallel to a certain direction  $z$  of frequency  $\omega$ :

$$E_\omega(z, t) = E_1 \cos(\omega t - k_1 z), \quad (1.11)$$

causes a nonlinear polarization response at the frequency  $2\omega$ :

$$P_{2\omega}(z, t) = \epsilon_0 \chi^{(2)} E_\omega^2 = \frac{1}{2} \epsilon_0 \chi^{(2)} E_1^2 \cos(2\omega t - 2k_1 z), \quad (1.12)$$

where  $E_1$  and  $k_1$  are the oscillation amplitude and the wave vector  $E_\omega$ , respectively.

The generated wave at the frequency  $2\omega$  at the exit from the crystal will have the form:

$$\begin{aligned} E_{2\omega}(L, z, t) &= E_0 \cos(2\omega t - 2k_1 z - k_2(L - z)) = \\ &= E_0 \cos(2\omega t - \Delta k z - k_2 L), \end{aligned} \quad (1.13)$$

where  $k_2$  is the wave vector of the wave with the frequency  $2\omega$ ,  $E_0 \sim \chi^{(2)} E_\omega^2$  characterizes the amplitude of the wave with the frequency  $2\omega$ ,  $\Delta k = 2k_1 - k_2$  is the detuning of the wave vectors.

During interaction, secondary waves propagating in space will be generated at each point of the nonlinear medium. Then at the exit from the nonlinear medium

(z=L) one can observe a wave with a frequency  $2\omega$ , which is the sum of all secondary waves. It can be shown:

$$E_{2\omega}(L, t) \sim L \frac{\sin(\Delta k L/2)}{\Delta k L/2}. \quad (1.14)$$

When the phase matching condition is realized, there is no phase mismatch  $\Delta k=0$ , which leads to an increase in the intensity of the second harmonic with distance (Figure 1.28). For the condition of phase matching to be fulfilled, the effect of birefringence is usually used, choosing a certain direction in the crystal. In the case of SHG, such a direction is chosen that for waves with frequencies  $\omega$  and  $2\omega$ , ordinary and extraordinary, respectively, the refractive indices are equal. However, the maximum value of the tensor  $\chi^{(2)}$ , does not correspond to the chosen direction, which leads to a decrease of the conversion efficiency. When the wave detuning is not equal to zero, oscillation of the wave intensity by twice the frequency will be observed with distance (Figure 1.28). Long coherence  $l_c = \frac{\pi}{\Delta k}$ . is the distance at which the amplitude of the second harmonic reaches its maximum.

The creation of an PDS with a width of stripe domains equal to  $l_c$  makes it possible to implement the condition of phase quasi-phase matching. In this case, the sign change  $\chi^{(2)}$  at the boundaries between the domains provides a further increase in the intensity of the propagating wave (Figure 1.28) [99,100]. The implementation of phase quasi-matching makes it possible to use directions with the maximum values of the tensor  $\chi^{(2)}$ , which provide a record efficiency of wavelength conversion.

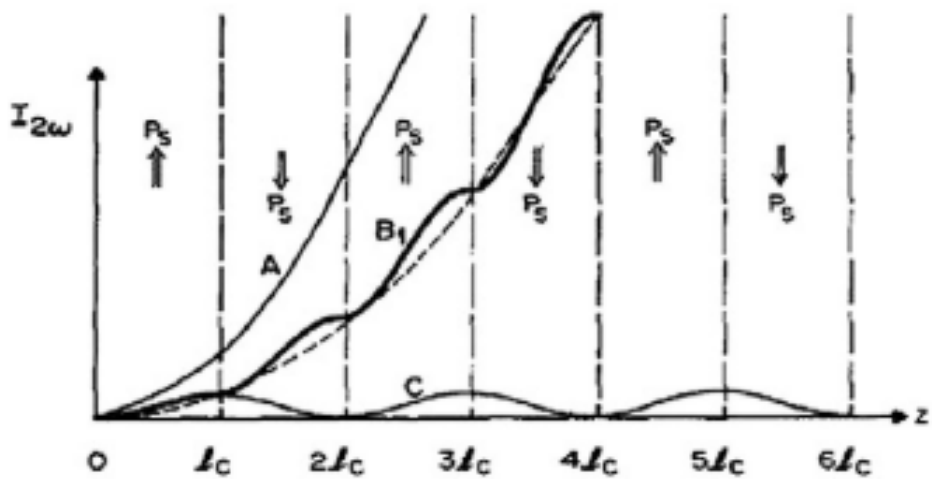


Figure 1.28 - The intensity of the second harmonic: (A) with phase matching in a single-domain crystal, (B) with phase quasi-matching, (C) in the absence of phase matching [9].

#### 1.4.2 Methods for creating regular domain structures.

In 1980, PDS was obtained for the first time in LN [104, 105], PDS was realized by alternating growth layers during crystal growth by the Czochralski method. In 1985, PDS was obtained in LN during crystal growth with a change in the electric field [106]. Miniature LN rods with PDS were also grown using laser heating [107]. Regular structures of shallow domains were created in channel waveguides obtained by Ti diffusion [108].

PDS with the application of an external electric field using periodic strip electrodes obtained by lithography was first fabricated in a thin CLN plate in 1992 [109]. Blue light SHG was obtained due to the structure with a period of 2.8  $\mu\text{m}$ . In a short period of time, polarization reversal by an external electric field was successfully applied to create a through PDS in CLN plates with a thickness of 0.5 mm. A number of nonlinear optical effects have been successfully demonstrated on samples with RDS [110–113]. Later, PDS was obtained in LN doped with MgO, which has an increased optical damage threshold [114, 115].

The method of using periodic strip electrodes has the following advantages: (1) a well-developed lithography method, applicable to any ferroelectric materials, (2) the ability to apply the method to the whole LN wafer, (3) relatively low cost, (4) a large selection of electrode materials and configurations as well as good control

over the process of application of an external electric field makes the method very flexible (5) the possibility of creating end-to-end DS, (6) the ability to combine with the production of waveguides. At present, the method of applying an inhomogeneous external electric field is the most developed, which makes it possible to obtain a commercially available LN with a through PDS with a period of up to 4  $\mu\text{m}$ .

The creation of an PDS with submicron periods opens new possibilities controlled by the electro-optical effect of Bragg gratings, as well as by backward-wave HHG. To implement such scenarios of nonlinear optical interactions, a structure period of about 300 nm is required. Implementation by switching by an external field with optimization of all stages made it possible to obtain a shallow PDS with a period of 400 nm [116, 117].

The use of various self-organization techniques can be an alternative technique for creating PDS with submicron periods. Nanodomains with a period of up to 100 nm were obtained by the method of controlled backswitching in CLN [118].

Despite the significant advantages of the described method, there are unsolved problems that prevent the creation of strip electrodes with submicron periods, such as domain fusion [119] and uncontrolled backswitching [118]. The search for alternative solutions leads to the development of new methods for creating PDS, for example, scanning with a focused electron beam.

#### **1.4.3 Electron beam lithography**

In 1986, the idea of creating an PDS was first proposed by teaching the surface of a ferroelectric material with a focused electron beam [120]. A periodic gold grating was deposited on the Z-polar surface of the CLN sample, a field of 10 V/cm was applied, and switching was carried out at a temperature of 580°C. Later, PDS was obtained in LN using a metal mask and with the same switching parameters [121].

Further development of the method of electron beam irradiation made it possible to create PDS at room temperature and without applying an external field

but using a grounded electrode on a non-irradiated surface [122, 123]. Using a scanning electron microscope with a lithographic attachment, PDS with a period of 6  $\mu\text{m}$  were obtained [124, 125].

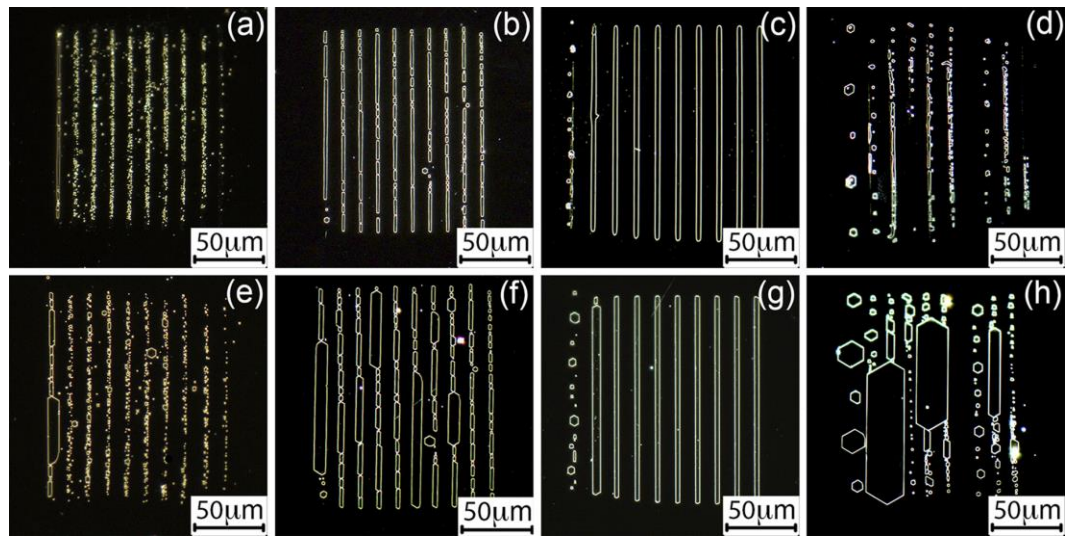


Figure 1.29 - Typical DS after irradiation with a focused electron beam in MgOLN: (a–d) Z- and (e–h) Z+ polar surfaces. (a) and (e)  $U = 7 \text{ kV}$ , (b) and (f)  $U = 8 \text{ kV}$ , (c) and (g)  $U = 10 \text{ kV}$ , (d) and (h)  $U = 12 \text{ kV}$ . Dose  $1.5 \text{ mC/cm}^2$  [132]

The deposition of a thin dielectric layer on the irradiated polar surface made it possible to localize electrons on the surface [126]. Thanks to the deposited photoresist layer, the accelerating voltage was reduced to 5 kV and one- and two-dimensional PDSs were obtained [127]. Optimization of the layer thickness and accelerating voltage made it possible to obtain a through DW in a CLN plate 1 mm thick [128]. Successful results of polarization reversal have been demonstrated on nonpolar cuts of lithium niobate [129], on the Z+ polar surface, and in waveguides fabricated by titanium diffusion [130] and proton exchange [131].

The author of [132] demonstrated a technique for creating a through PDS in LN doped with MgO (MgOLN). A foresist was used to localize electrons on the Z- polar surface of the sample. Figure 1.29 shows how the switched region changes with a change in the accelerating voltage.

## 1.5 Optical waveguides

### 1.5.1 Basic concepts

The twentieth century was marked by the rapid development of such industries as computer technology and microelectronics, which causes qualitative changes in the life of all humankind. New devices are being created that allow processing and storing information at a fundamentally new level. In terms of its significance, the creation of such technologies is comparable to the introduction of integrated circuits and microprocessors. Soon, the transition to fully optical information processing.

An optical waveguide is a structure in which, due to spatial inhomogeneity, light can propagate and serve to transmit it. Typically, the region of the waveguide intended to transmit light has a refractive index higher than the refractive index of the medium. It is now believed that optical waveguides are the most advanced technology for transmitting gigantic amounts of data over vast distances.

According to the type of construction, all optical waveguides can be divided into planar and channel (Figure 1.30). In a planar waveguide, light can propagate in two directions, and in a channel waveguide, in one direction.

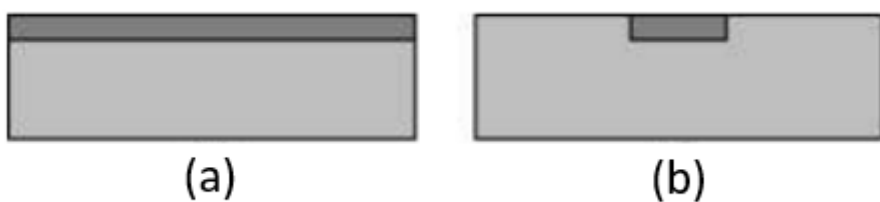


Figure 1.30 - Scheme (a) of a planar waveguide (b) of a channel waveguide

Optical fiber is a channel fiber waveguide widely used for information transmission. With the help of optical fiber, it is possible to transmit information over long distances. Integrated planar or channel waveguides are usually used in integrated optical circuits and serve for local transmission of light and information processing. The fiber is pulled out of the preform - a large glass rod.

Features of light propagation in optical waveguides are very different from classical "three-dimensional" optics.

Suppose there are two isotropic and homogeneous dielectrics with refractive indices  $n_1$  and  $n_2$ . Let there exist a light wave incident on the boundary of these materials and the angle of incidence to the normal drawn to the point of incidence equals  $\theta_1$ . Then the incident wave will separate. Part will be reflected at an angle  $\theta_1$ , and part will be refracted at an angle  $\theta_2$  (Figure 1.31). The angle of refraction is related to the angle of incidence by Snell's law:

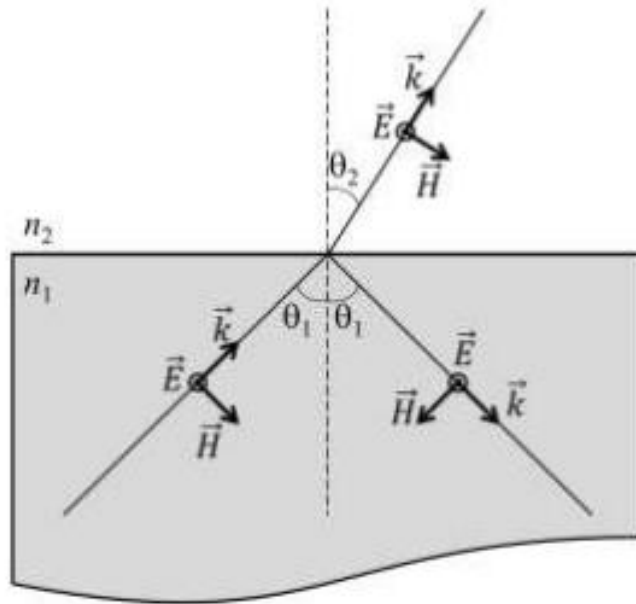


Figure 1.31 - Reflection of a light wave from the boundary of two media

All waves can be divided into two types of TE and TM waves. The difference between TE and TM waves lies in the plane of the electric field strength vector or wave polarization. For TM waves, the polarization vector lies in the plane of incidence, while for TE waves, the polarization vector is perpendicular to the plane of incidence (Figure 1.31).

It can be noted that if the angle of incidence in Snell's law corresponds to the  $n_1 \sin \theta_1 > n_2$  ratio, then the light will not be able to penetrate the medium whose refractive index is  $n_2$ , and the effect of total internal reflection will be observed. The critical angle  $\theta_c$  can be found as follows:

$$\sin \theta_c = \frac{n_1}{n_2} \quad (1.15)$$

If the propagation angle of the light wave  $\theta$  satisfies the condition of total internal reflection, then the light wave will always remain inside the waveguide. In a medium with a refractive index  $n_1$ , the direction of propagation of monochromatic light with a frequency  $\omega$  (wavelength  $\lambda$ ) is determined by the vector  $\vec{k}n_1$ , where  $\vec{k}$  is the wave vector ( $|\vec{k}| = k = 2p/l = w/c$ , and  $c$  is the speed of light in vacuum). The propagation constant of a light wave is the expression:  $\beta = kn_1 \sin \theta$  is the propagation constant of a light wave, which is the Z-component of the vector  $\vec{k}n_1$ .

All light waves inside the waveguide can be divided into waveguide and radiative. Radiative modes leave the waveguide and cannot propagate in it. The waveguide modes, on the other hand, satisfy the condition and form a standing wave between the waveguide boundaries and can propagate inside the waveguide. Such a mode arises only for certain discrete values of the angle  $\theta$  and the propagation constant  $\beta$ .

A simple model representation of a channel waveguide (Figure 1.32) can be a rectangular area with a changing jump refractive index. However, it has not yet been possible to find exact analytical solutions for channel waveguides.

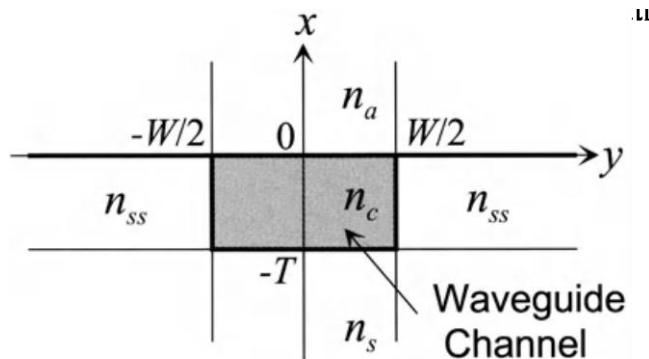


Figure 1.32 - Section of a rectangular channel waveguide [133]

To obtain the most accurate representation of the intensity  $|E_y(x, y)|^2$  (Figure 1.33) propagating through a channel waveguide, the Markatili method [134] can be used.

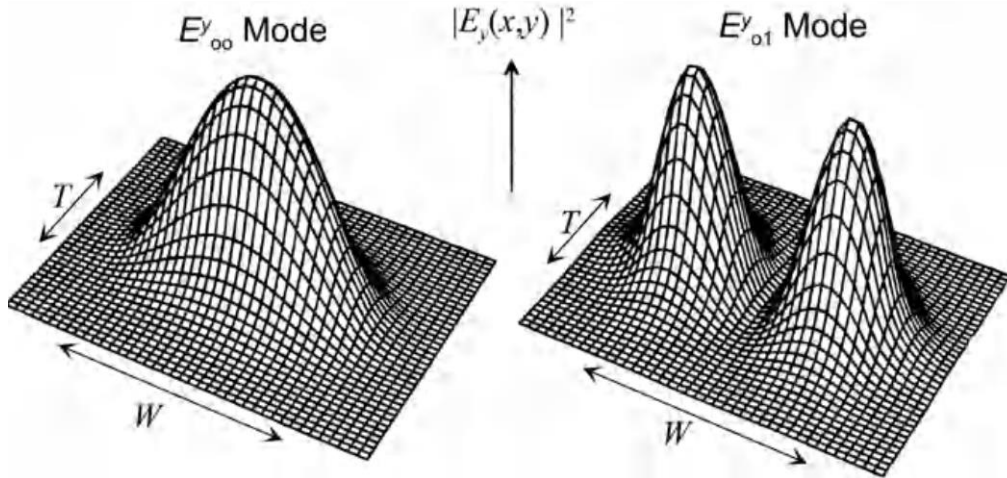


Figure 1.33 - An example of the intensity distribution of modes propagating along a channel waveguide [133]

The TE and TM modes propagate in the channel waveguide. Using computational techniques based on the finite element method [134] or the finite difference method [134], it is possible to obtain modes that are quasi-TE and quasi-TM.

Usually, for use in nonlinear optical devices, waveguides are created along one of the crystallographic axes of the crystal, which leads to a significant reduction in losses. So, for example in LN, waveguides are created along the X crystallographic direction. When creating a waveguide in LN cut perpendicular to the Z-axis, the refractive index for the extraordinary wave ne increases. Only the TM wave can propagate in such a waveguide.

### 1.5.2 Types of waveguides

All existing optical waveguides in CLN can be divided into three fundamentally different types: (1) ridge, in which, due to the removal of a part of the crystal, a ridge is formed on the surface, in which light propagates, (2) diffusion, created by changing the refractive index in the near-surface layer due to impurity diffusion, (3) recorded, a femtosecond laser is usually used to create a waveguide, laser radiation causes a rearrangement of the crystal lattice and refractive index.

Ridge waveguides are usually created in CLN. Recently, thin LN films on an insulating substrate (LNOI) have been used [135]. The ridge is created by: (1)

precision cutting [136], (2) ion beam etching [137], (3) chemical etching [138]. A clear advantage of ridge waveguides is the preservation of the optical properties of CLNs.

Diffusion waveguides are created by diffusion of titanium or zinc [139, 140]. The technique is as follows, a layer of titanium is applied to the surface of the crystal, and titanium is diffused at 1100°C. [141]. In a Ti-diffuse waveguide, the refractive index of both the ordinary and extraordinary waves changes (the maximum increase is  $\Delta n_e \sim 0.022$ ,  $\Delta n_o \sim 0.007$ ) [139]. It should be noted that the creation of a waveguide can lead to polarization reversal and the creation of an undesirable domain structure [142, 143]. Losses in such a waveguide can reach 0.15 dB/cm.

An alternative to Ti-diffuse waveguides are Zn-diffuse waveguides. The manufacturing technology of such waveguides is characterized by a lower temperature of about 900°C [144]. A change in the refractive index also occurs for both extraordinary and ordinary waves (the maximum increase is  $\Delta n_e = \Delta n_o \sim 0.005$ ) [145]. Losses in a Zn diffuse waveguide can be as high as 0.3 dB/cm [146].

Proton exchange consists in replacing lithium ions with hydrogen ions in the near-surface layer.

### **1.5.3 Method for creating waveguides by proton exchange.**

Proton exchange is a method of creating waveguides in LN, since  $\text{Li}^+$  ions are replaced by  $\text{H}^+$  protons from any source in the LN crystal lattice to form  $\text{Li}_{1-x}\text{H}_x\text{NbO}_3$ . Usually, a weak organic acid, in liquid or gaseous phase, acts as a source of protons. For example, benzoic acid (BA) and toluic acid. Proton exchange is carried out at temperatures from 150 to 400 °C, as a rule, in some closed medium. Usually, sealed glass ampoules or metal reactors are used. During proton exchange, the refractive index for the extraordinary wave in the modified layer increases, which makes the modified layer a waveguide.

Formed because of proton exchange, the modified layer with the composition  $\text{Li}_{1-x}\text{H}_x\text{NbO}_3$  has a complex phase composition. In total, seven phases are distinguished (called  $\alpha$ ,  $\kappa 1$ ,  $\kappa 2$ ,  $\beta 1$ ,  $\beta 2$ ,  $\beta 3$ ,  $\beta 4$ ) [147-149] depending on the proton

concentration  $x$  and crystallographic lattice parameters. The formation of certain phases depends on the temperature at which the exchange process takes place and the properties of the proton source (Figure 1.34) [148]. Usually  $x$  has a local character, the formation of new phases occurs in layers. The change in  $\Delta n_e$  caused by the change in the parameters of the crystallographic lattice occurs in jumps at the boundary between the layers. Each phase has its own nonlinear optical coefficients and optical losses. Changes in the duration and temperature of proton exchange determine not only the waveguide profile, but also the values of the electro- and nonlinear optical coefficients [150].

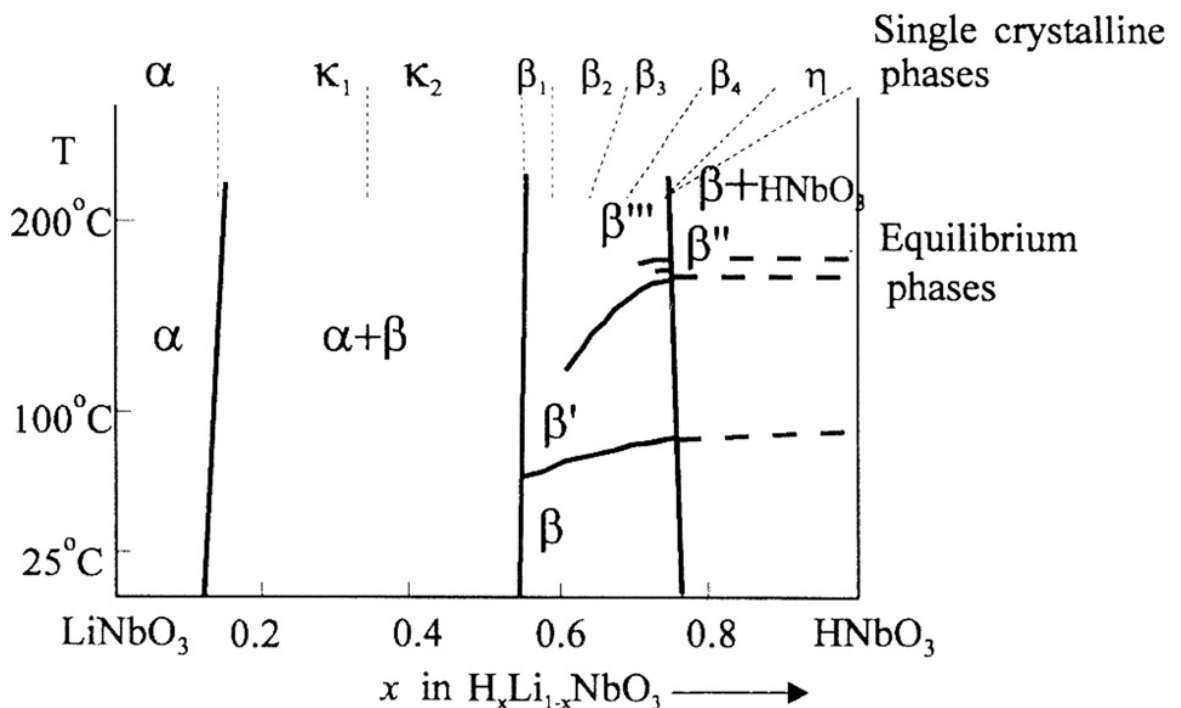


Figure 1.34 - Phase diagram of  $\text{Li}_1-x\text{H}_x\text{NbO}_3$  [148]

The use of proton exchange in pure benzoic acid usually causes the loss of ferroelectric and nonlinear optical properties in the modified layer. The refractive index for an extraordinary wave  $\Delta n_e$  in this case increases and can reach a value of 0.1. For waveguides obtained by exchange in pure benzoic acid, a stepped profile is characteristic, the refractive index for an extraordinary wave change abruptly with depth. Also, such waveguides are also characterized by a significant decrease of electro-optical coefficients, strong scattering, and losses, as well as instability in

time. These features make it impossible to use such waveguides in nonlinear optical devices.

In the case of additional annealing in air at a temperature of 300–400°C for several hours (annealed proton exchange, APE) [151,152], one can observe a partial recovery of the nonlinear optical coefficients and an increase in the optical damage threshold. The annealing process leads to the fact that the profile of the refractive index changes with depth and acquires a smooth, falling character, then such a profile is called a gradient. In a waveguide created by the APE method, in the near-surface modified layer, the nonlinear optical coefficients decrease and can reach zero. If annealing is carried out in an atmosphere rich in Li<sup>+</sup> ions at a temperature of 300-400 °C [153], one can observe a complete recovery of the nonlinear optical coefficients, a shift deep into the crystal of the maximum of the waveguide profile, this procedure is called reverse proton exchange (reverse proton exchange, RPE). Experiments with APE/RPE waveguides have shown that in the telecommunications wavelength range, the SHG efficiency  $\eta = 150\%/(W \cdot cm^2)$  was observed [154].

To slow down the process of diffusion of protons into the LN crystal and optimize the properties of the waveguides, lithium benzoate (LB) is added to the mixture for exchange into benzoic acid. The LB concentration can be defined as  $\rho = mLB/(mLB + mBA) \times 100\%$ , where  $mLB$  and  $mBA$  are the masses of LB and BA, respectively. Two types of proton exchange are distinguished using BL soft proton exchange (SPE) [155] when the concentration is more than 2.7% and soft proton exchange with a high refractive index change (High Index Soft Proton Exchange, HISoPE) [156] then the concentration of LB in the aisles is from 2.0 to 2.4%. The SPE and HISoPE processes are usually carried out at temperatures of 300–350°C [157]. The SPE process requires fewer phases than RPE, which makes it simpler [155], but the main thing is that SPE waveguides preserve the nonlinear optical and ferroelectric properties of the crystal. It is important to highlight the fact that during the process, good reproducibility of results and high electro-optical

efficiency are observed [158]. SPE waveguides are characterized by a gradient profile.

Using the SPE method, optical waveguides and devices are fabricated: optical modulators [159] and switches [160], multiplexers and splitters [161]. Losses in SPE waveguides are from 0.086 dB/cm.

## 1.6 Brief conclusions

Based on the literature review, the following brief conclusions can be drawn:

1. The process of polarization reversal is determined by the local electric field, in which it is necessary to consider both the external field applied to the sample and the residual depolarizing field.
2. In the evolution of the domain structure in the process of polarization reversal, the screening efficiency of the depolarizing field plays a key role.
3. Scanning probe microscopy methods can be used to create and visualize the domain structure in LN single crystals.
4. The shape of the growing domains in LN during polarization reversal is determined by the angular dependence of the velocity of the domain walls.
5. SPE LN waveguides, characterized by low losses and a gradient profile, are of interest for creating high-performance devices for wavelength conversion.
6. The study of the evolution of the domain structure in SPE CLN is of interest both from a practical point of view (creation of waveguides with PDS) and from a theoretical point of view for studying the kinetics of a domain structure under highly nonequilibrium conditions in the presence of a composition gradient.

## 2 Studied samples, experimental setups, and methods.

### 2.1 Studied samples.

Lithium niobate samples with a surface layer modified by the proton exchange were single-crystal single-domain CLN plates 0.5 mm thick and 5x5 mm<sup>2</sup>, cut perpendicular to the polar axis. The polar surfaces were polished to an optical quality. The plates were subjected to soft proton exchange lasting from 12 to 72 hours.

The proton exchange was carried out at a temperature of 300°C in benzoic acid with the addition of lithium benzoate. For proton exchange, the sample was fixed in the upper part of the zirconium container (Figure 2.1a). To reduce the effect of water vapor, the container with the sample was annealed in vacuum at 110°C. Subsequent manipulations with the container were carried out in a dry atmosphere. A source of protons was placed in the lower part of the container (Figure 2.1a). Then the container was hermetically sealed and pumped out to 10<sup>-3</sup> mbar.

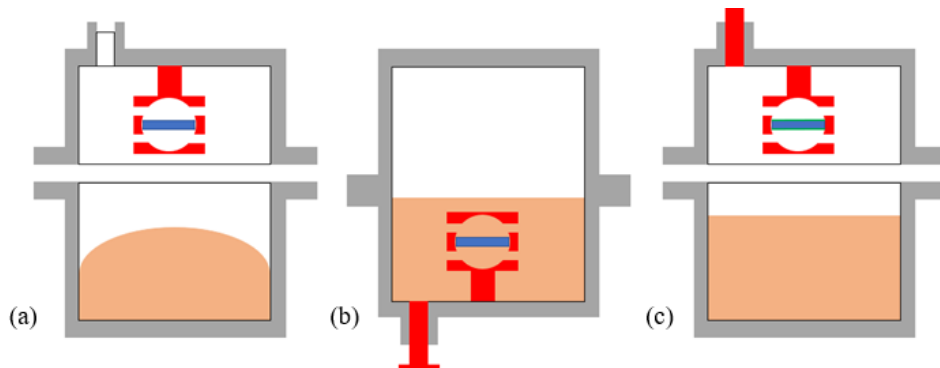


Figure 2.1 - Stages of the proton exchange. (a) – assembling of a cell, (b) – the proton exchange, (c) – completion of the proton exchange

The container heated up to 300°C would be turned over (Figure 2.1b) and the sample would be dived into the proton source. After the exchange had completed the container would be turned over and cooled down to the room temperature (Figure 1c). The rate of temperature changes did not exceed 5°C/min.

As a result of proton exchange, the  $H_xLi_{1-x}NbO_3$  compound was formed in the near-surface layer with an inhomogeneously distributed H<sup>+</sup> concentration over the depth.

## 2.2 Experimental methods

### 2.2.1 Study of the evolution of the domain structure during polarization reversal in a uniform electric field

For *in situ* imaging of the evolution of the domain structure during polarization reversal in a uniform field, the sample was placed in a cell with transparent liquid electrodes based on a saturated LiCl solution (Figure 2.2). The measurement setup was made based on an LMA10 optical microscope (Carl Zeiss, Germany) with a high-speed FC13 video camera (FastMotion, USA) with a frame rate of up to 400 fps and a maximum resolution of 1280x1024 pixels.

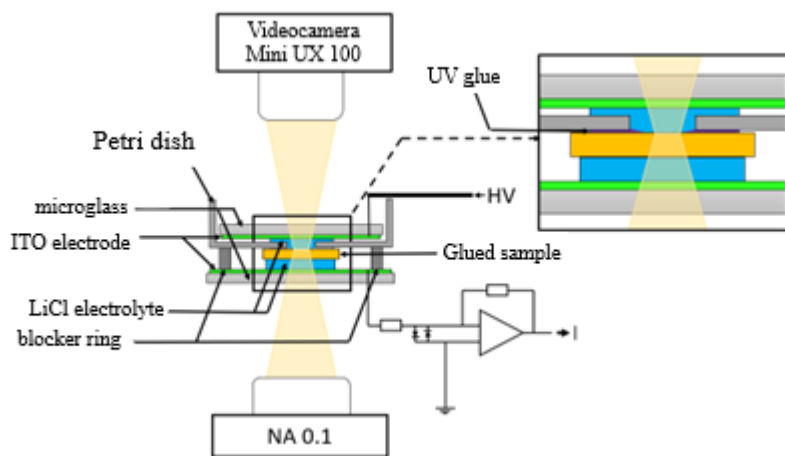


Figure 2.2 - Setup schema for switching polarization in the uniform field with *in situ* imaging of the domain structure kinetics.

Switching was carried out in a constant field with rectangular pulses (Figure 2.3a) with a duration of up to 300 s and an amplitude of 0.1 to 25 kV / mm, as well as in a growing field with triangular pulses (Figure 2.3b) with a field increase rate of 200 V / (mm·With). The pulses were generated by an ADC/DAC board PCI-6251 (National Instruments, USA) or an AFG1022 signal generator (Tektronix, USA) and amplified using a Trek 20/20c high-voltage amplifier (Trek inc., USA).

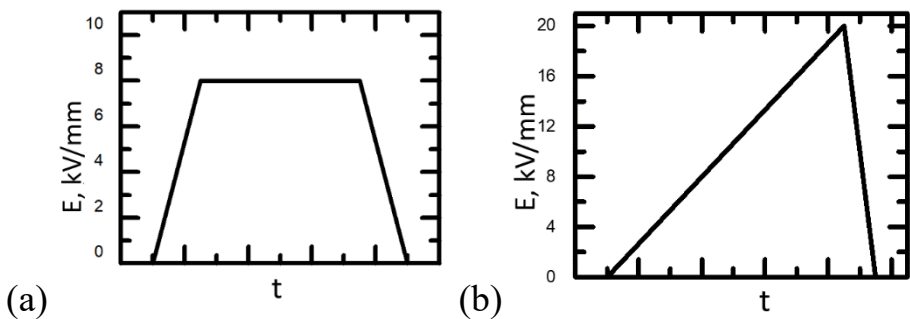


Figure 2.3. Pulse waveforms: (a) – steady-state field, (b) – growing field

To determine the values of the threshold fields corresponding to the appearance of the first optically distinguishable stripe domains, switching in a growing field was used (Figure 2.3). To determine the threshold field for the appearance of hexagonal domains, switching in a constant field by rectangular pulses with a duration of 100 ms was used.

### 2.2.2 Local switching

To create isolated domains and domain structures using the local switching method, as well as to visualize domain structures on the surface, the PFM method was used. PFM was performed using an Ntegra Aura scanning probe microscope (NT-MDT, Russia). Silicon probes with a carbon-tungsten conductive coating HA\_NC/W2C (ScanSens, Germany) were used. A voltage of up to 300 V was applied to the probe, the sample was heated to 100°C, while the controlled rate of heating and cooling did not exceed 5°C/min. Switching pulses were generated using an NI-6251USB data acquisition board (National Instruments, USA) and amplified using a Trek-677B high-voltage amplifier (TREK, USA).

Local switching was carried out in an atmosphere with a controlled humidity of 25%. Humidity was measured using a built-in humidity sensor.

### 2.2 Measuring the dependence of H<sup>+</sup> concentration on depth.

The depth dependence of the H<sup>+</sup> concentration (C(z)) near the sample surface was determined by CRM using a confocal Raman microscope Alpha 300 AR, WiTec (Germany), equipped with a solid-state laser with a wavelength of 488 nm and a power of up to 27 mW and a diffraction grating with 1800 pcs/mm, which provided

a spectral resolution of  $1.2\text{ cm}^{-1}$ . The spatial resolution for the 100x objective was about 300 nm.

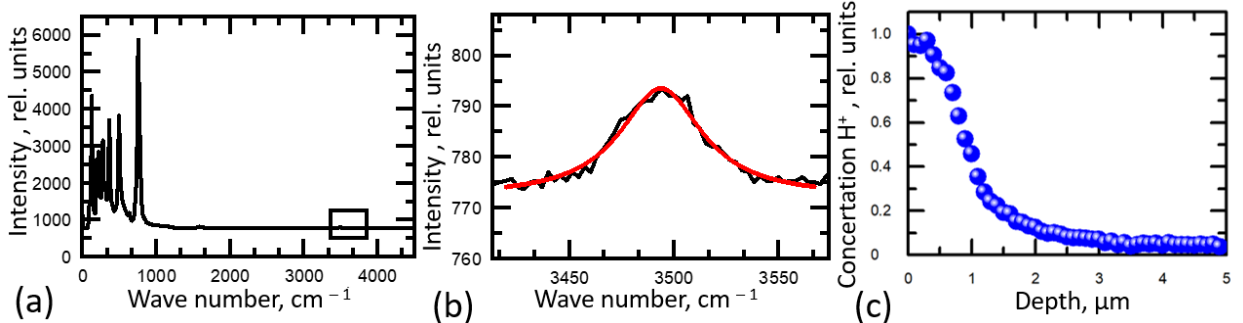


Figure 2.4 - (a) – Raman spectrum SPE CLN. (b) – Spectrum line  $3492\text{ cm}^{-1}$ , fitted by Lorentzian function. (c) – Dependence of the ions  $\text{H}^+$  relative concentration from depth.

The parameters of the line of the Raman spectrum at  $3492\text{ cm}^{-1}$ , corresponding to vibrations of the OH group, which is proportional to the concentration of  $\text{H}^+$  ions [162] (Figure 2.4a), were measured. The maximum line intensity was determined by approximating the measurement results with the Lorentz function (Figure 2.4b).

### 2.3 Visualization of the domain structure

The static domain structure was visualized both on the surface and in the bulk.

On a surface:

1) PFM method with a resolution of about 30 nm using an Ntegra Aura scanning probe microscope (NT-MDT, Russia) and MFP-3D (Oxford Instruments, USA) using an HA\_NC/W<sub>2</sub>C silicon probe (ScanSens, Germany) with a conductive tungsten coating and silicon probe with NSC 01 conductive platinum coating (Mikromash, Estonia). The piezoelectric response was measured because of the action of an alternating modulating voltage between the probe and the lower electrode with an amplitude  $U_{mod} = 3\text{--}5\text{ V}$  and a frequency  $f_{mod} = 20\text{ kHz}$  below the resonant frequency of the probe-sample system.

2) by optical microscopy with a resolution of about 500 nm using a polarizing microscope BX-61 (Olympus, Japan) in transmitted light.

In bulk:

1) by the CRM method based on the analysis of the spatial distribution of the shifts of the  $581\text{ cm}^{-1}$  E(TO<sub>8</sub>) and  $872\text{ cm}^{-1}$  A<sub>1</sub>(LO<sub>4</sub>) lines in the Raman spectrum

with a spatial resolution of about 500 nm. A lens with a magnification of 100x and a numerical aperture of 0.75 was used. A subject piezoelectric stage was used for scanning with a step of 0.1  $\mu\text{m}$ . The measured spatial distribution of spectral parameters sensitive to the domain structure was transformed into a two-dimensional image encoded by pseudocolor using the Control FOUR 4.1 software.

2) by the SHGM method using a setup based on Ntegra Spectra (NT-MDT, Russia) with a resolution of about 1  $\mu\text{m}$ . An IR laser with a wavelength of 1064 nm was used as a pump source. The pump beam, focused by a 100x objective with a numerical aperture of 0.80, was directed by galvanoelectric mirrors, which made it possible to scan with a step of 0.5  $\mu\text{m}$ .

## 2.4 Brief conclusions

Based on a review of the experimental setups and techniques used, the following brief conclusions can be drawn:

1 To study the evolution of the domain structure, we used CLN plates cut perpendicular to the polar axis with a surface layer modified by the soft proton exchange method.

2. *In situ* imaging of the evolution of the domain structure was carried out in SPE CLN samples using optical microscopy.

3. Confocal Raman microscopy was used to measure the depth dependence of  $\text{H}^+$  ion concentration in SPE CLN.

4. For local switching and imaging of the domain structure with submicron resolution, scanning microscopy of the piezoelectric response was used.

5. Imaging of the domain structure in the volume was carried out using second harmonic generation microscopy and confocal Raman microscopy.

### 3 Evolution of the domain structure in SPE CLN when switching in a uniform field.

#### 3.1 Anomalous kinetics of stripe domains.

The kinetics of the domain structure was studied during polarization reversal in a homogeneous field in plates with a soft proton exchange duration of 12 to 48 hours at 300°C and a concentration of lithium benzoate 3.0%. The studies were carried out when switching in a growing and steady-state field two months after the completion of the proton exchange process.

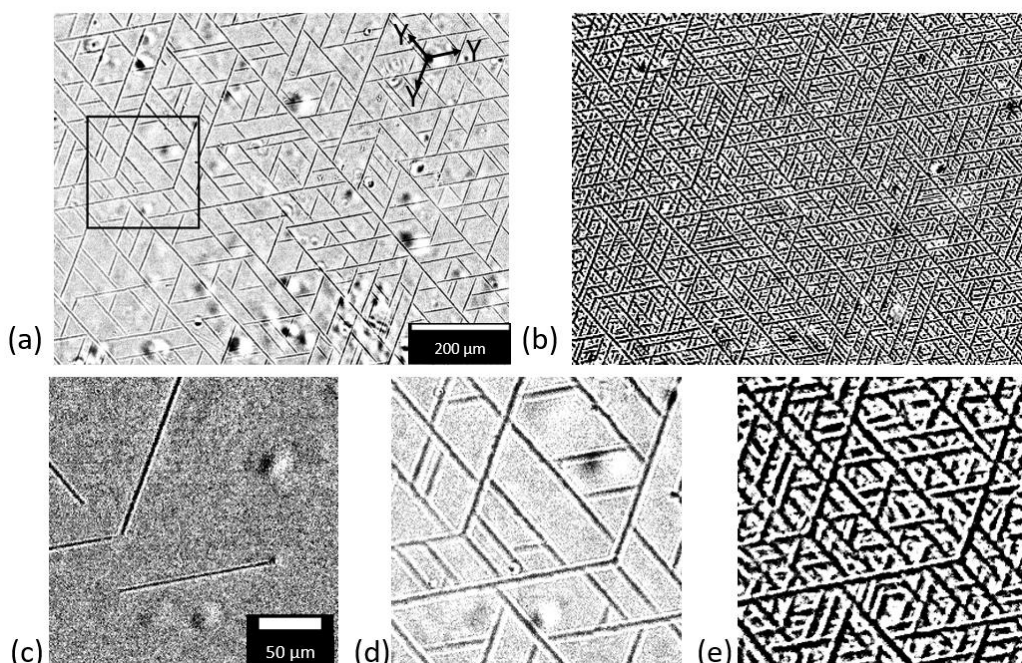


Figure 3.1 - Instantaneous optical images of the domain structure during switching polarization in a growing field at time intervals from the start of switching: (a) – 37 s ( $E = 8 \text{ kV/mm}$ ), (b) – 95 s ( $E = 19 \text{ kV/mm}$ ). The enlarged fragment of the image, highlighted on (a), at time points: (c) – 22 s ( $E = 4.5 \text{ kV/mm}$ ), (d) – 37 s ( $E = 8 \text{ kV/mm}$ ), (e) – 95 s ( $E = 19 \text{ kV/mm}$ ). The field growth rate is  $0.2 \text{ kV}/(\text{mm}\cdot\text{s})$ . The duration of proton exchange is 48 hours, at  $300^\circ\text{C}$ , the fraction of lithium benzoate is 3.0%.

In all the studied SPE CLN samples, when switching in a growing field, the kinetics of the domain structure starts in fields significantly lower compared to CLN crystals. An anomalous evolution of the domain structure was observed, which represented the formation of stripe domains and their growth in three selected

directions (Figure 3.1). The growth of the stripe domain stopped when approaching the stripe domain growing in the other direction. As a result of long-term switching, a net of stripe domains with an effective period of about 10  $\mu\text{m}$  was formed. It should be noted that the formation and anisotropic growth of submicron-width stripe domains were observed earlier for the domain structure formed because of pulsed heating of CLN by IR laser radiation [93].

The study of *in situ* imaging data of the kinetics of the domain structure revealed three stages in the evolution of the domain structure: (1) the formation and growth of isolated stripe domains, (2) the branching of stripe domains, (3) the formation of a net domain structure.

The formation of isolated stripe domains occurred on point defects of the sample in the area under the electrode. Domain growth started, as a rule, in one of the Y-directions in a field exceeding the threshold one ( $E_{th} = 2.4 \text{ kV/mm}$  for a sample with a proton exchange duration of 72 hours) (Figure 3.1b). The subsequent formation and growth of the second and third stripe domains from the same center along the two remaining Y-directions led to the formation of a domain in the shape of a dodecagon (Figure 3.1b, 3.2).

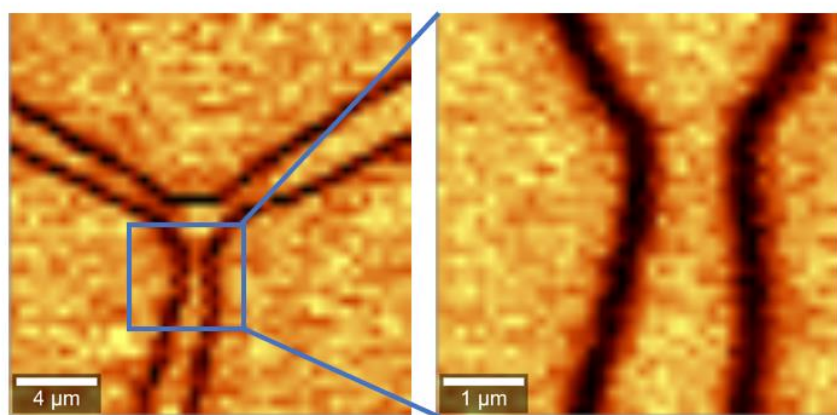


Figure 3.2 - CRM image of the central part of the domain in the shape of a dodecagon

Branching of the stripe domains was observed with a subsequent increase in the field ( $E_{th} > 7 \text{ kV/mm}$ ) and represented the formation and anisotropic growth of stripe domains from previously formed isolated domains (Figure 3.1. 6a, d).

The net domain structure was formed at the final stage of switching (Figure 3.1b, e). The resulting structure consists of domains about ten microns long. The typical effective period of the network structure was 10  $\mu\text{m}$ .

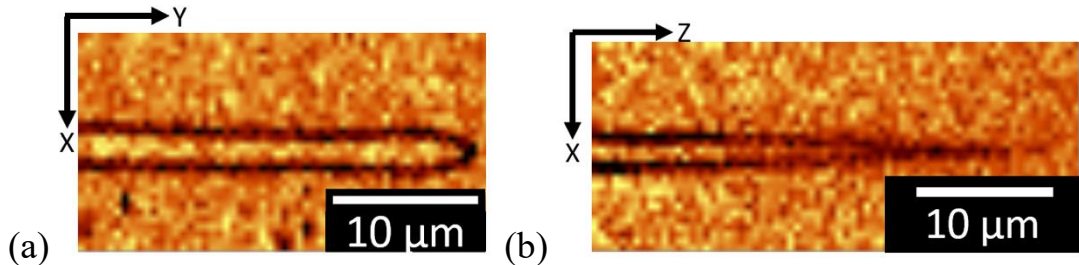


Figure 3.3 - CRM of the image of the stripe domain obtained by polarization reversal in a steady-state field of 5 kV/mm: (a) – on the polar surface, (b) – in the YZ cross-section. The proton exchange duration is 48 hours, at 300°C, the fraction of lithium benzoate is 3.0%.

The CRM imaging of the static domain structure made it possible to determine the average width of the stripe domains of about 4  $\mu\text{m}$  and a depth of up to 30  $\mu\text{m}$  (Figure 3.3).

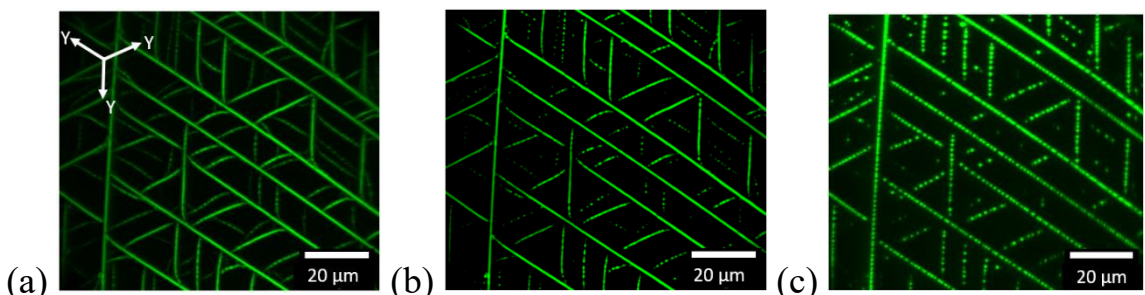


Figure 3.4 - SHGM images of the domain structure after partial switching in a growing field at different depths from the Z-polar surface,  $\mu\text{m}$ : (a) – 0, (b) – 8, (c) – 32. Field amplitude 20 kV/mm, pulse duration 100 s. The duration of proton exchange is 12 hours, at 300°C, the fraction of lithium benzoate is 3.0%.

The imaging of stripe domains in the volume by the SHGM method at different depths showed that stripe domains are observed only near the surface, and at a depth of more than 30  $\mu\text{m}$  they break up into chains of isolated domains with a diameter of about a micron. Thus, the domains have a comb shape (Figures 3.4,3.5) [94].

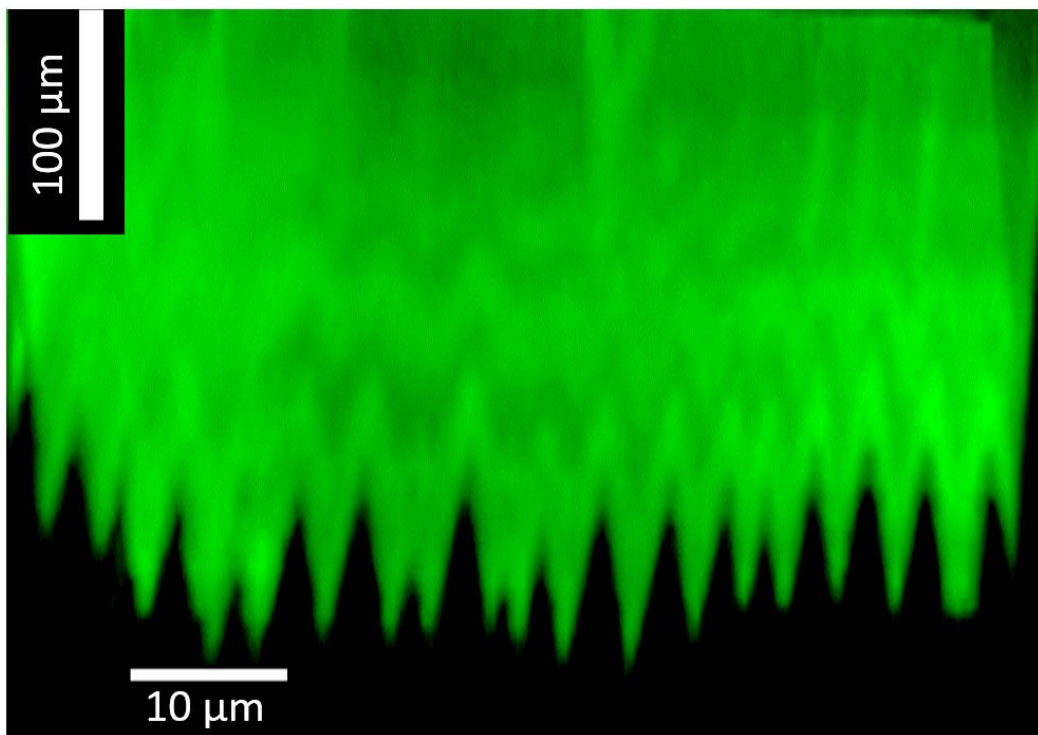


Figure 3.5 – SHGM is a three-dimensional image of a comb domain obtained by switching in a growing field. Field amplitude 20 kV/mm, pulse duration 100 s. Duration of proton exchange 48 hours at 300°C, proportion of lithium benzoate 3.0%.

For statistical analysis of the orientations of the stripe domains, the results of *in situ* imaging of the kinetics of the domain structure were processed using the following algorithm (Figure 3.6):

- 1) The background (the first frame of the video recording) was subtracted from all instantaneous images (Figure 3.6b).
- 2) The resulting images were binarized by the Lee algorithm [163].
- 3) The Fourier-transformed image of the binarized image was calculated (Figure 9c).
- 4) Angular dependence of the Fourier-transformed image relative to the center was performed (Figure 3.6d).

The algorithm for processing video recording frames and presenting the results was implemented by using OpenCV, Scipy, Skimage and Matplotlib libraries [164-167].

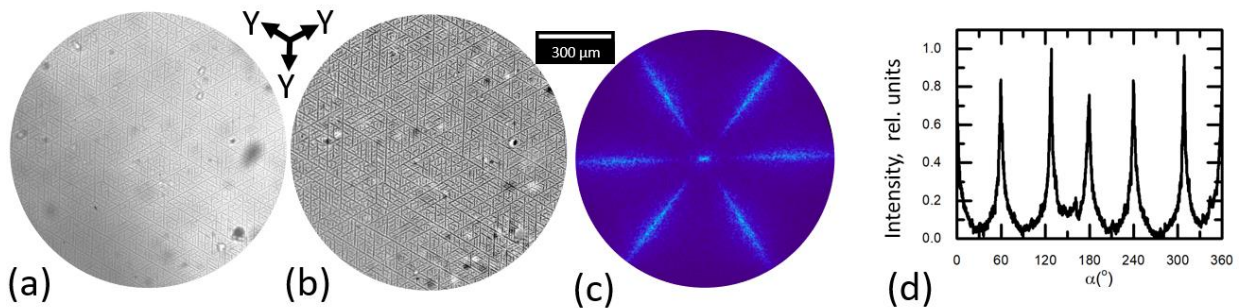


Figure 3.6 - (a) - an instantaneous optical image of the domain structure, (b) - an image after background subtraction, (c) - a Fourier-transformed image of the image. (d) - Angular folding of the Fourier-transformed image. Switching in a steady-state field of 8 kV/m. The duration of the proton exchange is 48 hours, the fraction of lithium benzoate is 3.0% at a temperature of 300°C.

The analysis showed that the stripe domains are oriented along three equivalent Y crystallographic directions in terms of CLN ( $C_{3v}$ ) symmetry.

### Statistical analysis

For quantitative description of the domain structure kinetics during switching in a growing field, the time dependence of the total length of the stripe domains  $L$  (Figure 3.1a) and the mean effective domain period  $T = A/L$ , where  $A$  is the area of the analyzed area, was analyzed. A modified Kolmogorov-Avrami approach was used [168-170], which was also used to analyze the time dependence of the total domain area in ferroelectrics [171]. At the same time, it was considered that at the initial stage, the increase in  $L$  occurs due to the growth of stripe domains that have arisen on surface defects, which corresponds to the Kolmogorov-Avrami  $\beta$ -model. With further switching after  $t_{cat}$  time, the evolution of the domain structure changes qualitatively and the formation and growth of stripe domains because of branching is observed, which corresponds to the Kolmogorov-Avrami  $\alpha$ -model (Figure 3.1d).

The experimentally measured time dependence of the total length of stripe domains  $L(t)$  was fitted by the formula (Figure 3.7a):

$$L(t) = \begin{cases} L_\beta(t), & t \leq t_{cat} \\ L_\alpha(t - \Delta t), & t \geq t_{cat} \end{cases} \quad (1)$$

At the first stage

$$L_\beta(t) = L_{max} \left( 1 - \exp \left( - \left( \frac{t-t_{st}}{t_\beta} \right)^2 \right) \right) \quad (2)$$

where  $t_\beta = (mbR/2)^{1/2}$ ,  $b$  is the concentration of the occurrence centers of stripe domains,  $\mu$  - the lability of the wall,  $t_{st} = E_{th}/R$  - the start time of the switching process,  $E_{th}$  - the threshold field,  $R = dE/dt$  - the rate of field increase,  $L_{max}$  - the maximum total length of domains.

At the second stage

$$L_\alpha(t) = L_{max} \left[ 1 - \exp \left( -a \left[ \frac{-1}{6} R(t^3 - t_{st}^3) + \frac{1}{2} E_{th}(t^2 - t_{st}^2) + \left( \frac{1}{2} R t^2 - E_{th} t \right) (t - t_{st}) \right] \right) \right] \quad (3)$$

where  $a = \alpha\mu$ ,  $\alpha$  - the probability of branching per unit length of stripe domains.

The time dependence of the mean effective domain structure period was approximated by the formula (Figure 3.7b):

$$T(t) = \frac{A}{L(t)} \quad (4)$$

As a result of the fitting of  $L(t)$  for SPE CLN with a proton exchange time of 48 hours at fixed parameters  $L_{max} = 96$  mm,  $R = 0.2$  kV/(mm·s) and  $E_{th} = 3.6$  kV/mm, the following parameter values were obtained:  $a = (7.1 \pm 0.5) \cdot 10^{-5}$  mm/(kV·c2),  $\Delta t = -(30 \pm 1)$  s,  $t_b = (25 \pm 1)$  s.

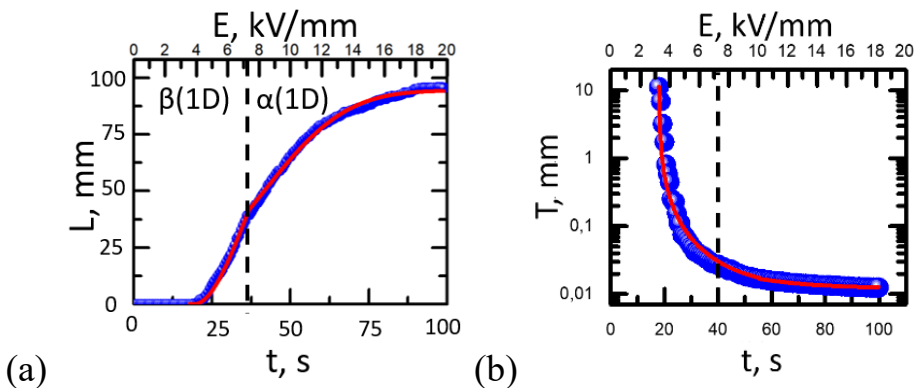


Figure 3.7 - Time dependences: (a) – the total length of the stripe domains and (b) – the effective period, approximated by equations (1) and (4) respectively. The duration of proton exchange is 48 hours, the fraction of lithium benzoate is 3.0%, at a temperature of 300°C.

### Growth of hexagonal domains

In fields of more than 21.5 kV/mm corresponding to the threshold field for switching polarization in CLN in all studied samples, the traditional growth of hexagonal domains with domain walls parallel to the Y crystallographic directions was observed. The hexagonal shape was rapidly restored after domain merging due to the growth of ultrafast short-lived walls [88], that is, typical of CLN shape stability effect (Figure 3.8).

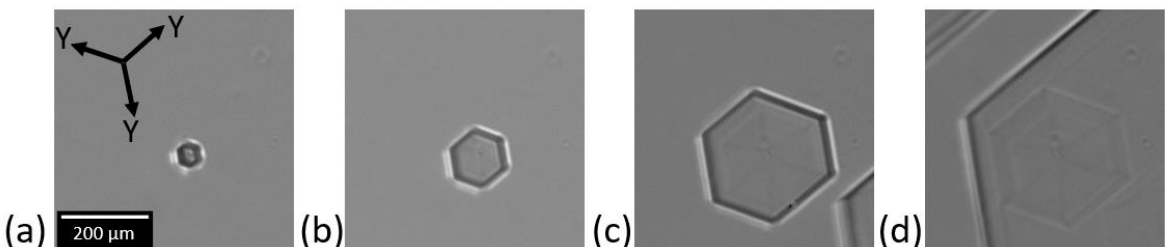


Figure 3.8 - Growth of hexagonal domains when switching polarization in a steady-state field of 22 kV/mm. Instant optical images of the domain structure. Time intervals from the start of switching, ms: (a) - 220, (b) - 228, (c) – 236, (d) – 244. Optical microscopy, transmitted light. The duration of proton exchange is 48 hours, with a fraction of lithium benzoate of 3.0% at a temperature of 300°C.

#### Transition mode

In the field range from 21 to 22 kV/mm, when switching in a constant field, a transitional growth regime was observed, in which first stripe domains formed and grew, and then polygon-shaped domains formed and grew (Figure 3.9a-b). During this process, polygons with concave corners were formed - "three-beam stars" (Figure 3.9).

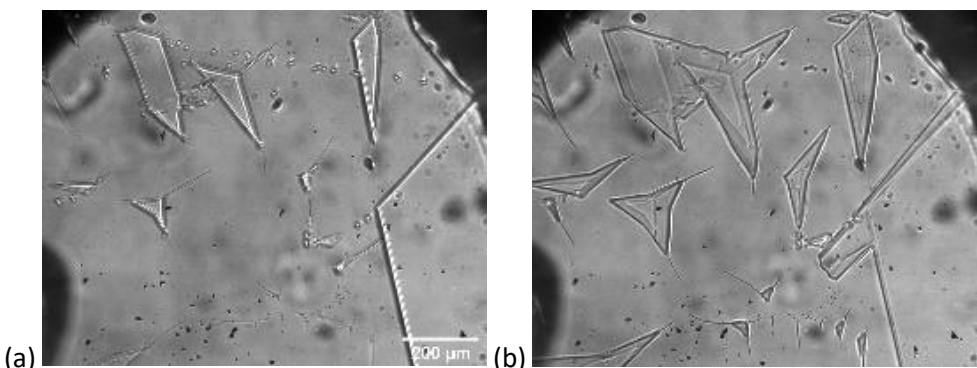


Figure 3.9 - Optical images of instantaneous domain configurations during polarization reversal in a field of 21 kV / mm in SPE CLN with a proton exchange duration of 72 hours for various time intervals after the start of switching: (a) 2 s, (b) 3 s.

Imaging of the domain structure at different depths from the surface using the CRM method showed that the motion of domain walls in this case is accompanied by the formation of nanodomains in front of the moving wall (Figure 3.10), that is, the effect of correlated nucleation is observed [32].

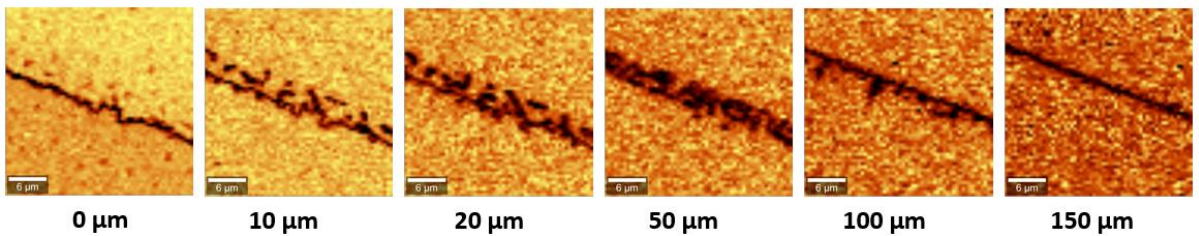


Figure 3.10 - CRM images of the domain wall in the shape of a three-beam star at different depths from the surface

### 3.2 Quasi-periodic domain structures

The process of formation of the quasi-periodic structures of the stripe domains after the change of the switching mode was studied. In this case, the switching process consisted of two stages. At the first stage, an extended domain wall was created near the edge of the electrode by switching in a field of 22 kV/mm. At the second stage, the sample was covered with a solid electrode, while switching by a series of rectangular pulses with an amplitude of 10 kV/mm and a duration of 100 ms with an interval between pulses of 10 s led to the formation of a quasi-periodic structure of stripe domains growing from the created domain wall along the Y crystallographic direction (Figure 3.11 a, b).

The width of the stripe domains was about 2  $\mu\text{m}$ , the length was up to 100  $\mu\text{m}$ , the average period was about 5  $\mu\text{m}$  (Figure 3.11b), the depth was up to 20  $\mu\text{m}$  (Figure 3.11d).

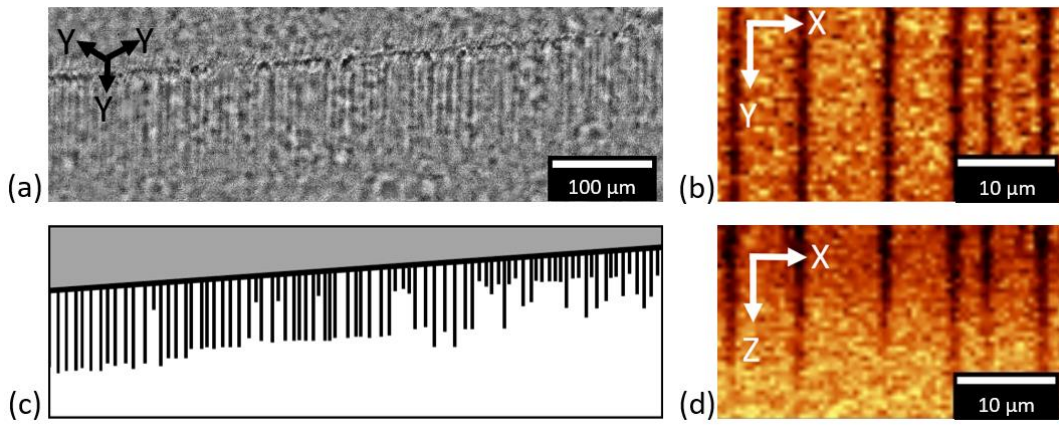


Figure 3.11 - Quasi-periodic structure of stripe domains growing from a plane domain wall because of polarization by a series of rectangular pulses. (a) – Optical image. CRM images: (b) – XY plane, (d) – XZ plane, (c) - a diagram of the domain structure.

The self-organized formation of a quasi-periodic structure consisting of parallel stripe domains in a homogeneous field is due to the electrostatic interaction of floating stripe domains with charged domain walls. The resulting effect opens possibilities for creating periodical DS in SPE optical waveguides.

### 3.3 Change in the evolution of the domain structure because of the long holding of the SPE CLN.

It was found that holding SPE CLN samples at room temperature and about 20% humidity for more than one year after the completion of the proton exchange led to a further decrease of the threshold field and a change in the evolution of the domain structure during polarization reversal in an increasing field. So, for a sample with a proton exchange duration of 48 hours, when measured two months after the completion of the proton exchange, the threshold field was 4 kV/mm, and after 12 months the threshold field decreased to 2.5 kV/mm. As in earlier measurements, similar three stages of domain structure evolution were observed, however, the orientation of the growing stripe domains changed significantly.

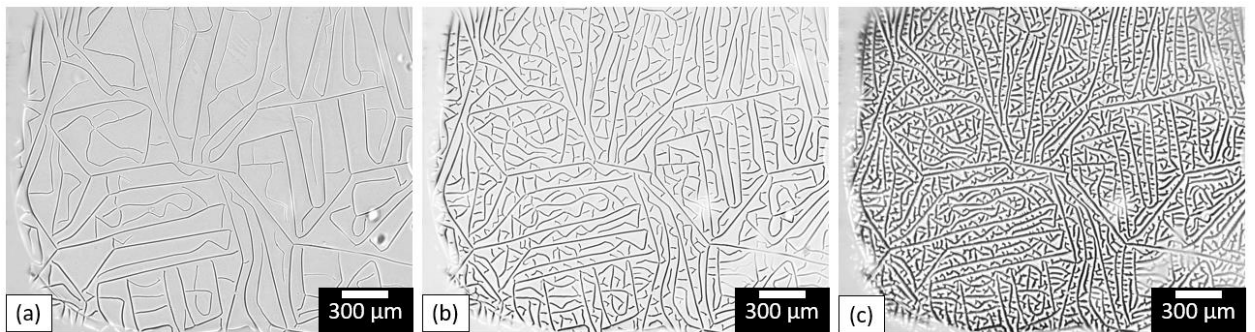


Figure 3.12 - (a)-(c) Optical images of instantaneous domain configurations during polarization reversal in a growing field in SPE CLN with a proton exchange duration of 48 hours: (a) 40 s,  $E = 8.3$  kV/mm, (b) 58 s,  $E = 12.4$  kV/mm, (c) 86 s,  $E = 18.4$  kV/mm. The measurements were taken 12 months after the completion of the proton exchange.

Isolated stripe domains, which were formed at the first stage, grew not only in Y, but also in X directions. In addition, the distances at which the interaction of the growing domains was manifested was much greater, which led to the manifestation of the effect of reflection of the growing domains (change in the direction of growth) when approaching the previously grown domains and their growth in arbitrary directions (Figure 3.12b,c).

The branching of the stripe domains was also largely chaotic with a lower concentration of branches and significant deviations of the growth directions from the X and Y crystallographic directions (Figure 3.12b, e).

The net domain structure that formed at the final stage of switching (Figure 3.12b, e) had a significantly smaller total length of the stripe domains. A typical effective period of the network structure was 20  $\mu\text{m}$ .

Reflection of stripe domains and chaotization of the structure of stripe domains were observed earlier when studying the evolution of a domain structure obtained because of pulsed laser heating and subsequent cooling [2].

The revealed changes in the evolution of the domain structure because of prolonged exposure of SPE CLN after the completion of soft proton exchange can be attributed in the framework of the kinetic approach to an increase in the electrostatic interaction between growing stripe domains. When explaining, it should

be considered that these domains are ridge and have charged domain walls in the bulk. The interaction between domains in this case depends on the efficiency of bulk screening. Within the framework of the proposed mechanism, the observed effect can be caused by a slowdown in bulk screening during long exposure. The mechanism will be refined in future studies.

The revealed effect, of course, should be considered in the manufacture of integrated optical converters of the laser radiation wavelength using the effect of phase quasi-phase matching. According to the results obtained, the creation of regular domain structures in waveguides must be carried out no later than two months after the completion of soft proton exchange.

### **3.4 Dependence of the threshold fields for the growth of stripe domains and the spatial distribution of the composition on the duration of the proton exchange**

Comparative studies of the spatial distribution of the composition and threshold fields were carried out for SPE CLN samples with different proton exchange durations of 12, 24, 36, and 48 hours at the same temperature of 300°C and a lithium benzoate concentration of 3.0%. The results of measurements of composition change with depth are shown in Figure 3.13.

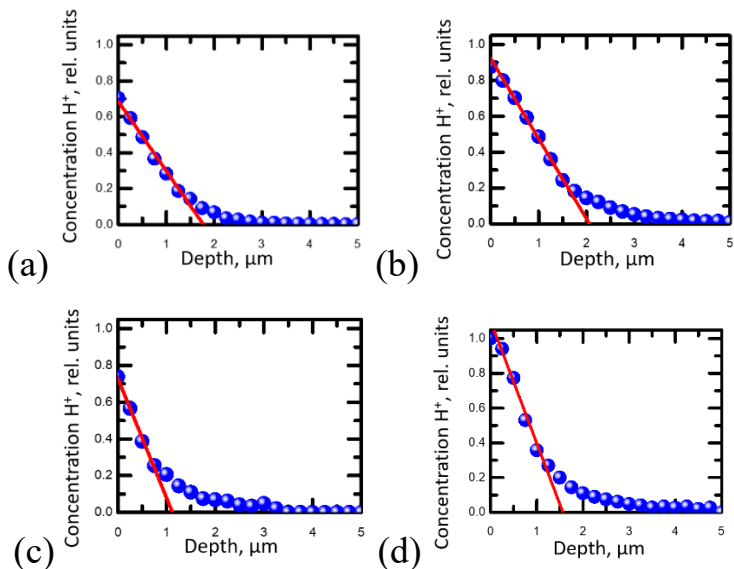


Figure 3.13 - The dependence of the concentration of  $H^+$  ions on the depth near the Z- polar surface for the proton exchange time: (a) - 12 h, (b) - 24 h, (c) – 36 h and (d) – 48 h at a temperature of 300°C with a fraction of lithium benzoate 3.0%

The obtained  $C(z)$  dependences near the polar surface were approximated by a linear dependence to determine the near-surface composition gradient  $dC/dz$  (Figure 3.14).

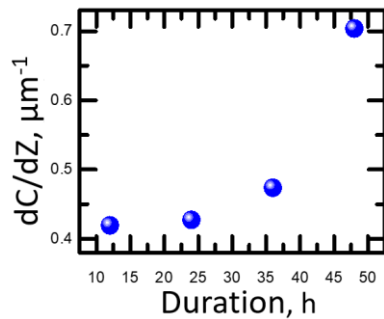


Figure 3.14 - Dependence on the duration of the proton exchange of the gradient of the relative concentration of  $H^+$  ions. Temperature 300°C, proportion of lithium benzoate 3.0%.

With an increase in the duration of the proton exchange, the composition gradient increases significantly (Figure 3.14).

The duration dependence of the proton exchange of the threshold fields measured during switching in a growing field is shown in Figure 3.15a.

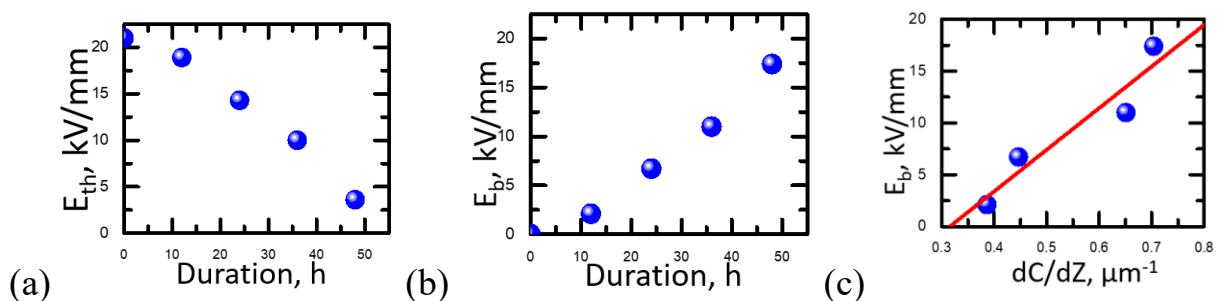


Figure 3.15 – Dependences of the duration of proton exchange on: (a) – the threshold field and (b) – the relative internal bias field. (c) - the dependence of the relative internal bias field on the  $H^+$  ions concentration gradient in the near-surface layer. Temperature 300°C, fraction of lithium benzoate 3.0%

With an increase in the duration of the proton exchange, the decrease of the threshold fields increases in comparison with the unmodified CLN (Figure 3.15b):

$$E_b(t_{PE}) = E_{th,CLN} - E_{th,SPE}(t_{PE}) \quad (3.5)$$

Previously, it was shown that the composition gradient in the surface layer of a uniaxial ferroelectric can be considered as a source of an internal field [35, 172].

The dependence of the threshold field on the composition gradient was analyzed. It was assumed that switching occurs under the action of  $E_{loc}$ , which is the sum of the applied field  $E_{ex}$  and the associated internal field  $E_b(t_{PE})$ , which is proportional to the gradient of the relative concentration of  $H^+$  ions.

$$E_{loc} = E_{ex} + E_b(t_{PE}) \quad (3.6)$$

$$E_b(t_{PE}) = k \frac{dC}{dz}(t_{PE}) \quad (3.7)$$

where  $k$  is the coefficient.

It is shown (Figure 3.15b) that under the experimentally implemented conditions, the bound internal field  $E_b$  increases with the duration of the proton exchange and reaches the value of 17 kV/mm at the proton exchange duration of 48 hours, which leads to a decrease of the threshold field to 4 kV/mm. Thus, the assumption is experimentally confirmed that the intensity of the bound internal field is proportional to the concentration gradient of  $H^+$  ions with the coefficient  $k = 38$  V (Figure 3.15c).

Therefore, the observed effect of a significant decrease of the threshold fields in SPE CLN can be attributed to the formation of a coupled internal field caused by the presence of a composition gradient in the surface layer.

### 3.5 Computer simulation of proton exchange in lithium niobate

To elucidate the mechanism of formation of the composition gradient in the surface layer because of soft proton exchange, computer simulation of the process of proton diffusion in the process of soft proton exchange was carried out. Diffusion of hydrogen ions into the bulk of the crystal and out-diffusion of lithium ions from the crystal with the formation of bulk vacancies were considered. To solve this problem, the model of Ganshin and Korkishko [173] was used.

The model is based on the following principles:

1) The behavior of particles in a crystal is described in accordance with the formalism of relative composing units. In this case, the crystal is considered as a set

of cationic (lithium), anionic, and interstitial sublattices. The diffusion of lithium and hydrogen over the sites of the cation sublattice together with cation vacancies is considered, as well as over interstices with the corresponding self-diffusion coefficients. It is assumed that anionic particles do not take part in diffusion.

2) The cationic and interstitial sublattices interact through the following reactions:



3) From a thermodynamic point of view, the "crystal-melt" system is open, but there are some characteristics that simplify the description. This system is isothermal and isobaric, that is, bulk changes can be neglected. Chemical reactions are not related to transfer processes, so equilibrium is reached instantly compared to the characteristic diffusion time, and a description based on the principles and laws of local chemical equilibrium is possible.

4) The temperature gradient, the stress tensor and the electric field inside the sample are assumed to be equal to zero.

The following equation was used to describe the diffusion of protons:

$$J_h = -b D_h (b - C_h)^{-1} \nabla C_h \quad (3.9)$$

where  $J_h$  is the flux of particles given particle type,  $D_k$  is the self-diffusion coefficient of the particle type,  $b = (D_l - D_v)/(D_h - D_v)$ ,  $u = b - 1 = (D_l - D_h)/(D_h - D_v)$ , ( $l$  are ions lithium,  $h$  are protons and  $v$  are vacancies),  $C_k$  is the concentration of this type of particles.

Then for each particle type:

$$\frac{\partial C_k}{\partial t} = - \frac{\partial J_k}{\partial x} \quad (3.10)$$

The following boundary conditions were used to solve the equation:

1)  $C_h(x, 0) = 0$  – at the initial moment of time, in all sections of the crystal, except for the surface, the concentration of hydrogen ions was assumed to be equal to zero.

2)  $C_h(\infty, t) = 0$  – at any moment of time at an infinite distance from the crystal boundary, the concentration of hydrogen ions was assumed to be zero.

3)  $C_h(0, t) = \text{const}$  – at any time at the crystal boundary, the concentration of hydrogen ions was a constant value.

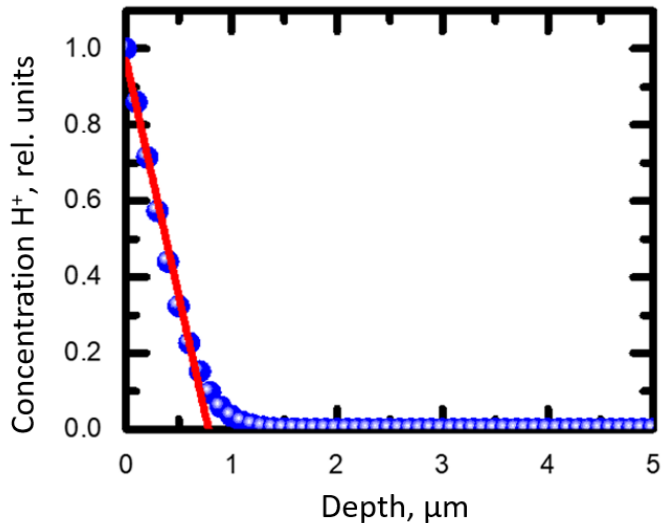


Figure. 3.16. – Results of a numerical experiment for a proton exchange duration of 24 hours

This non-stationary boundary value problem was solved numerically using the finite difference method with the explicit Euler time scheme. It is shown that the obtained dependences of the composition on depth (Figure 3.16) qualitatively correspond to the experimental data (Figure 3.13).

### 3.5 Brief conclusions

Based on the results obtained, the following main conclusions can be drawn:

1. Threshold fields in SPE CLN are much smaller than in CLN. In this case, stripe domains are formed and grow in three Y crystallographic directions. Three stages of evolution have been identified: (1) formation and growth of isolated stripe domains, (2) branching of stripe domains, (3) formation of a networked domain structure. The stripe domains are comb shaped.

2. The dependence of the total length of the stripe domains on time can be described within the framework of the modified Kolmogorov-Avrami approach, considering the change in the nature of the switching. At the same time, at the initial

stage, the stripe domains that have arisen on defects grow, which corresponds to the  $\beta$  model, and branching predominates, which corresponds to the  $\alpha$  model.

3. The creation of a quasi-periodic stripe domain structure based on the creation of a flat domain wall by a single high-field pulse and the growth of stripe domains from it from a flat domain wall with the application of many short weak-field pulses is demonstrated. The width of the stripe domains is about 2  $\mu\text{m}$ , the length is up to 100  $\mu\text{m}$ , the average period is about 5  $\mu\text{m}$ , and the depth is up to 20  $\mu\text{m}$ .

4. It was shown that exposure of SPE CLN samples at room temperature and 20% humidity for more than 12 months after the completion of proton exchange led to a further decrease of the threshold field and a change in the evolution of the domain structure. In this case, the stripe domains grew in Y and X crystallographic directions. The interaction of growing domains led to a change in the direction of growth when they approached each other.

5. It is shown that the decrease of threshold fields in SPE CLN is due to the formation of a coupled internal field caused by the presence of a composition gradient in the surface layer.

6. It has been shown by computer simulation that the appearance of a near-surface layer with a composition gradient during soft proton exchange is caused by diffusion of hydrogen ions into the bulk of the crystal and out-diffusion of lithium ions with the formation of bulk vacancies.

## 4 Local switching and creation of regular structures in SPE CLN

To study local polarization reversal, we used 0.5 mm thick SPE CLN plates cut perpendicular to the polar axis and polished to optical quality. The plates were subjected to soft proton exchange for 12, 24, 36, 48, and 72 hours at 300°C and a lithium benzoate concentration of 3.0%. Two switching modes were used: point and line scanning.

### 4.1 Local point switching

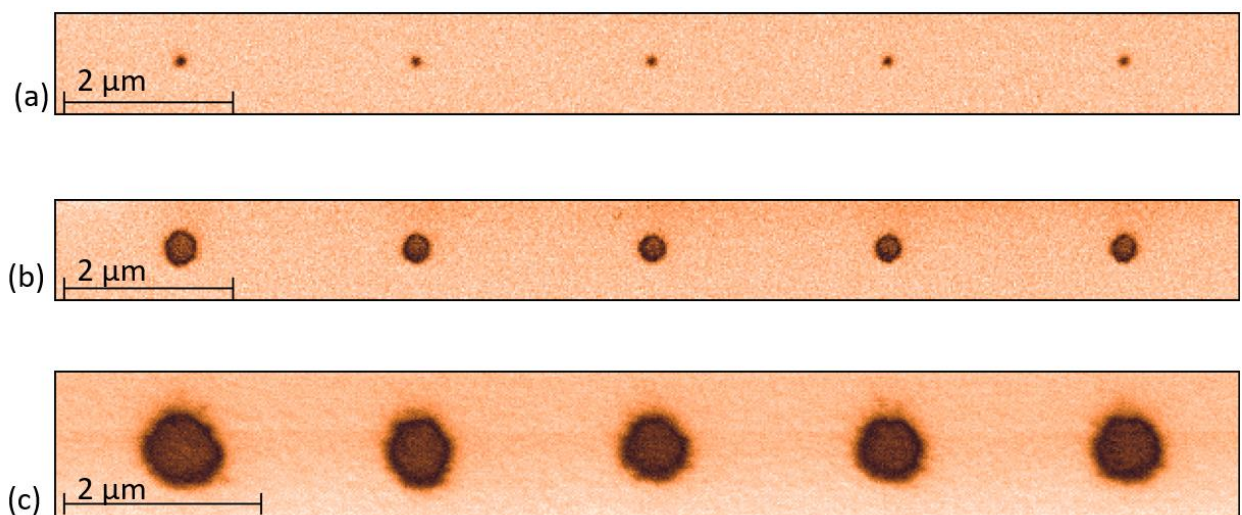


Figure 4.1. – PFM images of domain chains obtained by point switching at a pulse duration of 1 s and different voltages: (a) 75 V, (b) 200 V, (c) 300 V. Proton exchange duration 72 hours, 300°C, lithium benzoate fraction 3 .0%

It was established that in samples with a proton exchange duration of less than 48 hours, it was not possible to obtain domain chains in the whole range of voltages and durations. Therefore, all further studies were carried out in samples with a proton exchange duration of 48 and 72 hours.

Dependences of the effective radius of point domains on the duration (Figure 4.3) and amplitude of the voltage pulse (Figure 4.3) were analyzed. The resulting dependence of the diameter on the applied voltage was approximated by the equation [174]:

$$r(U_{tip}) = \sqrt{a\left(\frac{U_{tip}}{E_{th}}\right)^{2/3} - R_{tip}^2} \quad (4.1)$$

where  $a = \sqrt[3]{\frac{CR_{tip}}{2\pi\varepsilon_0(1+\varepsilon)}}$ ,  $U_{tip}$  – applied voltage,  $R_{tip}$  – probe curvature radius,

$E_{th}$  threshold field,  $C$  is the capacitance of the probe,  $\varepsilon_0$  - vacuum permittivity,  $\varepsilon$  - permittivity of the sample,  $E_{th}$  - the threshold field.

The resulting threshold voltage value for the pulse duration of 1 s is about 50 V.

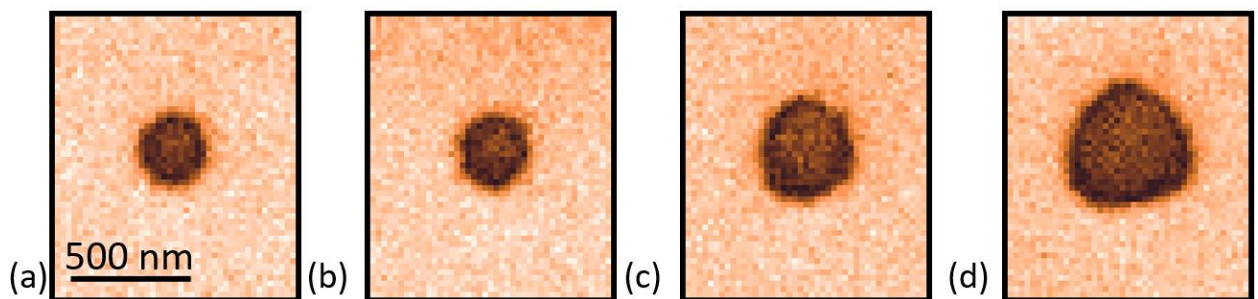


Figure 4.2. – (a) PFM images of isolated domains obtained by point switching at different pulse durations, voltage 200 V. Proton exchange duration 72 hours, 300°C, lithium benzoate fraction 3.0%

For round domains with a pulse duration of less than 10 s, a logarithmic dependence of the domain diameter on the pulse duration, traditional for local switching in uniaxial ferroelectrics, was observed (Figure 4.3). With a pulse duration of more than 10 s, the dependence became linear (Figure 4.3b, inset). The observed feature can be attributed to the transition from stochastic nucleation to deterministic nucleation with a change in the shape of domains (Figure 4.2) [174].

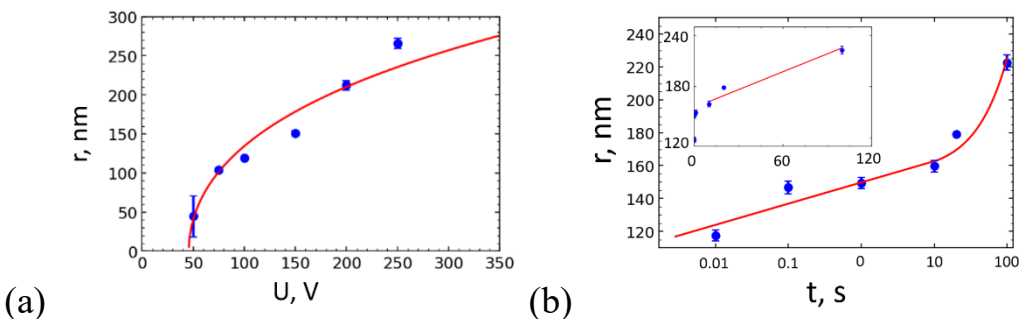


Figure 4.3 - Dependences of the effective radius of the domains: (a) - on voltage at a pulse duration of 1 s, approximated by equation (4.1) (b) - on the pulse duration at a voltage of 200 V,

approximated by a logarithmic function up to 10 s and linear after. Proton exchange duration 72 hours, 300°C, lithium benzoate content 3.0%

The dependence of the sizes of point domains in the chain on the period was investigated. It was shown that the circular domain shape was distorted for distances between the centers of voltage application less than 500 nm and the domain diameter decreased with period decreasing (Figure 4.4a).

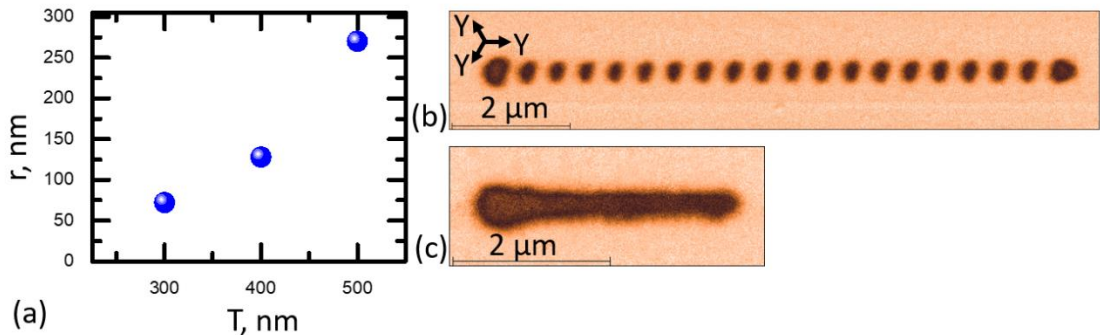


Figure 4.4 - (a) – The dependence of the effective domain diameter on the chain period. PFM images of the point domains with different periods, nm: (b) - 500, (c) – 150. Duration of proton exchange 72 hours, temperature 300°C, fraction of lithium benzoate 3.0%.

The reduction in size is caused by two effects: (1) by reducing the domain switching field due to the contribution of the depolarizing field created by the previous domain in the chain, (2) by partial polarization reversal of the switched domain under the action of the depolarizing field of the created domain. The first effect manifests in a decrease of the size of domains in the chain compared to the first domain, and the second one leads to a distortion of the circular domain shape (Figure 4.4b). For period below 300 nm, the domain merge led to formation of a stripe domain with width about 150 nm, which does not depend on the period (Figure 4.4c).

Thus, local switching can be used to create regular domain structures with submicron periods.

## 4.2 Line scan switching

Stripe domains were created by scanning along the Y crystallographic direction (Figure 4.5). In this case, the domains were formed at voltages above 150 V (Figure

18b-d). At voltages above 150 V, it was possible to create stable stripe domains of submicron width, which depended on the applied voltage (Figure 4.5a, b).

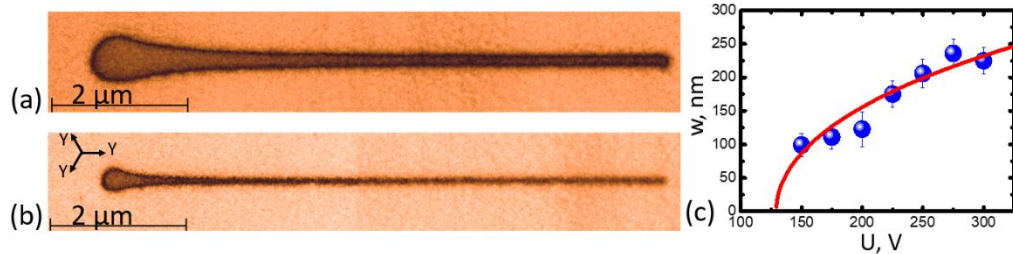


Figure 18 PFM images of stripe domains obtained via switching by scanning at different voltages, V: (a) – 150, (b). – 270. (c) Voltage dependence of the stripe domain width. The scanning rate is 1  $\mu\text{m}/\text{s}$ . Duration of proton exchange 72 hours, temperature 300°C, fraction of lithium benzoate 3.0%

The voltage dependence of the steady-state width of the stripe domain was analyzed. The resulting dependence was approximated by equation (4.1). In this case, the threshold value was 130 V, and the maximum width reached 250 nm.

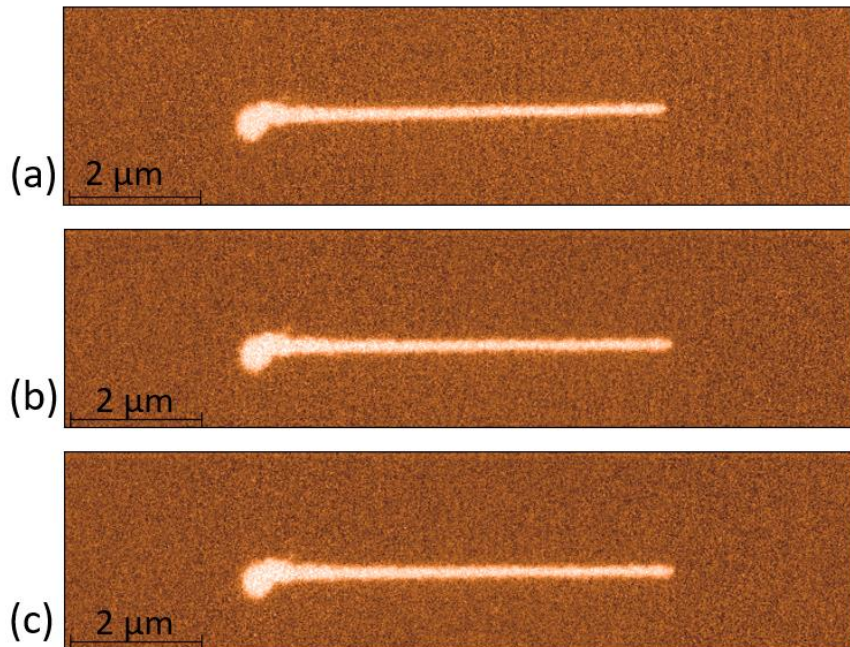


Figure 4.6 - PFM image of the stripe domain during multiple imaging with a time interval between scans of 30 minutes

It was found that even with repeated imaging for 90 minutes, there was no noticeable change in the size of the created stripe domain structure. (Figure 4.6).

### 4.3 Creation of regular domain structures

To create regular domain structures using the local switching method by line scanning, each stripe domain was created using sequential scanning: from left to right and from right to left.

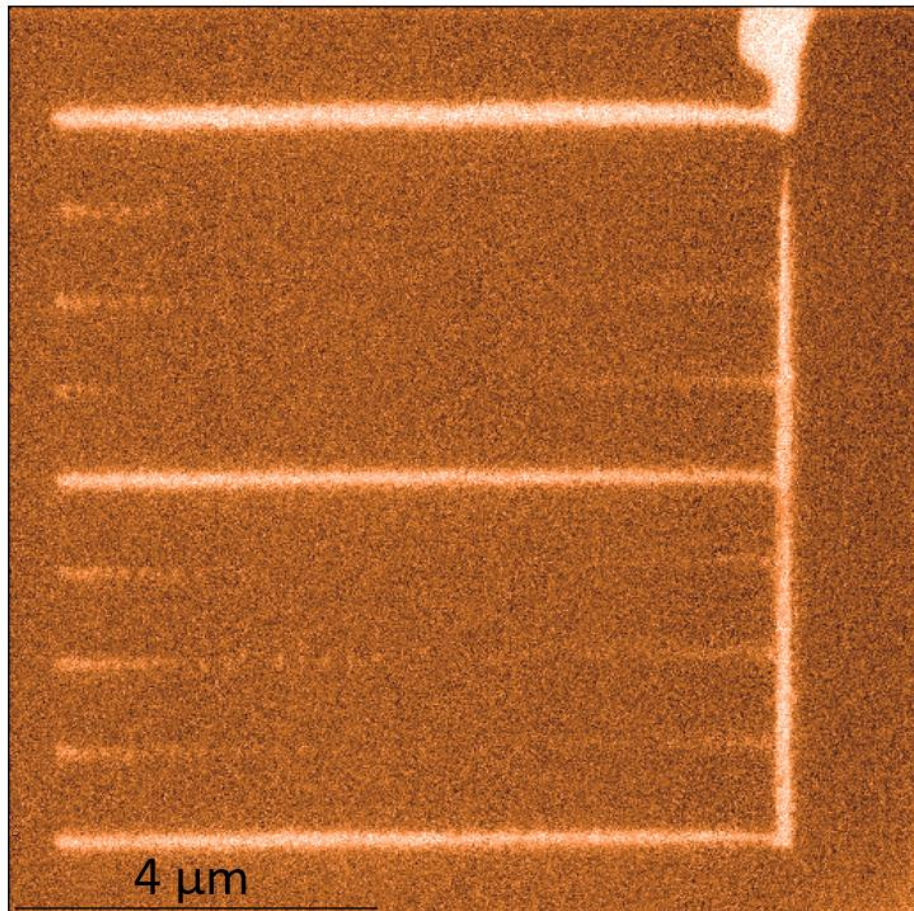


Figure 4.7 - Unsuccessful attempt to create a regular domain structure with a period of 1  $\mu\text{m}$  by linear scanning at room temperature.

At room temperature, it was not possible to obtain PDS even with a micron period (Figure 4.7), which is caused by the effect of electrostatic interaction of domains, previously identified with point switching.

Switching at elevated temperatures has been investigated to reduce the interaction. It is shown that the acceleration of bulk screening and the decrease of the threshold field led to a significant improvement in the regularity of the domain structure and the possibility of obtaining PDS with submicron periods.

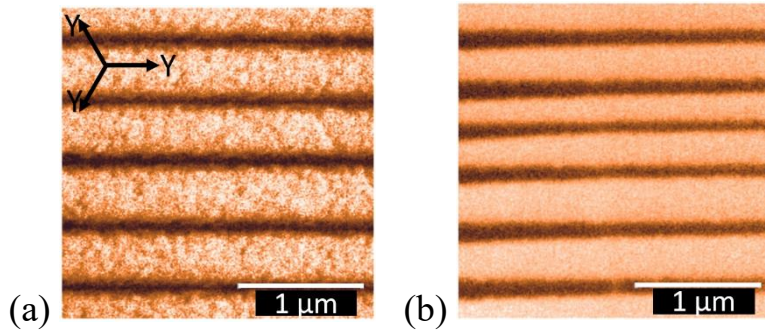


Figure 4.8 - PFM images of periodic domain structures created by scanning with period 500 nm. Duration of proton exchange (a) – 48 h, (b) – 72 h, at a temperature of 300°C with a fraction of lithium benzoate 3.0%.

The studies performed made it possible to choose the optimal switching parameters: voltage 200 V, temperature 85°C, using which it was possible to create a stable PDS with a period of 500 nm in samples with a proton exchange duration of 48 and 72 hours (Figure 4.8).

#### 4.5 Brief conclusions

Based on the results obtained, the following main conclusions can be drawn:

1. It is shown that local switching of polarization by a conducting SPM probe leads to the formation of rounded domains. It has been established that the dependence of the radius of an isolated domain on the amplitude of the switching pulse is described in terms of a simplified model, according to which the domain wall stops at the point where the field generated by the probe is equal to the threshold field.

2. It is shown that the dependence of the radius of an isolated domain on the duration of the switching pulse for durations less than 10 s is logarithmic, and for durations greater than 10 s it is linear. The observed feature is attributed to the change in the shape of the domains caused by the transition from stochastic to deterministic generation of steps on the domain wall.

3. It is shown that when writing chains of isolated domains, the round shape of the domains is distorted at distances between the voltage application points (period) of less than 500 nm. The size of the domains decreases with a further decrease of the period. The effect is attributed to a decrease of the local field and a

partial backswitching caused by the contribution of the depolarizing field created by the neighboring domain.

4. It is shown that linear scanning by a conducting SPM probe with a probe voltage of more than 150 V makes it possible to create stable submicron-wide stripe domains. In this case, the dependence of the stripe domain width on the applied voltage is described in terms of the model used to describe the dependence of the isolated domain radius on the switching pulse amplitude.

5. It is shown that polarization reversal at a temperature of 85°C makes it possible to create a stable regular domain structure of stripe domains with a period of 500 nm.

## **5 Second harmonic generation in MgOCLN with PDS created by scanning with a focused electron beam.**

The dependence of the SHG efficiency on the pump wavelength, temperature, and crystal rotation angle was studied, as well as the homogeneity of the end face area in single crystals of magnesium-doped lithium niobate with an PDS with a period of 2  $\mu\text{m}$  created by scanning the polar surface with a focused electron beam.

### **5.1 Creation of a periodic domain structure by a focused electron beam**

The lithium niobate doped with Mg (MgOCLN) with a periodic domain structure was studied. A periodic domain structure was created by scanning the Z-polar surface of MgOCLN plates with a thickness of 1 mm, cut perpendicular to the polar axis and polished to optical quality, with a focused electron beam. Before scanning, the irradiated Z-polar surface was covered by centrifugation with a layer of AZ nLOF 2020 photoresist (MicroChemicals, Germany) 2  $\mu\text{m}$  thick. A copper electrode 100 nm thick was deposited on the opposite Z+ polar surface by magnetron sputtering. The period of the created RDS was 2  $\mu\text{m}$  with an area of 1.5x0.5 mm<sup>2</sup>.

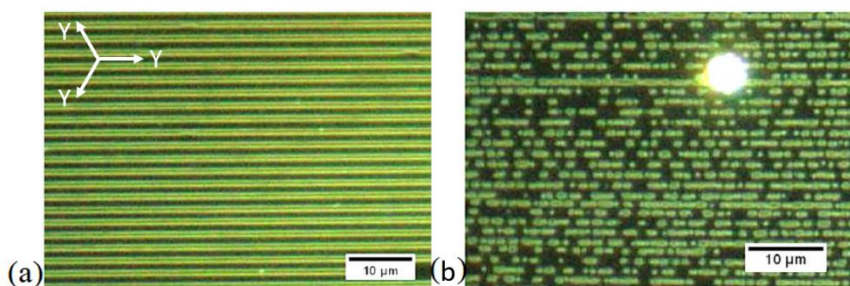


Figure 5.1 - A periodical domain structure with 2- $\mu\text{m}$ -period on (a) – Z- and (b) – Z+ polar surfaces. Revealed by selective chemical etching. Optical microscopy, dark field.

A scanning electron microscope Auriga Crossbeam Workstation (Carl Zeiss, Germany) with an electron-beam lithography system Elphy Multibeam (Raith GmbH, Germany) was used to create the PSD. The accelerating voltage was 8 kV, the beam current was 1.29 nA, the scanning speed was 0.52 mm/s, and the radiation

dose was  $2.5 \text{ mC/cm}^2$ . After creating the PDS, the input and output ends of the crystal were polished to optical quality.

Optical images of the created domain structure on both polar surfaces are shown in Figure 5.1. The structure is non-through.

## 5.2 Measurement of second harmonic generation

To study the second harmonic generation (SHG), the linearly polarized pump radiation of a Ti:Sapphire laser MBR-110 (Coherent, USA) with a power of 100 mW was focused by a lens with a focal length of 30 mm.

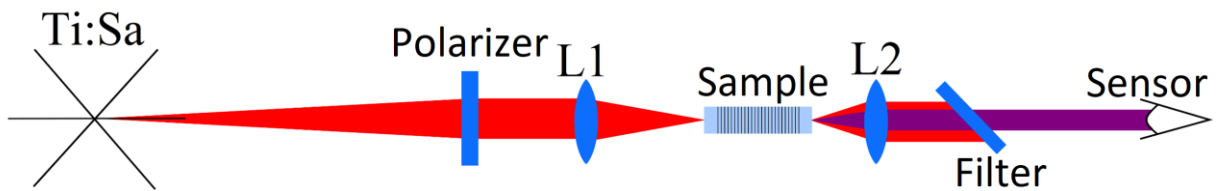


Figure 5.2 - Scheme of the experimental setup for studying the generation of the second harmonic in crystals with PDS.

The beam waist diameter was  $30 \mu\text{m}$ . The power of the SHG signal extracted with a BrightLine 375/110 nm single-band filter (Semrock, USA) was measured with an S130VC photodiode (Thorlabs, USA).

## 5.2 Features of second harmonic generation.

Measurement of the dependence of the SHG power on the pump wavelength (Figure 5.4 a) showed that the maximum conversion efficiency is observed at 744 - 747 nm. The FWHM of the main peak is 4 nm, which indicates a high sensitivity of the SHG process to the pump wavelength. The normalized SHG efficiency in the created regular domain structure 1.5 mm long was  $0.3\%/(W \text{ cm})$ .

The dependence of the SHG power on the position of the pump radiation focus when moving along the Z coordinate showed that the depth of the RDS, in which the second harmonic is effectively generated, was about  $300 \mu\text{m}$  (Figure 5.4 b). Comparison of images of the domain structure obtained on opposite polar surfaces

(Figure 5.1) suggested that the regular domain structure decays at a depth of 300  $\mu\text{m}$ .

The quasi phase-matching temperature for the pump wavelength of 747 nm was 32°C (Figure 5.4c), which is close to the calculated value of 47°C obtained using the Sellmeier equation [175].

$$n^2(\lambda) = 1 + \frac{B_1\lambda^2}{\lambda^2-C_1} + \frac{B_2\lambda^2}{\lambda^2-C_2} + \frac{B_3\lambda^2}{\lambda^2-C_3} \quad (5.1)$$

where  $B_1$ ,  $B_2$ ,  $B_3$ ,  $C_1$ ,  $C_2$ ,  $C_3$  are the Sellmeier coefficients and  $\lambda$  is the wavelength of the light passing through the sample.

The following Sollmeyer coefficients were used, as shown in Table 1.

Table 1 - Sollmeyer coefficients for congruent lithium niobate doped with 5% MgO

Coefficient	Value
$B_1$	2.4272
$B_2$	1.4617
$B_3$	9.6536
$C_1$	0.01478
$C_2$	0.05612
$C_3$	371.216

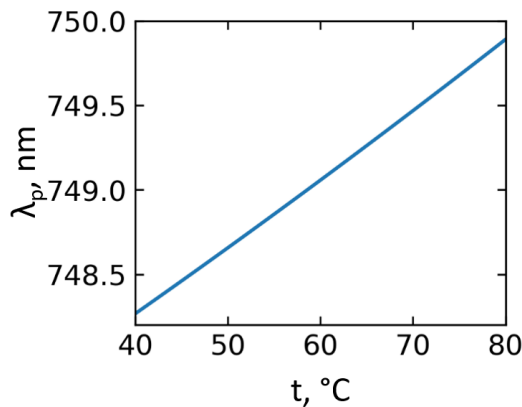


Figure 5.3. – Theoretical calculation of the temperature dependence of the phase quasi-phase-matching wavelength for a regular structure with a period of 2  $\mu\text{m}$  in MgOCLN

The normalized efficiency of second harmonic generation in an element 1.5 mm long, considering losses due to reflection, was 0.4%/(W·cm).

Rotation of the crystal with RDS relative to the Z axis at room temperature showed an almost threefold increase in power for an angle of 5 degrees (Figure 5.4 d). Estimates show that rotation of the RDS by a given angle corresponds to an effective increase in the period of the structure by 8 nm.

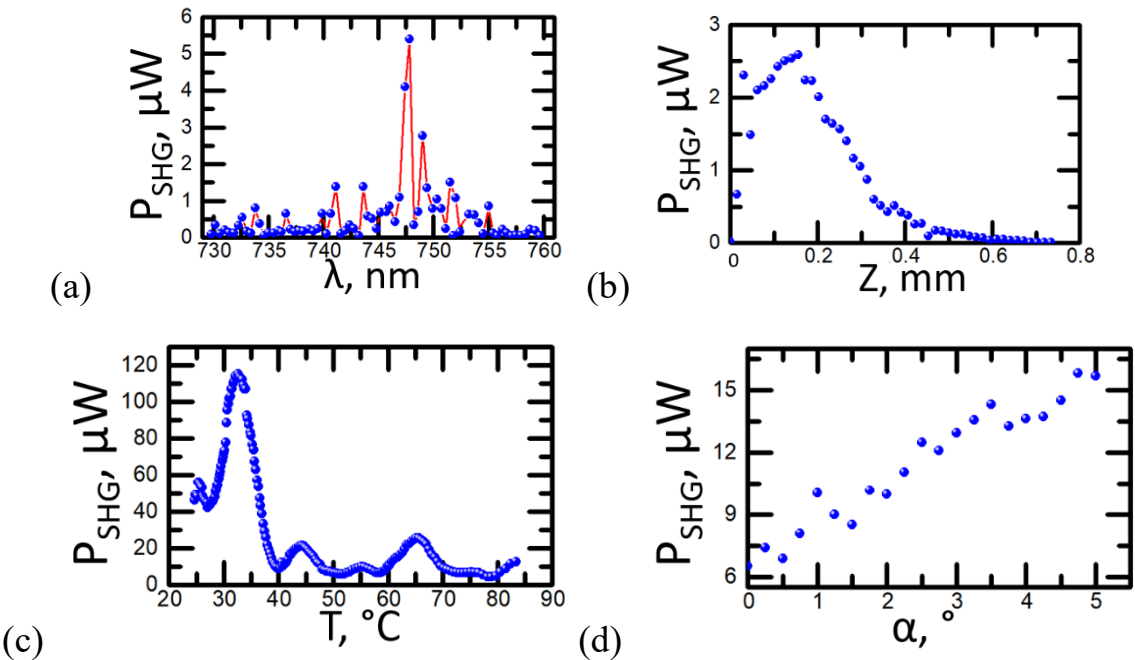


Figure 5.4 - The dependence of the SHG power on: (a) the pumping wavelength, (b) the Z coordinates of the pumping beam, (c) the temperature, (d) the angle of rotation of the sample relative to the Z axis. The pumping wavelength in (b-d) is 747 nm.

Thus, for the first time, it was possible to obtain radiation with a wavelength of 373 nm by the second-harmonic generation in a crystal of magnesium doped lithium niobate with an PDS with a period of 2  $\mu\text{m}$ , created by scanning with a convergent electron beam.

### 5.3 Brief conclusions.

Based on the results obtained, the following main conclusions can be drawn:

1. It is shown that scanning with a focused electron beam makes it possible to create in MgOLN regular domain structures with a small period (2  $\mu\text{m}$ ), which can be used for efficient generation of the second harmonic in a bulk crystal.

2. It was found that the normalized efficiency of second harmonic generation in the created regular domain structure 1.5 mm long (without antireflection coating) was 0.3%/(W·cm).

3. It was found that the depth of the regular domain structure created by scanning with a focused electron beam, in which the second harmonic was effectively generated, was about 300  $\mu\text{m}$ .

## **Conclusion**

1. The abnormal growth of stripe domains on the Z-polar surface during polarization switching in lithium niobate single crystals modified by soft proton exchange was studied for the first time.
2. The dependences of abnormally low values of threshold fields of domain formation on the Z-polar surface on the duration of the proton exchange process are revealed.
3. The effect of the formation of quasi-periodic domain structures with the growth of stripe domains from a planar domain wall was found.
4. The observed anomalous decrease in the threshold field of stripe domain growth as a result of soft proton exchange is attributed to the formation of bound internal field caused by the presence of a composition gradient in the near-surface layer.
5. It is shown that the composition gradient in the near-surface layer increases with an increase in the duration of the proton exchange process, which leads to a decrease in the threshold field.
6. The possibility of creating a stable periodic domain structure with a period of 500 nm by local switching using the probe of a scanning probe microscope is demonstrated.
7. For the first time, radiation with a wavelength of 374 nm was obtained by the method of the second-harmonic generation in a crystal of magnesium doped lithium niobate with a 2- $\mu\text{m}$ -period domain structure created by scanning with a focused electron beam.

### **Prospects for further development of the topic**

The results obtained during the research will be used to development of domain engineering methods for creating periodic domain structures in optical waveguides. Methods will be developed for creating optical waveguides with a periodic domain structure for wavelength conversion using quasi-phasematching. Optical

waveguides fabricated by soft proton exchange in lithium niobate crystals with a precise periodic domain structure will be used in quantum communication devices.

## **List of author's publications on the theme of the thesis**

- A1. Second harmonic generation in periodically poled MgO:LN crystal with 2  $\mu\text{m}$  period created by e-beam irradiation / **E. D. Savelyev**, A. R. Akhmatkhanov, D. S. Chezganov, E. O. Vlasov, E. A. Pashnina, V. Ya. Shur, H. Tronche, F. Doutre, T. Lunghi & P. Baldi // Ferroelectrics. – 2021. – Vol. 576. – P. 50-54, DOI: 10.1080/00150193.2021.188825.
- A2. Domain growth in LiNbO<sub>3</sub> with surface layer modified by soft proton exchange / **E. D. Savelyev**, A. R. Akhmatkhanov, E. D. Greshnyakov, A. S. Abramov, H. Tronche, F. Doutre, T. Lunghi, P. Baldi, M. M. Neradovskiy, V. Ya. Shur // Ferroelectrics. – 2022. – Vol. 592. – P. 64-71. DOI: 10.1080/00150193.2022.2052247.
- A3. Abnormal domain growth during polarization reversal in lithium niobate crystal modified by proton exchange / **E. Savelyev**, A. Akhmatkhanov, M. Kosobokov, H. Tronche, F. Doutre, T. Lunghi, P. Baldi, V. Shur // Crystals. – 2023. – Vol. 13. – P. 72. DOI: 10.3390/crust13010072.

## List of conventions and abbreviations

$\alpha$	– probability of nucleation in the $\alpha$ -model of the K-A theory
$\beta$	– density of nuclei in the $\beta$ -model of the K-A theory
$\lambda$	– radiation wavelength
$\Delta n$	– refractive index anisotropy in birefringence
$\Delta E_{loc.k}$	– exceeding the local field over the threshold value for kinks generation
$\Delta E_{loc.st}$	– exceeding the local field over the threshold value for step generation
$\epsilon_0$	– vacuum permittivity
$\epsilon_L$	– permittivity of the layer
$\tau$	– bulk screening time constant
$v_k$	– kink speed
$\mu$	– domain boundary mobility
$\mu_k$	– kink mobility
$\sigma_b$	– charge density
$\chi^{(i)}$	– $i$ -th order susceptibility
$A$	– switchable area
APE	– annealed waveguide after proton exchange
AFM	– atomic force microscope
$C$	– capacitor
CDW	– charged domain walls
CLN	– congruent lithium niobate
CRM	– confocal Raman microscopy
$C(z)$	– Depth dependence of $H^+$ concentration
$dC/dz$	– surface gradient composition
$dE/dt$	– rate of change of field with time
$D_k$	– self-diffusion coefficient
$dn_s/dt$	– step generation rate
DS	– domain structure

$E$	– electric field strength
$E_{ac}$	– activation field
$E_b$	– internal bias field
$E_{bscr}$	– bulk screening field
$E_{dep.z}$	– depolarizing field
$E_{ex.z}$	– external electric field
$E_{loc.z}$	– local field on the domain wall
$E_{scr.z}$	– outer screening field
$E_{th}$	– polarization reversal threshold field
$E_{th.k.}$	– threshold field for kink motion
$E_{th.st}$	– threshold field for step generation
$E_{rd}$	– residual depolarizing field
HISoPE	– soft proton exchange with high refractive index change
ITO	– indium tin oxide
$J_h$	– particle flow
$\vec{k}$	– wave vector
K-A	– Kolmogorov-Avrami theory
$L$	– dielectric layer thickness
$L(t)$	– total length of stripe domains versus time.
LB	– lithium benzoate
LN	– lithium niobate $\text{LiNbO}_3$
$n_s$	– concentration steps
MgOLN	– LN, doped with 5 mol.% magnesium oxide
$n$	– refractive index
PDS	– periodic domain structure
PFM	– piezoelectric force microscopy
PE	– proton exchange
PPLN	– lithium niobate with a periodic domain structure
$\vec{P}_S$	– spontaneous polarization vector

- RT – room temperature
- $R_{tip}$  – rounding radius of tip
- RPE – reverse proton exchange
- $T_C$  – ferroelectric phase transition temperature
- $t_{0\alpha}, t_{0\beta}$  – characteristic times in the  $\alpha$  and  $\beta$  models of K-A
- $U_{tip}$  – voltage applied to the probe
- SPE – soft proton exchange
- SHG – second harmonic generation
- SHGM – second-harmonic generation microscopy of the Cherenkov type
- SPM - scanning probe microscopy
- SEM - scanning electron microscopy

## CITED LITERATURE

1. High-frequency resonance in acoustic superlattice of LiNbO<sub>3</sub> crystals / Y. Zhu, et al. // Appl. Phys. Lett. – 1988. – Vol. 53. – P. 2278–2280.
2. Khan A.I. The future of ferroelectric field-effect transistor technology / A.I. Khan, A. Keshavarzi, S. Datta // Nat. Electron. – 2020. – Vol. 3. – P. 588–597.
3. Hu X. Nonlinear beam shaping in domain engineered ferroelectric crystals / X. Hu, Y. Zhang S. Zhu // Adv. Mat. – 2020. – Vol. 32 – P. 1903775.
4. Nanodomain engineering for programmable ferroelectric devices / A. Lipatov et al. // Nano Lett. – 2019. – Vol. 19. – P. 3194.
5. Kores C C. Quasi-phase matching waveguides on lithium niobate and KTP for nonlinear frequency conversion: A comparison / C. C. Kores, C. Canalias, F. Laurell // APL Photonics. – Vol. 6. – 2021. – P. 091102.
6. Bazzan M. Optical waveguides in lithium niobate: Recent developments and applications. / M. Bazzan, C. Sada // Appl. Phys. Rev. – Vol. 2:4. – 2015. – P. 040603.
7. Soft-proton-exchange tapers for low insertion-loss LiNbO<sub>3</sub> devices / D. Castaldini, et al. // IEEE J. Light. Technol. – Vol. 25. – 2007. – P. 1588–1593.
8. Soft proton exchange on periodically poled LiNbO<sub>3</sub>: A simple waveguide fabrication process for highly efficient nonlinear interactions / L. Chanvillard et al. // Appl. Phys. Lett. – Vol. 76:9. – 2000. – P. 1089–1091.
9. Hum, D. S. Quasi-phasematching / D. S. Hum, M. M. Fejer // Comptes Rendus Phys. – 2007. – Vol. 8:2. – P. 180–198.
10. Reduction of lattice defects in proton-exchanged lithium niobate waveguides / H. G. Muller et al. // J. Appl. Phys. – 2011. – Vol. 110. – P. 033539.

11. Shur V.Ya. Nano- and micro-domain engineering in normal and relaxor ferroelectrics / V.Ya. Shur // Handbook of Advanced Dielectric, Piezoelectric and Ferroelectric Materials. – Elsevier, 2008. – P. 622-669.
12. Shur V.Ya. Fast Polarization Reversal Process : Evolution of Ferroelectric Domain Structure in Thin Films / V.Ya. Shur // Ferroelectric thin film: synthesis and basic properties / ed. G.W.T.C.P. de A. James F. Scott. – Gordon and Breach Science Publ., 1996. – P. 153-192.
13. Lines M. Ferroelectrics and related materials / M. Lines, A. Glass. - Moscow: Mir, 1981. - P. 735.
14. Shur V.Ya. Domain shapes in bulk uniaxial ferroelectrics / V.Ya. Shur, E. V. Pelegova, M.S. Kosobokov // Ferroelectrics. – 2020. – Vol. 569. – P. 251-265.
15. Lambeck P.V. The nature of domain stabilization in ferroelectric perovskites. / P.V. Lambeck, G.H. Jonker. // J. Phys. Chem. Solids. – 1986. – Vol. 47:5. – P. 453-461.
16. Forward growth of ferroelectric domains with charged domain walls. Local switching on non-polar cuts / V.Ya. Shur et al. // J. Appl. Phys. – 2021. – Vol. 129. – P. 044103.
17. Shur V.Ya. Kinetics of ferroelectric domains: Application of general approach to LiNbO<sub>3</sub> and LiTaO<sub>3</sub> / V.Ya. Shur // J. Mater. Sci.. – 2006. – Vol. 41:1. – P. 199-210.
18. Shapes of isolated domains and field induced evolution of regular and random 2D domain structures in LiNbO<sub>3</sub> and LiTaO<sub>3</sub> / A. Chernykh et al. // Mater. Sci. Eng. B: Solid-State Materials for Advanced Technology. – 2005. – Vol. 120:1-3. – P. 109-113.
19. Shape evolution of isolated micro-domains in lithium niobate / V.Ya. Shur et al. // Ferroelectrics. – 2007. – Vol. 360. – № 1 PART 2. – P. 111-119.

20. Abnormal domain growth in lithium niobate with surface layer modified by proton exchange / M.A. Dolbilov et al. // Ferroelectrics. – 2010. – Vol. 398. – P. 108-114.
21. Formation of nanodomain structure in front of the moving domain wall in lithium niobate single crystal modified by proton exchange / M. A. Dolbilov et al. // Ferroelectrics. – 2013. – Vol. 442:1. – P. 82-91.
22. Formation of self-organized domain structures with charged domain walls in lithium niobate with surface layer modified by proton exchange / V.Ya. Shur et al. // J. Appl. Phys.. – 2017. – Vol. 121:10. – P. 104101.
23. Esin A.A. Tilt control of the charged domain walls in lithium niobate / A.A. Esin, A.R. Akhmatkhanov, V.Ya. Shur // Appl. Phys. Lett.. – 2019. – Vol. 114. – P. 9.
24. Formation of self-organized nanodomain patterns during spontaneous backswitching in lithium niobate / V.Ya. Shur et al. // Ferroelectrics. – 2001. – Vol. 253. – P. 105-114
25. Merz W.J. Switching time in ferroelectric BaTiO<sub>3</sub> and its dependence on crystal thickness / W.J. Merz // J. Appl. Phys. – 1956. – Vol. 27:1954. – P. 938-943.
26. Volk T. Lithium Niobate : Springer Series in Materials Science. Vol. 115 / T. Volk, M. Wöhlecke. – Berlin, Heidelberg: Springer Berlin Heidelberg, 2009. – P. 250.
27. Lambeck P. V. Ferroelectric domain stabilization in BaTiO<sub>3</sub> by bulk ordering of defects / P. V. Lambeck, G.H. Jonker // Ferroelectrics. – 1978. – Vol. 22:1. – P. 729-731.
28. Domain reversal and nonstoichiometry in lithium tantalate / S. Kim et al. // J. Appl. Phys. – 2001. – Vol. 90:6. – P. 2949.

29. Polarization fatigue in ferroelectric films: Basic experimental findings, phenomenological scenarios, and microscopic features / A.K. Tagantsev et al. // J. Appl. Phys. – 2001. – Vol. 90:3. – P. 1387.
30. Miller R.C. Mechanism for the Sidewise Motion of 180° Domain Walls in Barium Titanate / R.C. Miller, G. Weinreich // Phys. Rev. – 1960. – Vol. 117:6. – P. 1460-1466.
31. Udalov A. R. Origin of jump-like dynamics of the plane domain wall in ferroelectrics / A. R. Udalov, A. L. Korzhenevskii V. Ya. Shur // Ferroelectrics. – 2015. – Vol. 476. – P. 17-27.
32. Shur V.Y. Correlated Nucleation and Self-Organized Kinetics of Ferroelectric Domains. In Nucleation Theory and Applications / V.Y Shur / ed. J.W.P. Schmelze. – Verlag: Wiley-VCH. – 2005. – P. 178-214.
33. Drougard M.E. On the dependence of the switching time of barium titanate crystals on their thickness/ M.E. Drougard, R. Landauer // J. Appl. Phys. – 1959. – Vol. 30:11. – P. 1663-1668.
34. Movement of a flat domain wall in ferroelectric-ferroelastic gadolinium molybdate / V.Ya. Shur et al. // FTT. - 1999. - T. 41: 1. – pp. 126-129
35. Domain structure of lead germanate / V.Ya. Shur et al. // Ferroelectrics. – 1989. – Vol. 98. – P. 29-49.
36. Shur V.Ya. Domain structure of uniaxial ferroelectrics: Thes. doc. Phys.-Math. Sciences. Sverdlovsk, 1990. 335 C.
37. Formation of broad domain boundary in congruent lithium niobate modified by proton exchange / V. Ya. Shur et al. // Ferroelectrics. – 2015. – Vol. 476. – P. 146-155.
38. Hooton J. Etch patterns and ferroelectric domains in BaTiO<sub>3</sub> single crystals / J. Hooton, W. Merz // Phys. Rev. – 1955. – V. 98. – P. 409-413.

39. Differential etch rates in Z-cut LiNbO<sub>3</sub> for variable HF/HNO<sub>3</sub> concentrations / C.L. Sones et al. // J. Mater. Chem. – 2002. – Vol. 12. – P. 295-298.
40. Kuzminov Yu., Electro-optical and nonlinear optical crystal of lithium niobate // M.: Nauka, 1987. - 264 p.
41. Rearrangement of ferroelectric domain structure induced by chemical etching / V. Shur et al. // Appl. Phys. Lett. – 2005. – Vol. 87. – P. 022905-22908.
42. Fatuzzo E., Merz W., Ferroelectricity // Amsterdam: North-Holland Publishing Company, 1967. – P. 287.
43. D. Barfoot, D. Taylor, Polar dielectrics and their application // M.: Mir, 1981. - 526 p.
44. Iona F., Shirane D., Ferroelectric crystals // M.: Mir, 1965. - 555 p.
45. Merz W. Domain formation and domain wall motions in ferroelectric BaTiO<sub>3</sub> single crystals / W. Merz // Phys. Rev. – 1954. – Vol. 95. – P. 690-698.
46. Kinetics of the domain structure upon ultrafast polarization reversal in lead germanate / V. Shur et al. // JETP Letters. - 1991. - T. 53. - S. 591-594.
47. Gopalan V. In situ video observation of 180° domain kinetics in congruent LiNbO<sub>3</sub> / V. Gopalan, Q. Jia, T. Mitchell // Appl. Phys. Lett. – 1999. – Vol. 75. – P. 2482-2484.
48. Paranin V.D. Methods to control parameters of a diffraction grating on the surface of lithium niobate electro-optical crystal /V.D. Paranin // Tech. Phys. – 2014. – Vol. 59. – P. 1723–1727.
49. Yu. Kuzminov, Lithium niobate and tantalate - materials for nonlinear optics // M.: Nauka, 1975. - 224 p.
50. Otko A.I. Volumetric visualization of 180° ferroelectric domains in LiNbO<sub>3</sub> using electro-optical effects / A.I. Otko, A.E. Nosenko, I.M. Solsky, Ya.V. Burak // FTT. - 1989. - T. 31. - S. 42-47.

51. Gopalan V. In situ video observation of 180° domain switching in LiTaO<sub>3</sub> by electro-optic imaging microscopy / V. Gopalan, T. Mitchell // J. Appl. Phys. – 1999. – Vol. 85. – P. 2304-2311.
52. Le Bihan R. Study of ferroelectric and ferroelastic domain structures by scanning electron microscopy / R. Le Bihan // Ferroelectrics. – 1989. – Vol. 97. – P. 19-46.
53. Tanaka M. Electron optical studies of barium titanate single crystal films / M. Tanaka, G. Honjo // J. Phys. Soc. Japan. – 1964. – Vol. 19. – P. 954-970.
54. Ivantsov V. Observation of the development of the domain structure of NaNO<sub>2</sub> single crystals in a scanning electron microscope / V. Ivantsov, V. Nikolaev, I. Popov, FTT. - 1987. - T. 29. - S. 1855-1857.
55. Sogr A.A., Repolarization of ferroelectrics in a scanning electron microscope / A.A. Sogr, V.Z. Borodin // Proceedings of the Academy of Sciences of the USSR, ser. physical - 1977. - T. 41. - S. 1498-1501.
56. Sogr A.A. Observation of the dynamics of the domain structure of ferroelectrics in a scanning electron microscope / A.A. Sogr, V.Z. Borodin // Proceedings of the Academy of Sciences of the USSR, ser. physical - 1984. - T. 48. - S. 1086-1089.
57. Shakmanov V., Spivak G. Observation of the domain structure of thin ferroelectric films in a transmission electron microscope / V. Shakmanov, G. Spivak // Izvestiya AN SSSR, ser. physical - 1966. - T. 30. - S. 823-828.
58. Observation of polarization reversal of BaTiO<sub>3</sub> single-crystal films using a stroboscopic transmission electron microscope / Shakmanov V. et al. // Crystallography. - 1972. - T. 17. - S. 351-355.
59. Yakunin S., Shakmanov V., Spivak G., Vasil'eva N. Microstructure of domains and domain boundaries of barium titanate single-crystal films // Crystallography. - 1972. - T. 14. - S. 372-377.

60. Ivantsov V. Observation of the development of the domain structure of NaNO<sub>2</sub> single crystals in a scanning electron microscope / V. Ivantsov, V. Nikolaev, I. Popov // FTT. - 1987. - T. 29. - S. 1855-1857.
61. Wang Y. Study on surface and domain structures of PbTiO<sub>3</sub> crystals by atomic force microscopy / Y. Wang, J. Dec, W. Kleemann // J. Appl. Phys. – 1998. – Vol. 84. – P. 6795-6799.
62. Yamamoto T. Surface and domain structure of pure PbTiO<sub>3</sub> and Pb(Zn<sub>1/2</sub>Nb<sub>1/2</sub>)<sub>0,91</sub>Ti<sub>0,09</sub>O<sub>3</sub> single crystals by atomic force microscopy / T. Yamamoto, K. Kawano, M. Saito, S. Omika // Jap. J. Appl. Phys. – 1997. – Vol. 36. – P. 6145-6149.
63. Study of ferroelectric domains in BaTiO<sub>3</sub> crystalline films and bulk crystals by atomic force and scanning electron microscopies / Tsunekawa S. et al. // J. Appl. Phys. – 1998. – Vol. 84. – P. 999-1002.
64. Kalinin S. Electrostatic and Magnetic Force Microscopy / S. Kalinin, D. Bonnell // Scanning Probe Microscopy and Spectroscopy: Theory, Techniques, and Applications / D. A. Bonnell, Ed. Wiley-VCH, 2001, pp. 205–251.
65. Gruverman A. Scanning force microscopy as a tool for nanoscale study of ferroelectric domains / A. Gruverman, O. Auciello, Y. Hatano, H. Tokumoto // Ferroelectrics. – 1996. – Vol. 184. – P. 11-20.
66. Gruverman A. Scanning force microscopy of domain structure in ferroelectric thin films: imaging and control / A. Gruverman, O. Auciello, R. Ramesh, H. Tokumoto, // Nanotechnology B. – 1997. – Vol. 8. – P. A38-A43.
67. Residual stress estimation in ferroelectric PbTiO<sub>3</sub> thin films by Raman spectroscopy / Bartasyte A. et al. // Phys. Rev. B. – 2009. – Vol. 79. – P. 104104
68. Gouadec G. Raman Spectroscopy of nanomaterials: How spectra relate to disorder, particle size and mechanical properties / G. Gouadec, P. Colomban,

// Progress in Crystal Growth and Characterization of Materials. – 2007. – Vol 53. – P. 1-56.

69. Jach T. Long-range strains and the effects of applied field at 180 deg ferroelectric domain walls in lithium niobate / T. Jach, V. Gopalan, S. Durbin, D. Bright // Phys. Rev. B. – 2004. – Vol 69. – P. 064113
70. .Observation of ferroelectric domains in bismuth-layer-structured ferroelectrics using Raman spectroscopy/ Osada M. et al. // Mater. Sci. Eng. B. – 2005. – Vol. 120. – P. 95- 99.
71. Dierolf V. Sandmann C., Inspection of periodically poled waveguide devices by confocal luminescence microscopy / V. Dierolf // Appl. Phys. B. – 2004. – Vol. 78. – P. 363-366.
72. The asymmetry between the domain walls of periodically poled lithium niobate crystals / Kong Y., Jingjun X. et al// Opt. Mat. – 2004. – Vol. 27. – P. 471-473.
73. Raman probe on PPLN microstructures / Fontana M. et al. // Ferroelectrics. – 2008. – Vol. 373. – P. 26-31.
74. Hammoum R. Raman micro-spectroscopy as a probe to investigate PPLN structures / R. Hammoum, M. Fontana, P. Bourson, V. Shur, // Ferroelectrics. – 2007. – Vol. 352. – P. 106-110.
75. Hammoum R. Characterization of PPLN-microstructures by means of Raman spectroscopy / R. Hammoum, M. Fontana, P. Bourson, V. Shur, // Appl. Phys. A. – 2008. – Vol. 91. – P. 65-67.
76. High-resolution study of incoherent twin boundaries and of isolated wedge microt-wins in rare-earth monoclinic sesquioxides ( $\text{Ln}_2\text{O}_3\text{-B}$ ) / B. Yangui et al. // Phylos. Mag. A. – 1982. – Vol. 45. – P. 443-454.

77. Campagnola, P.J. Second harmonic generation microscopy: principles and applications to disease diagnosis / P.J. Campagnola, C.Y. Dong // Laser & Photon. Rev. – 2011. – Vol. 5. – P. 13-26.
78. Three-dimensional ferroelectric domain visualization by Čerenkov-type second harmonic generation / Y. Sheng, et al// Opt. Express. – 2010. – Vol. 18. – P. 16539-16545.
79. Beating the superparamagnetic limit with exchange bias / V. Skumryev et al. // Nature. – 2003. – Vol. 423. – P. 850–853.
80. Houé, M. An introduction to methods of periodic poling for second-harmonic generation / M. Houé, P. D. Townsend // J. Phys. D: Appl. Phys. – 1995. – Vol. 28:9. – P. 1747–1763.
81. Weis R. Lithium niobate: summary of physical properties and crystal structure / R. Weis, T. Gaylord // Appl. Phys. A. – 1985. – Vol. 37:4. – P. 191–203.
82. Volk, T. Lithium Niobate: Defects, Photorefraction and Ferroelectric Switching / T. Volk, M. Wöhlecke // Springer Science & Business Media. – Berlin : Springer. – 2009. – P. 249.
83. Volk, M. Optical ridge waveguides in lithium niobate and potassium titanyl phosphate: PhD thesis / Martin Volk ; Helmut Schmidt University. – Hamburg, 2018. – 126 p.
84. Arizmendi, L. Photonic applications of lithium niobate crystals /L. Arizmendi // Phys. Status Solidi. – 2004. – Vol. 201:2. – P. 253–283.
85. Sturman, B. I. The Photovoltaic and Photorefractive Effects in Noncentrosymmetric Materials / B. I. Sturman, V. M. Fridkin – Portland: CRC Press, 1992 – 264 p.
86. Abe R. Theoretical treatment of the movement of 180 ° domain in BaTiO<sub>3</sub> single crystal / R. Abe // J. Phys. Soc. Jpn. – 1959. – Vol. 14:5. – P. 633-642.

87. Hayashi M. Kinetics of domain wall motion in ferroelectric switching. I. general formulation / M. Hayashi // J. Phys. Soc. Jpn. – 1972. – Vol. 33:3. – P. 616-628.
88. Investigation of jerky domain wall motion in lithium niobate / I.S. Baturin et al. // Ferroelectrics. – 2008. – Vol. 374]. – P. 136-143.
89. Domain shape in congruent and stoichiometric lithium tantalate / V.Ya. Shur et al. // Ferroelectrics. – 2002. – Vol. 269. – P. 195-200.
90. Optical properties and ferroelectric engineering of vapor-transport-equilibrated, near-stoichiometric lithium tantalate for frequency conversion / D.S. Hum et al. // J. Appl. Phys. – 2007. – Vol. 101:9. – P. 093108.
91. Light-mediated ferroelectric domain engineering and micro-structuring of lithium niobate crystals / C.Y.J. Ying et al. // Laser & Photonics Rev. – 2012. – Vol. 6:4. – P. 526-548.
92. Discrete Switching by Growth of Nano-Scale Domain Rays Under Highly-Nonequilibrium Conditions in Lithium Niobate Single Crystals / A. I. Lobov et al. // Ferroelectrics. – 2008. – Vol. 373. – P. 99-108.
93. In situ investigation of formation of self-assembled nanodomain structure in lithium niobate after pulse laser irradiation/ V.Ya. Shur et al. // Appl. Phys. Lett. – 2011. – Vol. 99 – P. 082901.
94. Dimensionality increase of ferroelectric domain shape by pulse laser irradiation / V.Ya. Shur et al. // Acta Mat. – 2021. –Vol. 219. – P. 117270
95. Shape of isolated domains in lithium tantalate single crystals at elevated temperatures / V.Ya. Shur et al. // Appl. Phys. Lett. – 2013. –Vol. 103. – P. 242903
96. Esin A. A. Superfast domain wall motion in lithium niobate singlecrystals. Analogy with crystal growth / A. A. Esin ; A. R. Akhmatkhanov ; V. Ya. Shur // Appl. Phys. Lett. – 2019. –Vol. 114. – P. 192902

97. Tailored domain patterns in piezoelectric crystals / R.E. Newnham et al. // Phys. Stat. Sol. (a). – 1975. – Vol. 32:1. – P. 69-78.
98. Micro- and nano-domain engineering in lithium niobate / V.Ya. Shur, A.R. Akhmatkhanov, and I.S. Baturin // Appl. Phy. Rev. – 2015. –Vol. 2:4. – P. 040604.
99. Interactions between light waves in a nonlinear dielectric / J. A. Armstrong et al. // Phys. Rev. – 1962. – Vol. 127:6. – P. 1918–1939.
100. Giordmaine, J. A. Tunable coherent parametric oscillation in LiNbO<sub>3</sub> at optical frequencies / J. A. Giordmaine, R. C. Miller // Phys. Rev. Lett. – 1965. – Vol. 14:14. – P. 973–976.
101. Highly efficient photon-pair source using periodically poled lithium niobate waveguide / S. Tanzilli et al. // Electron. Lett. – 2001. – Vol. 37:1. – P. 26–28.
102. Byer, R. L. Optical parametric oscillation and amplification introduction / R. L. Byer, A. Piskarskas // J. Opt. Soc. Am. B. – 1993. – Vol. 10:11. – P. 2148–2150.
103. Nonlinear phase shift at 1.55 μm in CW single-pass cascaded parametric interactions in PPLN waveguides / P. Baldi et al. // Electron. Lett. – 1999. – Vol. 35:3. – P. 217–219.
104. Enhancement of second-harmonic generation in LiNbO<sub>3</sub> crystals with periodic laminar ferroelectric domains / D. Feng et al. // Appl. Phys. Lett. – 1980. – Vol. 37:7. – P. 607.
105. Ming N.-B. The growth striations and ferroelectric domain structures in Czochralski-grown LiNbO<sub>3</sub> single crystals / N.-B. Ming, J.-F. Hong, D. Feng // J. Mat. Sci. – 1982. – Vol. 17:6. – P. 1663- 1670.

106. Feisst A. Current induced periodic ferroelectric domain structures in LiNbO<sub>3</sub> applied for efficient nonlinear optical frequency mixing / A. Feisst, P. Koidl // Appl. Phys. Lett. – 1985. – Vol. 47:11. – P. 1125
107. Periodically poled LiNbO<sub>3</sub> for high-efficiency second-harmonic generation / D.H. Jundt et al. // Appl. Phys. Lett. – 1991. – Vol. 59:21. – P. 2657.
108. Blue light generation by frequency doubling in periodically poled lithium niobate channel waveguide / E.J. Lim et al. // Electron. Lett. – 1989. – Vol. 25:11. – P. 731-732.
109. First-order quasi-phase matched LiNbO<sub>3</sub> waveguide periodically poled by applying an external field for efficient blue second-harmonic generation / M. Yamada et al. // Appl. Phys. Lett. – 1993. – Vol. 62:5. – P. 435.
110. Quasi-phase-matched blue light generation in bulk lithium niobate, electrically poled via periodic liquid electrodes / J. Webjörn et al. // Electron. Lett. – 1994. – Vol. 30:11. – P. 894.
111. Quasi-phase-matched 1.064-μm-pumped optical parametric oscillator in bulk periodically poled LiNbO<sub>3</sub> / L.E. Myers et al. // Opt. Lett. – 1995. – Vol. 20:1. – P. 52.
112. Quasi-phase-matched optical parametric oscillators in bulk periodically poled LiNbO<sub>3</sub> / L.E. Myers et al. // J. Opt. Soc. Am. B. – 1995. – Vol. 12:11. – P. 2102.
113. 55% conversion efficiency to green in bulk quasi-phase-matching lithium niobate / J. Webjörn et al. // Electron. Lett. – 1995. – Vol. 31:8. – P. 669.
114. McElhanon R.W. Blue light generation in bulk periodically field poled LiNbO<sub>3</sub> / R.W. McElhanon, W.K. Burns, L. Goldberg // Electron. Lett. – 1995. – Vol. 31:18. – P. 1576-1577

115. 42%-efficient single-pass cw second-harmonic generation in periodically poled lithium niobate / G.D. Miller et al. // Opt. Lett. – 1997. – Vol. 22:24. – P. 1834.
116. Surface domain inversion in ferroelectric lithium niobate / A.C. Busacca et al. // Ferroelectrics. – 2003. – Vol. 296. – P. 91-97.
117. Surface domain engineering in congruent lithium niobate single crystals: A route to submicron periodic poling / A.C. Busacca et al. // Appl. Phys. Lett. – 2002. – Vol. 81:26. – P. 4946.
118. Backswitch poling in lithium niobate for high-fidelity domain patterning and efficient blue light generation / R.G. Batchko et al. // Appl. Phys. Lett. – 1999. – Vol. 75:12. – P. 1673
119. Visible quasi-phase-matched harmonic generation by electric-field-poled lithium niobate / G.D. Miller et al. // Proceedings of the SPIE. – 1996. – Vol. 2700. – P. 34-45.
120. Haycock P.W. A method of poling  $\text{LiNbO}_3$  and  $\text{LiTaO}_3$  below  $T_c$  / P.W. Haycock, P.D. Townsend // Appl. Phys. Lett. – 1986. – Vol. 48:11. – P. 698.
121. Fabrication of domain reversed gratings for SHG in  $\text{LiNbO}_3$  by electron beam bombardment / R.W. Keys et al. // Electron. Lett. – 1990. – Vol. 26:3. – P. 188.
122. Ito H. Fabrication of periodic domain grating in  $\text{LiNbO}_3$  by electron beam writing for application of nonlinear optical processes / H. Ito, C. Takyu, H. Inaba // Electron. Lett. – 1991. – Vol. 27:14. – P. 1221
123. Yamada M. Fabrication of periodically reversed domain structure for SHG in  $\text{LiNbO}_3$ , by direct electron beam lithography at room temperature / M. Yamada, K. Kishima // Electron. Lett. – 1991. – Vol. 27:10. – P. 828-829.

124. Kurimura S. Domain inversion by an electron-beam-induced electric field in MgO:LiNbO<sub>3</sub>, LiNbO<sub>3</sub> and LiTaO<sub>3</sub> / S. Kurimura, I. Shimoya, Y. Uesu // Jap. J. Appl. Phys. – 1996. – Vol. 35. –Part 2, No. 1A. – P. L31-L33.
125. Ferroelectric domain inversion by electron beam on LiNbO<sub>3</sub> and Ti:LiNbO<sub>3</sub> / C. Restoin et al. // J. Appl. Phys. – 2000. – Vol. 88:11. – P. 666
126. Electron-beam-induced domain poling in LiNbO<sub>3</sub> for two-dimensional nonlinear frequency conversion / Y. Glickman et al. // Appl. Phys. Lett. – 2006. – Vol. 88:1. – P. 011103
127. Domain patterning in LiNbO<sub>3</sub> and LiTaO<sub>3</sub> by focused electron beam / X. Li et al. // J. of Crystal Growth. – 2006. – Vol. 292:2. – P. 324- 327.
128. Fabrication of domain inverted structures by direct electron bombardment in LiNbO<sub>3</sub> crystals and its characterization / P. Molina et al. // Ferroelectrics. – 2006. – Vol. 334. – P. 67-72.
129. Kokhanchik L.S. Domain structure fabrication in Z and Y-cuts of LiTaO<sub>3</sub> crystals by point e-beam writing in the SEM / L.S. Kokhanchik, D.V. Irzhak // Ferroelectrics. – 2009. – Vol. 390. – P. 87-98.
130. Electron-beam poling on Ti:LiNbO<sub>3</sub> / C. Restoin et al. // Appl. Optics. – 2001. – Vol. 40:33. – P. 6056
131. LiNbO<sub>3</sub> waveguide quasi-phase-matching second harmonic generation devices with ferroelectric-domain-inverted gratings formed by electron-beam scanning / M. Fujimura et al. // J. Lightwave Tec. – 1993. – Vol. 11:8. – P. 1360-1368
132. Domain patterning by electron beam of MgO doped lithium niobate covered by resist / V.Y. Shur et al. // Appl. Phys. Lett. – 2015. – Vol. 106:23. – P. 232902
133. Suhara, T. Waveguide Fabrication and Characteristics / T. Suhara, M. Fujimura. — Luxembourg: Springer, 2003. — P. 315

134. Suhara T. Theoretical Background / T. Suhara, M. Fujimura // Waveguide Nonlinear-Optic Devices / coll. T. Kamiya et al. – Berlin, Heidelberg: Springer Berlin Heidelberg, 2003. – Vol. 11. – P. 9-33.
135. Rabiei P. Lithium niobate ridge waveguides and modulators fabricated using smart guide / P. Rabiei, W. Steier // Appl. Phys. Lett. – 2005. – Vol. 86. – P. 161115.
136. Takigawa R., Tanemasa. (2014). Lithium niobate ridged waveguides with smooth vertical sidewalls fabricated by an ultra-precision cutting method /R. Takigawa, E. Higurashi, T. Kawanishi, T. Asano, // Optics Exp. –2014. – Vol. 22. – P. 27733.
137. Rabiei P. Optical and electro-optical properties of submicrometer lithium niobate slab waveguides prepared by crystal ion slicing and wafer bonding / P. Rabiei, P. Gunter, // Appl. Phys. Lett. – 2005. – Vol.85. – P. 4603–4605.
138. Supercontinuum generation in lithium niobate ridge waveguides fabricated by proton exchange and ion beam enhanced etching / B.-X. Xiang et al. // Chinese Phys. Lett. – 2017. – Vol. 34. – P. 024203.
139. Schmidt V. Metal-diffused optical waveguides in LiNbO<sub>3</sub> R. / V. Schmidt, I. P. Kaminow // Appl. Phys. Lett. – 1974. – Vol. 25. – P. 458–460.
140. Sugii, K. A study on titanium diffusion into LiNbO<sub>3</sub> waveguides by electron probe analysis and X-ray diffraction methods / K. Sugii, M. Fukuma, H. Iwasaki // J Mater. Sci. – 1978. – Vol. 13. – P. 523–533
141. Fukuma M. Optical properties of titanium-diffused LiNbO<sub>3</sub> strip waveguides and their coupling-to-a-fiber characteristics / M. Fukuma, J. Noda // Appl. Opt. – 1980. – Vol. 19. – P. 591-597.
142. Miyazawa S. Ferroelectric domain inversion in Ti-diffused LiNbO<sub>3</sub> optical waveguide / S. Miyazawa // J. Appl. Phys. – 2008. – Vol. 50. – P. 4599–4603.

143. Thaniyavarn S. Domain inversion effects in Ti-LiNbO<sub>3</sub> integrated optical devices / S. Thaniyavarn, T. Findakly, D. Booher, J. Moen // Appl. Phys. Lett. – 1985. – Vol. 46:10. – P. 933–935.
144. High conversion efficiency single-pass second harmonic generation in a zinc-diffused periodically poled lithium niobate waveguide / L. Ming et al. // Opt. Express. – 2005. – Vol. 13. – P. 4862-4868.
145. Arizmendi L. Review Article: Photonic applications of lithium niobate crystals / L Arizmendi // Phys. Stat. Sol. (a). – 2004. – Vol. 201. – P. 175-175.
146. Photorefractive-damage-resistant Zn-diffused waveguides in MgO:LiNbO<sub>3</sub> / W. M. Young et al. // Opt. Lett. – 1991. – Vol. 16. – P. 995-997.
147. Christova K. Stress in LiNbO<sub>3</sub> proton-exchanged waveguide layers / K. Christova, M. Kuneva, S. Tonchev // J. Phys. Conf. Ser. – 2010. – Vol. 253. – P. 012057
148. Korkishko Y.N. Ion exchange in single crystals for integrated optics and optoelectronics / Y.N. Korkishko, V.A. Fedorov / Cambridge: Cambridge Internat. Science Publ. – 1999. – P. 516.
149. Korkishko Y.N. Structural phase diagram of H<sub>x</sub>Li<sub>1-x</sub>NbO<sub>3</sub> waveguides: The correlation between optical and structural properties / Y.N. Korkishko, V.A. Fedorov // IEEE J. Sel. Top. Quantum Electron. – 1996. – Vol. 2:2. – P. 187-196.
150. Relationships between structural and optical properties of proton-exchanged waveguides on Z-cut lithium niobate / Y.N. Korkishko et al. // Appl. Opt. – 1996. – Vol. 35:36. – P. 7056.
151. Bortz M.L. Annealed proton-exchanged LiNbO<sub>3</sub> waveguides / M.L. Bortz, M.M. Fejer // Optics Letters. – 1991. – Vol. 16:23. – P. 1844.

152. Bortz M.L. Depth profiling of the  $d_{33}$  nonlinear coefficient in annealed proton exchanged LiNbO<sub>3</sub> waveguides / M.L. Bortz, L.A. Eyres, M.M. Fejer // Appl. Phys. Lett. – 1993. – Vol. 62:17. – P. 2012.
153. Reverse proton exchange for buried waveguides in LiNbO<sub>3</sub> / Y.N. Korkishko et al. // J. Opt. Soc. Am. A. – 1998. – Vol. 15:7. – P. 1838.
154. Highly efficient second-harmonic generation in buried waveguides formed by annealed and reverse proton exchange in periodically poled lithium niobate / K.R. Parameswaran et al. // Opt. Lett. – 2002. – Vol. 27:3. – P. 179.
155. Soft proton exchange on periodically poled LiNbO<sub>3</sub>: A simple waveguide fabrication process for highly efficient nonlinear interactions / L. Chanvillard et al. // Appl. Phys. Lett. – 2000. – Vol. 76:9. – P. 1089
156. Highly Confining Proton Exchanged Waveguides on Z-Cut LiNbO<sub>3</sub> With Preserved Nonlinear Coefficient / O. Stepanenko et al. // IEEE Photonics Technol. Lett. – 2014. – Vol. 26:15. – P. 1557-1560.
157. Crystalline and optical quality of proton exchanged waveguides / M. de Micheli et al] // J. Light. Technol. – 1986. – Vol. 4:7. – P. 743-745.
158. Subsurface disorder and electro-optical properties of proton-exchanged LiNbO<sub>3</sub> / S.M. Kostritskii et al. // J. Eur. Opt. Soc.: Rapid Publ. – 2014. – Vol. 9. – P. 14055.
159. Rei-Shin Cheng. Mach-Zehnder modulators with lithium niobate ridge waveguides fabricated by proton-exchange wet etch and nickel indiffusion / Rei-Shin Cheng, Wei-Lin Chen, Way-Seen Wang // IEEE Photonics Technol. Lett. – 1995. – Vol. 7:11. – P. 1282-1284.
160. High performance digital optical switch / G. Singh et al. // Photon. Lett. Poland. – 2011. – Vol. 3:1. – P. 38-40.
161. Broadband optical modulators: science, technology, and applications / A. Chen / Boca Raton: CRC Press. – 2012. – P. 548.

162. Pershin S. M. Raman spectroscopy of the OH group vibrations in structural complexes of liquid water / S. M. Pershin // Opt. Spectrosc. – 2005. – Vol. 98. – P. 543–554.
163. Li C.H. Minimum cross entropy thresholding / C.H. Li and C.K. Lee // Pattern Recognition. – Vol. 26. – 1993. – P. 617.
164. Bradski G. The OpenCV library / G. Bradski // Dr. Dobb's J. Softw. Tools. – 2000. – Vol. 120. – P. 122–125.
165. SciPy 1.0: fundamental algorithms for scientific computing in Python / P. Virtanen et al. // Nat Methods. – 2020. – Vol. 17. – P. 261–272.
166. Scikit-image: image processing in Python / S. van der Walt et al. // PeerJ. – 2014. – Vol. 2. – e453
167. Hunter J.D. Matplotlib: A 2D graphics environment / J.D. Hunter // Comput. Sci. Eng. – 2007. – Vol. 9. – P. 90-95.
168. Kolmogorov A.N. On the statistical theory of crystallization of metals / A.N. Kolmogorov. // Izvestiya Rossiiskoi Akademii Nauk. Seriya Matematicheskaya. – 1937. – Vol. 3. – P. 355–359.
169. Avrami M. Kinetics of phase change. I General theory. / M. Avrami // J. Chem. Phys. – 1939. – Vol. 7. – P. 1103-1112.
170. Shur V. Kinetics of phase transformations in real finite systems: Application to switching in ferroelectrics / V. Shur, E. Rumyantsev, S. Makarov // J. Appl. Phys. – 1998. – Vol. 84:1. – P. 445.
171. Abnormal domain growth during polarization reversal in lithium niobate crystal modified by proton exchange / E. Savelyev et al.// Crystals – 2023. – Vol. 13. – P. 72. – 82.
172. Shur V.Ya. Arising and evolution of the domain structure in ferroics / V.Ya. Shur, E.L. Rumyantsev // J. Korean Phys. Soc. – 1998. – Vol. 32. – P. 727–732.

173. Ganshin V.A. Kinetic model of proton-lithium exchange in LiNbO<sub>3</sub> and LiTaO<sub>3</sub> crystals: The role of cation vacancies / V.A. Ganshin, Yu.N. Korkishko // Sol. St. Ionics. – 1992. – Vol. 58. – P. 23.
174. Domain structure formation by local switching in the ion sliced lithium niobate thin films // B. N. Slautin at al. / Appl. Phys. Lett. – 2020. – Vol. 116. – P. 152904
175. Jundt D.H. Temperature-dependent Sellmeier equation for the index of refraction, ne, in congruent lithium niobate / D.H. Jundt // Opt. Lett. – 1997. – Vol. 22:20. – P. 1553–1555.